AD-A064 179 AIR FORCE INST OF TECH WRIGHT-PATTERSON AFB OHIO SCH--ETC F/G 8/11
ANALYSIS AND IMPLEMENTATION OF OPTIMAL ESTIMATION AND CONTROL F--ETC(U)
DEC 78 P L TOLER

UNCLASSIFIED AFIT/GE/EE/78D-45 NL

1 OF 2
AD
A064179

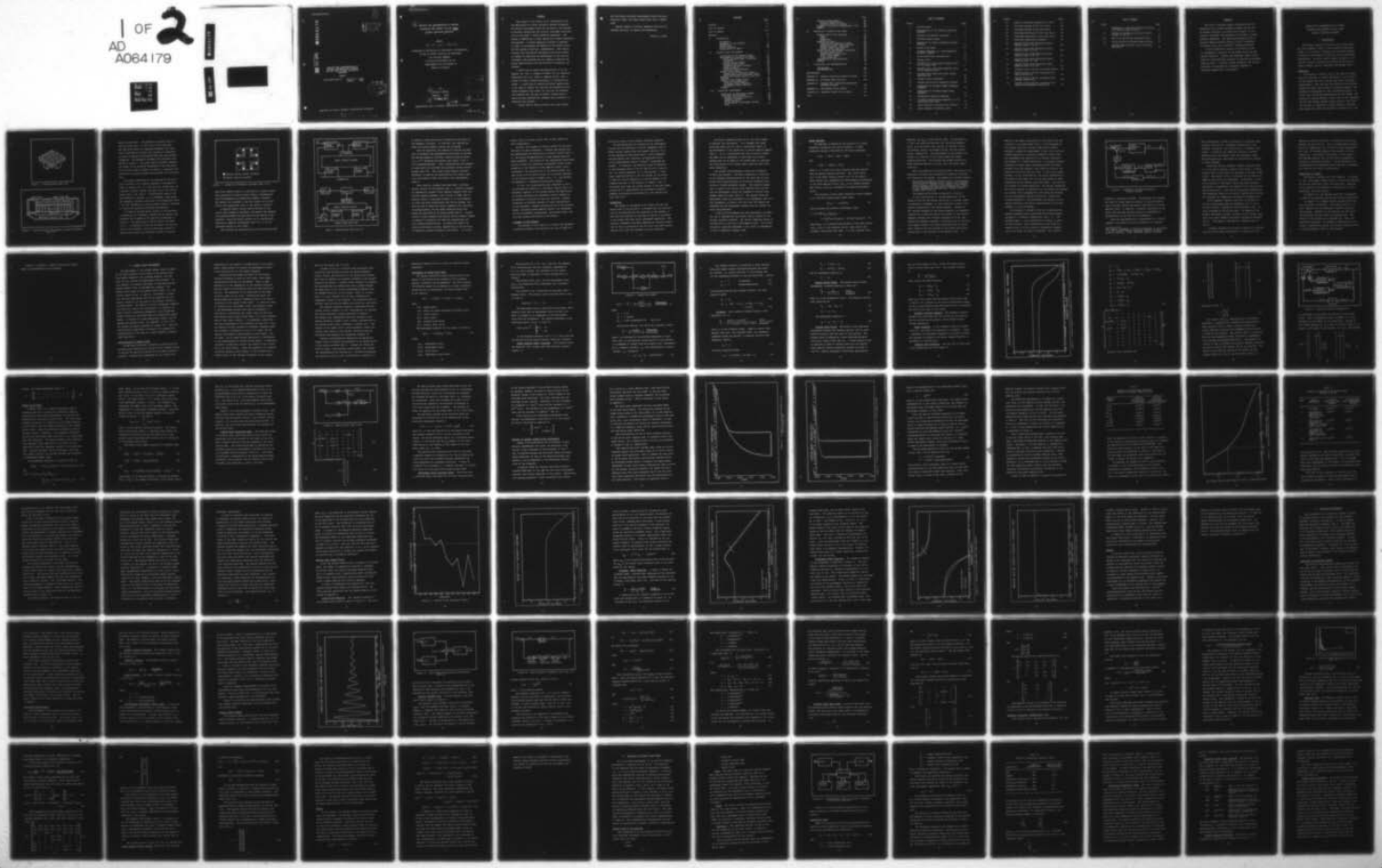

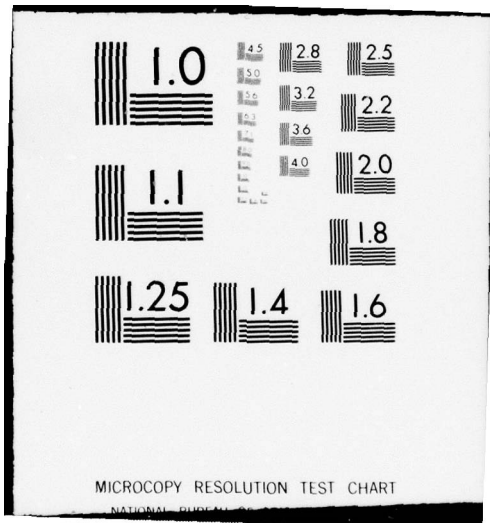
1.0
1.1
1.25
1.4
1.6
1.8
2.0
2.2
2.5
2.8
3.2
3.6
4.0
4.5
5.0
5.6
6.3
MICROCOPY RESOLUTION TEST CHART

ADA064179

AFIT/GE/EE/78D-45

(1)

LEVEL II

AD A064179

DDC FILE COPY

ANALYSIS AND IMPLEMENTATION OF OPTIMAL ESTIMATION AND CONTROL FOR THE FJSRL SEISMIC ISOLATION PLATFORM

THESIS

AFIT/GE/EE/78D-45 Phillip L. Toler
Captain USAF

DDC
RECEIVED
FEB 6 1979
A

Approved for public release; distribution unlimited

79 01 30 113

(14) AFIT/GE/EE/78D-45

(6) ANALYSIS AND IMPLEMENTATION OF OPTIMAL ESTIMATION AND CONTROL FOR THE FJSRL SEISMIC ISOLATION PLATFORM.

THESIS

(9) Master's thesis,

Presented to the Faculty of the School of Engineering

of the Air Force Institute of Technology

Air Training Command

in Partial Fulfillment of the

Requirements for the Degree of

Master of Science

ACCESSION for
NTIS White Section
DDC Buff Section
UNANNOUNCED
JUSTIFICATION
BY
DISTRIBUTION/AVAILABILITY CODES
Dist. AVAIL. and/or SPECIAL
A

by

(10) Phillip L. Toler

Captain USAF

(11) December 1978

(12) 146p.

Approved for public release; distribution unlimited

012 225

Preface

This report is the result of an investigation into the application of linear stochastic optimal estimation and control techniques toward the solution of the problem of actively controlling the inertial instrument test platform at the Frank J. Seiler Research Laboratory. The system is modeled as a linear system with random (stochastic) disturbances. A forced separation concept is employed in order to investigate the effects of the Kalman filter and the optimal controller, independently. The results indicate that the optimal estimation and control system is capable of improving the performance of the inertial instrument test platform but not capable of meeting the design specifications for the platform as presently configured.

I would like to extend my appreciation to my lab sponsor, Mr. Bill J. Simmons of FJSRL, for his technical assistance and to Dr. Peter S. Maybeck and Dr. John J. D'Azzo for their valuable assistance in reviewing this thesis. I would like to extend particular appreciation to Dr. Gary B. Lamont, not only for the guidance he provided throughout this study, but also for his guidance and tutelage over the past 18 months, without which I would not have obtained the academic tools necessary to undertake this project.

I would like to thank my family and close friends

who continually provided encouragement during the many difficult times; they were always there when I needed them.

Special thanks is due Mrs. Margaret Voigt for her patience and skill in typing this manuscript.

Phillip L. Toler

Contents

List of Figures

List of Tables

Abstract

The study is directed toward the analysis and implentation of an optimal estimator (Kalman filter) and an optimal regulator to provide active control of the inertial instrument test platform at the Frank J. Seiler Research Laboratory. The design specifications are to maintain angular position within $\pm 1.0 \times 10^{-3}$ arsceconds and angular rate with $\pm 1.667 \times 10^{-5}$ arcseconds/seconds.

A forced separation concept is utilized to allow the independent evaluation of the Kalman filter and the optimal regulator. Optimal and suboptimal Kalman filter models are developed and evaluated at physically realizable sampling rates. A general optimal estimation and control algorithm is developed and a proposed sequence of algorithm computations is presented.

ANALYSIS AND IMPLEMENTATION OF OPTIMAL ESTIMATION AND CONTROL FOR THE FJSRL SEISMIC ISOLATION PLATFORM

I. Introduction

The Seismic Isolation Platform at the United States Air Force Academy's Frank J. Seiler Research Laboratory (FJSRL) is an inertial instrument test platform designed to provide a high degree of isolation from environmental disturbances. An active control system is needed to provide the isolation required for testing and evaluating highly advanced inertial components and systems (Ref 1).

Background

As depicted in Figures 1 and 2, the inertial instrument test platform, as viewed from above, is a 25 feet by 25 feet square with nine circular test tables extending approximately 2 feet from the top surface of the platform. Viewed from below, the platform is cruciform shaped. The platform is constructed of steel reinforced concrete, is 9 feet high, and weighs approximately 450,000 pounds. The platform is located beneath a false floor in the laboratory and the test tables protrude through holes in this floor. The platform is supported by twenty pneumatic cylinders that essentially float the platform a fraction of an inch

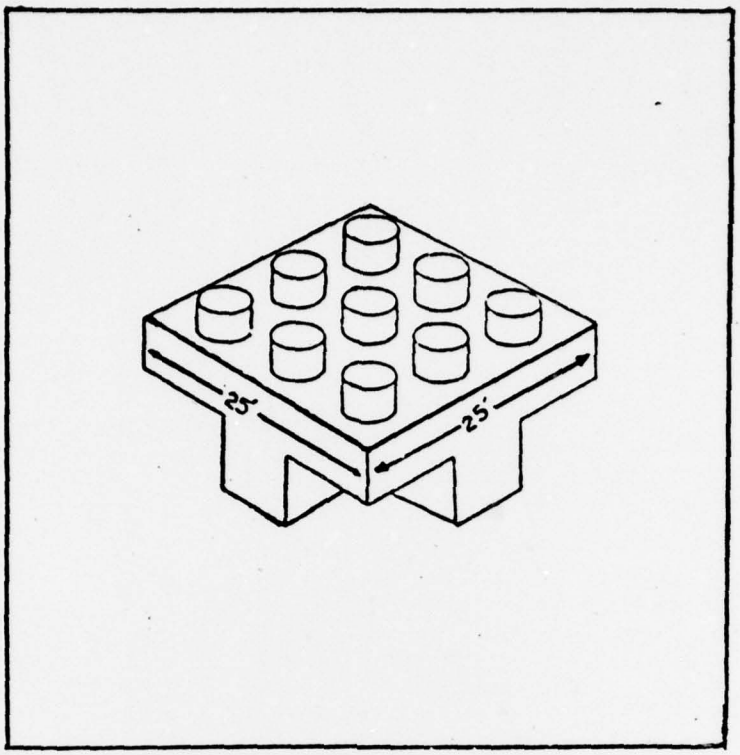

Figure 1. Concrete Block (Ref 2:14)

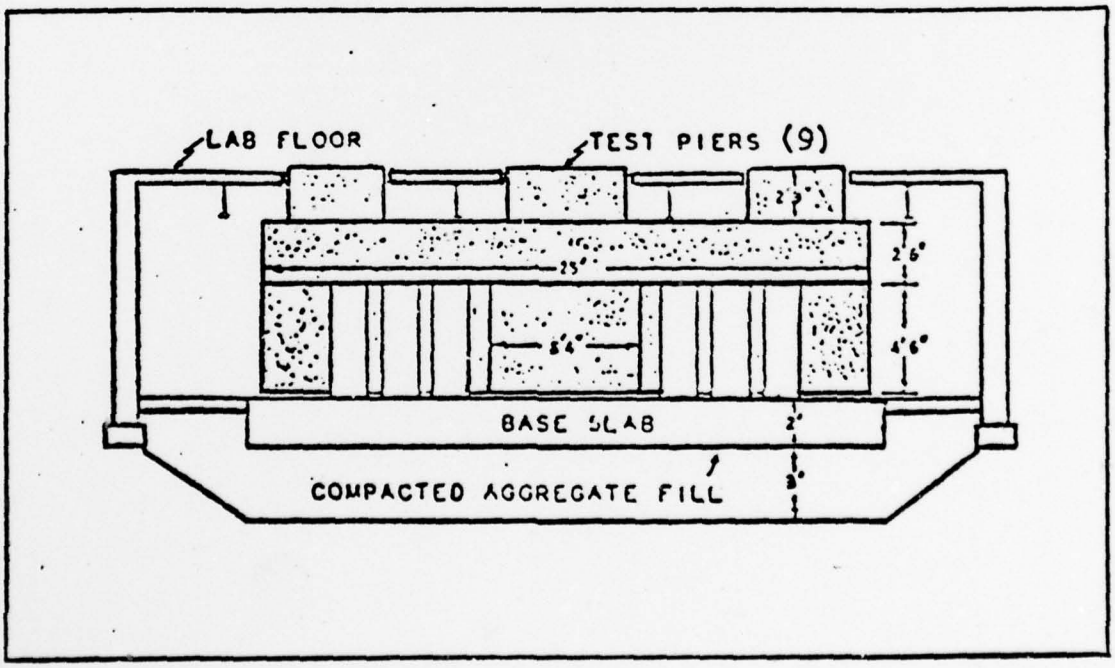

Figure 2. Cross-Section of the Seismic Isolation Platform (Ref 2:15)

above the base slab. The pneumatic cyclinders rest on red oak blocks that, in turn, rest on the base slab. The base slab rests on a compacted aggregate fill base that is designed to minimize the coupling of vibrations in order to separate the platform base from the building foundation. The pneumatic cylinders are arranged as depicted in Figure 3. The inner twelve cylinders regulate the height of the platform (referenced to the base slab) and the outer eight cylinders are used in a push-pull configuration to regulate angular motion about the horizontal axis.

The system consisting of the platform and the pneumatic cylinders has a natural frequency, as measured by FJSRL in January 1977, of 1.3Hz and acts, effectively, as a passive isolation system (low pass filter) for disturbances above 1.3Hz (Ref 3). Unfortunately, many of the disturbances of interest, e.g. earthquakes, ocean waves, and barometric pressure variations, have frequencies below 1.3Hz and, therefore, an active control system is required to isolate the platform from these disturbances.

In order to provide active control of the platform, a combination of tiltmeters, angular motion sensors, and actuators are attached to the platform as depicted in Figure 4. The eight angular motion control cylinders (Fig 3), in combination with the tiltmeters (on the surface of the platform), provide closed-loop control of angular motion about the platform's center of gravity.

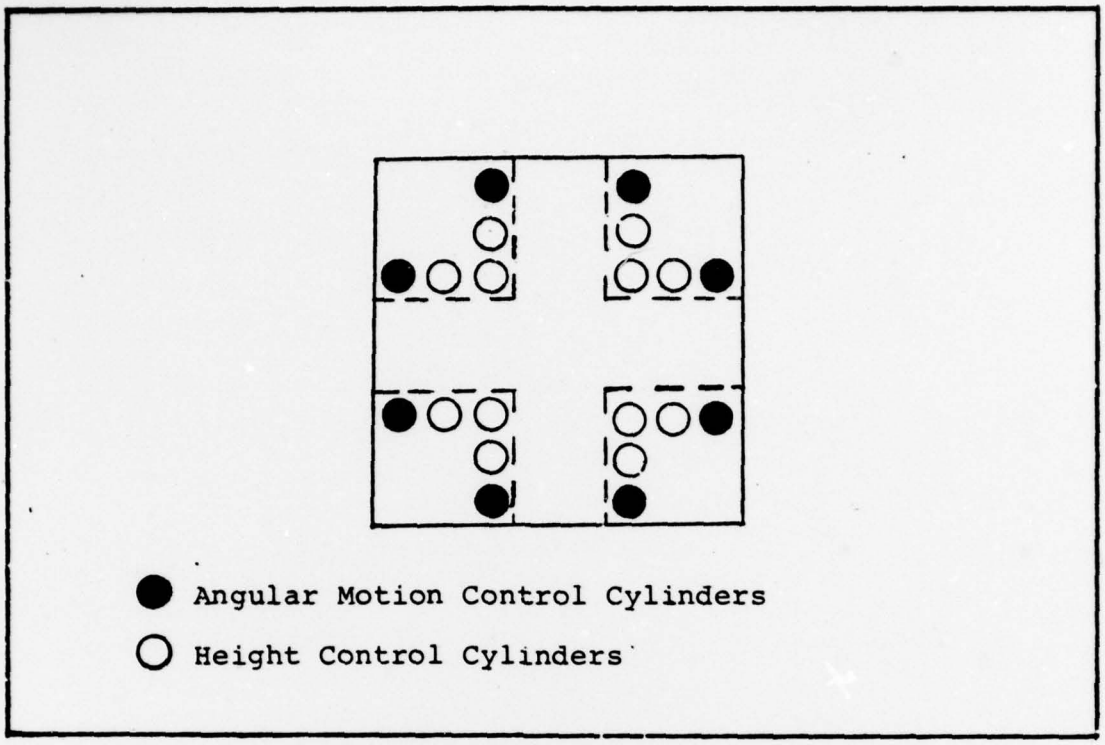

Figure 3. Location of Pneumatic Cylinders (Ref 2; 17)

Additional damping control is provided by a second control loop consisting of angular motion sensors (seismometers) and electromagnetic one-dimensional dampers (shakers). The shakers are attached at the four corners of the platform at the approximate level of the center of gravity.

A separate height control system consists of the twelve inner pneumatic cylinders, and sensors that measure the distance between the base slab and the bottom of the platform. Since the height control is not significantly affected by external disturbances (Ref 4:3), it is not mentioned further in this study.

The platform was constructed with the cruciform bottom

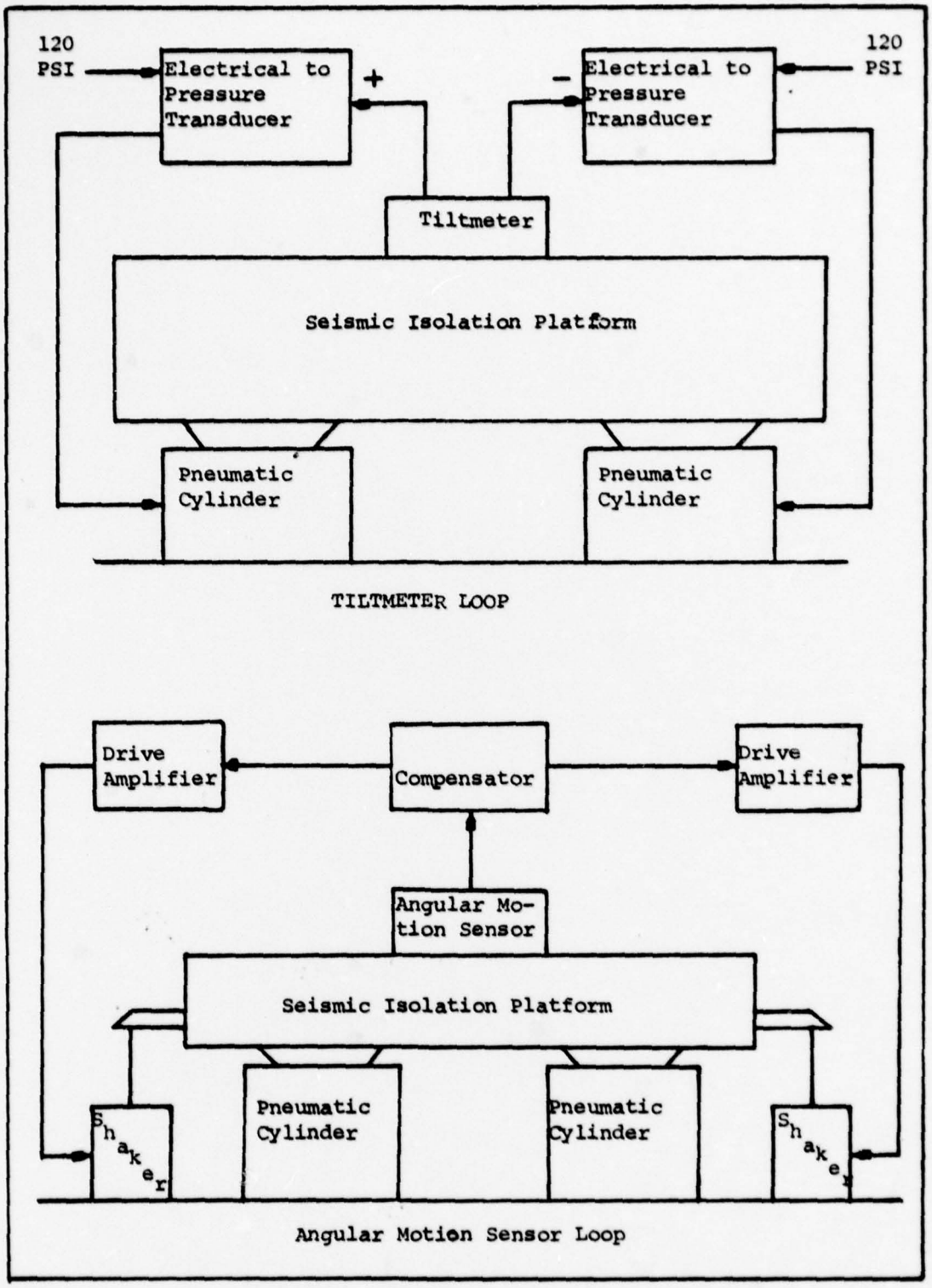

Figure 4. Platform Control Loops (Ref 4:3)

in order to locate the center of gravity at the level of the pneumatic cylinders. In this way, the coupling between the various modes of motion are minimized.

From the beginning, the problem of interest has been that of designing and implementing controllers to provide the desired degree of isolation (angular position within $\pm 1.0 \times 10^{-3}$ arcsecond and angular rate within $\pm 1.667 \times 10^{-5}$ arcseconds/second). Early investigations and attempts at stabilizing the platform were primarily analog control systems (Ref 5-8). The latest analog design, although successful in meeting the specification for angular position, was unable to meet the angular rate requirements (Ref 8).

More recently, attempts have been made to provide digital control to the platform (Ref 1), including attempts at implementing various Finite Impulse Response (FIR) and Infinite Impulse Response (IIR) filters at FJSRL (Ref 9). Digital control is desirable because it is less affected by noise and other disturbances than analog systems, permits the use of sensitive control elements with relatively low energy signals, and has phase characteristics that cannot be duplicated by an analog system (Ref 9). Digital control is more flexible than analog control because changes in sensors or actuators can often be incorporated with only software modifications. An additional benefit of digital controllers is their adaptability to the solution of stochastic optimal estimation and control. It is this

latter trait of digital control that is most useful for this investigation.

To date, the attempts at digital control of the platform have not been successful. Although some design work has demonstrated the feasibility of digital control (Ref 1: 9), the actual implementations of these designs have not been successful. The failure of the implemented controllers/filters to meet the theoretical performance levels is due primarily to the effects of slow sampling rates, finite wordlengths, the uncertainties in the system models, process noise, and the sensitivities of the sensors employed. In the previous digital attempts (Ref 1: 9), the platform was modeled as a completely deterministic system.

In 1976, two investigations were completed in which the platform was modeled as a stochastic system (Ref 2: 4). Stochastic modeling of the system permits the application of optimal estimation and stochastic control methods to the problem of isolation of the test platform. Optimal estimation is desirable because it allows consideration of the stochastic (random) characteristics of the platform system, including system modeling errors, the randomness of the environmental disturbances, the process noise, and the error sources attributed to the sensors.

Statement of the Problem

The purpose of this study is to analyze and implement an optimal estimator and controller for use at FJSRL for

the active control of the seismic isolation platform.

The specifications are dictated by the performance criteria for new generation inertial components (Ref 5). These criteria require that the angular position (tilt) of the platform be maintained within ±0.001 arcseconds and the angular rate (velocity) be maintained within ±0.001 arcseconds per minute (1.667×10^{-5} arcseconds per second). In addition, the controller must be effective in the frequency band of 0-20 Hz (Ref 8) with a step input (for testing purposes) of 2.5 foot-pounds. A step input, applied directly to the top surface of the block, is used for testing because it is easily modeled in the s-domain and also in the discrete (z) domain. The 2.5 foot-pound step input was chosen because it has been demonstrated that it approximates the disturbance caused by moderate environmental disturbances on the passive platform (Ref 2:20).

Assumptions

The system is considered to be linear over the frequency band of 0-20 Hz and it is assumed that the construction of the platform and the locations of the sensors is such that the coupling of the modes of motion is minimized to the extent that they can be considered separately. The linearity assumption has been supported by previous studies (Ref 8) and is justified by the fact that only small perturbations occur when the platform is being controlled.

Structural resonances above 20 Hz (the total number is unknown) are disregarded. It is assumed that these structural modes will not have a significant impact on the performance of the system due to natural passive damping (Ref 8). If it is determined that they do have an effect, the model can be redesigned to take them into account. Pseudo-noise can be added to the system model to represent the inaccuracies in the system model resulting from structural resonances.

The process and measurement noises can be modeled as White and Gaussian. The White assumption is valid due to the wideband characteristics of the noise and the very narrow band characteristics of the system (wideband noise driving a limited bandwidth system). The Gaussian assumption is based on the Central Limit Theorem since the process and measurement noises are composed of several independent additive noises (Ref 10). The process noise and measurement noise are considered to be independent (Ref 4:6). This assumption is based on the fact that the sensors are separated and the measurement process does not corrupt the state being measured.

A PDP-11/03 minicomputer has been designated, by FJSRL, for use in implementing the digital control system for the seismic isolation platform. The central computing system in the PDP-11/03 is the LSI-11 minicomputer board. The filter/controller algorithm developed in this study is implemented in LSI-11 compatible assembly code.

Design Approach

The approach is defined as the solution of a linear stochastic estimation and control problem. A linear stochastic system is described by the matrix equations

$$\dot{\underline{x}}(t) = F\underline{x}(t) + L\underline{u}(t) + G\underline{w}(t) \quad (1)$$

and

$$\underline{z}(t_k) = H\underline{x}(t_k) + \underline{v}(t_k) \quad (2)$$

where F, L, G, and H are time invariant matrices derived from the system transfer functions. The column vector $\underline{x}(t)$ is the state variable vector, $\underline{u}(t)$ is the control input vector, $\underline{w}(t)$ represents the environmental disturbances to the noise shaping filter, $\underline{z}(t_k)$ is the sampled measurement vector, and $\underline{v}(t_k)$ represents the sampled measurement noise.

The objective of the linear stochastic control problem is to find the discrete-time control input

$$\underline{u}(t_k) = -C(t_k)\hat{\underline{x}}(t_k) \quad (3)$$

that minimizes the quadratic performance index

$$J = E\{1/2\underline{x}^T(t_{N+1})V_f\underline{x}(t_{N+1}) + \Sigma\, 1/2[\underline{x}^T(t_k)V(t_k)\underline{x}(t_k) + \underline{u}^T(t_k)U(t_k)\underline{u}(t_k)]\} \quad (4)$$

where $\hat{\underline{x}}(t_k)$ is a discrete-time estimate of the state vector, $\underline{x}(t_k)$, $\underline{u}(t_k)$ is the discrete control input vector (put through a zero-order hold, ZOH). E is the expected value

operator, and t_{N+1} is the terminal time. The matrices V_f, V, and U are weighting matrices that assign performance costs, over the entire time interval of interest, due to the terminal states, the present states, and the control inputs, respectively. The performance of the optimal controller is a function of the values chosen for these weighting matrices. Only through the proper selection of these weighting matrices can $\underline{u}(t_k)$ meet the design specifications.

With the assumptions previously stated, employment of the Separation Principle was considered to simplify the design and analysis of the system. The Separation Principle states:

> The optimal stochastic controller for a linear system driven by white Gaussian noise, subject to a quadratic cost criterion, consists of an optimal linear Kalman filter cascaded with the optimal feedback grain matrix of the corresponding deterministic optimal control problem (Ref 11:II-16).

The Separation Principle is depicted in Figure 5.

In the investigation, a "forced separation" of the Kalman filter and the optimal controller is invoked, based on engineering judgement, to take advantage of some of the physical properties of the system elements. Because of the inherent dynamics of the system elements (the pneumatic actuator has a settling time of 20 seconds and the electromagnetic actuator has a natural frequency of 26 Hz) and, because the pneumatic actuator is actually part of the platform support system, the states associated with the pneumatic actuator are not included in the system state space models used in the analyses of the Kalman filter. In

addition, the states associated with the sensors are not included in the system model used in the development of the optimal controller because these states contain stochastic properties (measurement noises) and it was considered desirable to eliminate stochastic effects from the development and analysis of the optimal controller. The concept of a "forced separation" is necessary because, although the system being investigated meets the White Gaussian noise and quadratic cost function criteria, the Separation Principle does not apply, in the strict sense, because, in this investigation, the states represented by the Kalman filter model are not the same states as those represented by the optimal controller model. By utilizing the concept of "forced separation", the optimal estimation and control problem is separated into the design and analysis of a Kalman filter independent of the design and analysis of the corresponding optimal controller. Without the "forced separation", the development and analysis of the optimal estimation and control problem would be far more complex, if at all tractable.

The designs of a Kalman filter and a deterministic optimal controller were investigated by Richard Brunson and Martin J. Burkhart, respectively (Ref 2: 4). The approach taken in this investigation is based, in part, on their efforts. Both investigations were based on a sampling rate of 200 Hz (based on engineering judgment, using five times the Nyquist frequency*) and involved,

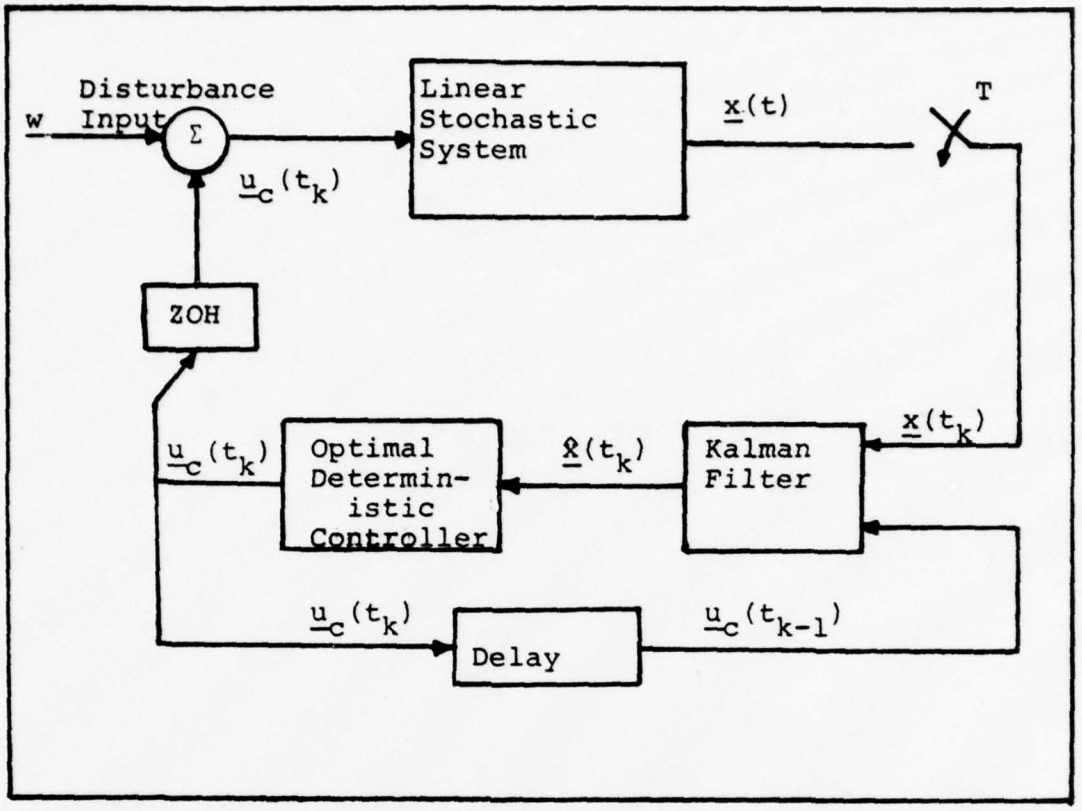

Figure 5. Separation of Linear Stochastic Control Problem

primarily, feasibility studies. The approach here extends the study to a more specific analysis of various combinations of Kalman filters and optimal controllers at various sampling rates. In addition, a specific algorithm for the filter that provides the best results is developed for implementation on the PDP-11/03 minicomputer.

Since the implementation is accomplished on a digital computer, the effects of finite wordlength are examined.

---

*The Nyquist frequency is twice the bandwidth of the system. It is the minimum sampling frequency required to avoid aliasing (folding). Also, reference Shannon's Theorem.

The investigation includes the effects of conversion quantization (A/D and D/A), coefficient quantization, and roundoff, truncation, and overflow due to arithmetic operations. In addition the numerical precision problems associated with the Kalman filter are discussed, along with the appropriate techniques for decreasing the effects of these problems.

Previously derived component transfer functions (Ref 2: 4) are used to develop a system "truth model", in state variable form, as the basis for designing an optimal Kalman filter. The optimal filter is analyzed for the effects of sampling rate and finite wordlength. In addition, a sensitivity analysis is performed (using covariance analysis techniques) to demonstrate the effects of the various noise sources separately. Using various simplifying assumptions, four suboptimal Kalman filter models (reduced order filters) are developed for comparison and possible implementation.

Using component transfer functions, an optimal controller is developed under the assumption that it is receiving "perfect" information from the Kalman filter, i.e. exact knowledge of the entire state. The design of the optimal controller is based, primarily on the linear quadratic full-state feedback controller developed by Burkhart (Ref 2). This model is derived for a sampling rate of 200 Hz.

A general estimation and control algorithm is designed and each filter model investigated (in cascade with the

appropriate optimal controller) to determine which filter provides the best results. This is accomplished by determining the computation time involved for each combination and, thus, the maximum sampling rate possible for each combination. Each Kalman filter model is then tuned at this maximum sampling rate and the results compared by utilizing a covariance analyses. A brief description of considerations for implementing the algorithm is presented as a baseline for future investigations.

Organization of Report

The report is divided into five chapters. In Chapter II, the "truth model" Kalman filter is derived and analyzed and various suboptimal filters are developed. Prominent in the analysis are the effects of sampling rate, finite wordlength, and noise sources.

In Chapter III, the optimal controller is discussed in terms of the expected results and previous conclusions.

In Chapter IV, a general optimal estimation and control algorithm is developed. Each Kalman filter is, in turn, combined with the appropriate optimal controller and analyzed. Prominent in the analysis are the filter tuning process and the effects of sampling rate. The results of this analysis are compared and a "best cut" combination selected. The effects of quantization, conversion, computational delay, and specific characteristics of the minicomputer (LSI-11) are discussed.

Finally, in Chapter V, general and specific conclusions and recommendations are discussed.

II. Kalman Filter Development

The development of the optimal Kalman filter is based on the state variable (truth) model of the seismic platform system composed of the platform dynamics, the sensors, and the process and measurement noise sources. In this chapter, the system truth model is developed and the optimal Kalman filter is designed and analyzed. The Kalman filter based on the system "truth" model, i.e. the optimal Kalman filter, is used as a "benchmark" to determine the best performance that can be expected from the optimal estimation of the state of the seismic isolation platform system. The effects of finite wordlength, sampling rate and noise levels are investigated. In addition, by making various simplifying assumptions, four sub-optimal Kalman filters are developed based on reduced-order system models. In Chapter IV, these suboptimal filters, and the appropriate optimal filter, are combined, in turn, with the optimal controller developed in Chapter III. Each filter/controller combination is analyzed and compared for implementation in the form of a Linear Quadratic Gaussian (LQG) controller.

Justification for Kalman Filter

As mentioned previously, attempts at controlling the platform using deterministic digital control methods failed to provide the specified control of the seismic isolation platform. Deterministic approaches do not include con-

siderations of the effects of uncertainties in the system model, random effects of process and measurement noises, or the sensitivities of the sensors employed.

Although the best model available for the seismic isolation platform is used for this study, there remain uncertainties that must be considered. There is some question as to the homogeneity of the platform structure and this leads to uncertainties about the exact center of gravity. The assumption of the decoupling of the modes of motion might not be valid. Uncertainties about the bending modes and resonant frequencies add to the overall inaccuracy of the system "truth model". In addition, there is process noise, measurement noise, and possible biases in the measurement sensors that must be considered. A difficulty in determining the current state of the platform angular rate arises because there is no direct measurement of this state; rather, it is determined, indirectly, from the measurements of the platform tilt and rate. Also, the sensors are most accurate in different frequency bands. The tiltmeter is effective in the 0-1 Hz range, and the angular rate sensor is more accurate in the higher, 1-20 Hz range. All of these factors contribute to inaccuracies in the determination of current system states. A stochastic estimator is required to filter the effects of the "noise" due to the above factor. Under the assumption of linearity and white Gaussian noise sources, it can be shown that a Kalman filter is the "optimal" estimator of the current

state of the system (Ref 11:I-44).

A Kalman filter is a recursive data processing algorithm that uses information about the system dynamics, initial states, and statistics of the process and measurement noise to generate an "optimal" estimate of the current states of the system. A Kalman filter attempts to minimize the uncertainties and random noise from a system through the application of all current measurements combined with the assumed statistics of the system. Since it is recursive, it is not required that all past information be remembered (stored in the computer); the estimation and covariance from the previous update are sufficient statistics.

The optimal estimation problem is separated from the optimal control problem, in this investigation, by invoking the forced separation concept described in Chapter I. This permits the independent design and analysis of the optimal estimator (Kalman filter) without consideration of the optimal control gain (addressed in Chapter III). The outputs of the Kalman filter (state estimates) become the current state inputs to the optimal controller when the controller and estimator are recombined (Chapter IV).

Brunson investigated the feasibility of employing a Kalman filter to improve the estimates of the system states of the seismic platform (Ref 4). Because the design was based on early, less accurate, system models and, because the implementation was analyzed for a HP-21MX minicomputer, the results are used in this investigation, primarily, as

background reference and as a basis for possible design techniques.

Development of System Truth Model

The seismic isolation platform system used for the design of the Kalman filter consists of the platform, sensors (tiltmeters and seismometers), and noise sources. The platform system can be modeled as a linear stochastic system and can be represented, in state variable form, by the equation

$$\dot{\underline{x}}(t) = F(t)\underline{x}(t) + G(t)\underline{w}(t) + L(t)\underline{u}(t) \qquad (5)$$

where

$F(t)$ system matrix

$G(t)$ matrix of states corrupted by process noise

$L(t)$ control matrix

$\underline{x}(t)$ state vector

$\underline{w}(t)$ process noise vector

$\underline{u}(t)$ control input vector

The measurement equation for the system is given by

$$\underline{z}(t_k) = H(t_k)\underline{x}(t_k) + \underline{v}(t_k) \qquad (6)$$

where

$\underline{z}(t_k)$ measurement vector

$H(t_k)$ measurement matrix

$\underline{x}(t_k)$ state vector

$\underline{v}(t_k)$ measurement noise vector

The matrices F(t), G(t), L(t), and H(t) are assumed to be time-invariant and are, therefore, expressed as F, G, L, and H through the remainder of this thesis. The truth model is depicted, in block diagram form, in Figure 6.

The process noise, $\underline{w}(t)$, and the measurement noise, $\underline{v}(t_k)$, are considered to be independent and, therefore, uncorrelated.

The process noise is described as zero-mean, White Gaussian noise. The process noise covariance matrix, Q(t), is given by

$$E[\underline{w}(t)\underline{w}(t+\tau)] = Q\delta\tau \tag{7}$$

The measurement noise is described as zero-mean, White Gaussian noise and the measurement noise from the tiltmeter is assumed to be independent of the measurement noise from the seismometer. The sampled measurement noise covariance matrix, $R(t_k)$, is given by

$$E[\underline{v}(t_i)\underline{v}(t_k)^T] = \begin{cases} R(t_i) & i=k \\ 0 & i\neq k \end{cases} \tag{8}$$

In the following sections, the F, G, L, and H matrices are derived from the system transfer functions (s-domain).

System Dynamics Model (Platform). The platform transfer function, for a torque input and horizontal angular output, is

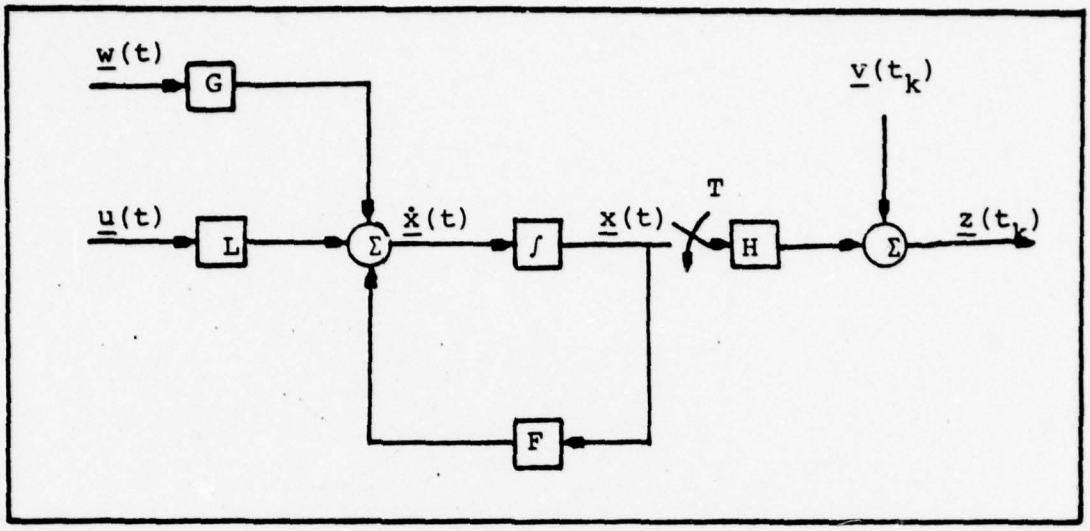

Figure 6. System Truth Model

$$G_b(s) = \frac{\theta}{T} = \frac{K_b \omega_b^2}{s^2 + 2\zeta_b \omega_b s + s_b^2} \quad \frac{\text{Arcseconds}}{\text{Foot-pounds}} \qquad (9)$$

where

$\zeta_b = 0.05$

$\omega_b = 7$ rad/sec

$K_b = 0.044$ arcsecond/ft-lb (Ref 2:16)

Solving the equation, for the given variables, yields

$$\frac{\theta}{T} = \frac{2.156}{s^2 + 0.07s + 49} \quad \frac{\text{Arcseconds}}{\text{Foot-pounds}} \qquad (10)$$

where θ is the angle of the platform referenced to local level and T is the external torque applied to the platform. T is composed of torques from the process noise, represented by T_w, pneumatic actuator, u_p, and electromagnetic actuator (shaker), u_s. Therefore,

$$T = T_w + u_p + u_s \quad \text{(Foot-pounds)} \qquad (11)$$

The transfer function is converted to state variable form using phase variable techniques because the states of interest, i.e. angular position (θ) and angular rate ($\dot{\theta}$) are represented directly in the resulting form. Letting

$$x_1 = \theta \qquad \text{(Arcseconds)} \tag{12}$$

$$x_2 = \dot{\theta} \qquad \text{(Arcseconds/Second)} \tag{13}$$

and cross-multiplying the transfer function, the state equation become

$$\dot{x}_1 = x_2 \tag{14}$$

$$\dot{x}_2 = -49x_1 - 0.7x_2 + 2.156T_w + 2.156u_p + 2.156u_s \tag{15}$$

Tiltmeter. The tiltmeter transfer function, from Reference 4:12, is

$$\frac{V_1}{\theta} = \frac{19.84(1 - 0.1531s^2)}{s^3 + 12.56s^2 + 77.6s + 198.4} \quad \frac{\text{Volts}}{\text{Arcsecond}} \tag{16}$$

where V_1 is the tiltmeter output. Based on results from Brunson (Ref 4:48), the tiltmeter model, and subsequent component models are derived in physical variable form. Therefore, letting

$$x_3 = V_1 \tag{17}$$

the state equations become

$$\dot{x}_3 = -3.037504x_1 - 12.56x_3 + x_4 \tag{18}$$

$$\dot{x}_4 = -77.6x_3 + x_5 \tag{19}$$

$$\dot{x}_5 = 19.84x_1 - 198.4x_3 \tag{20}$$

and the measurement equation is

$$z_1 = x_3 \tag{21}$$

Angular Motion Sensor. The angular motion sensor (seismometer) transfer function is (Ref 4:12)

$$\frac{V_2}{\theta} = \frac{s^2}{s^2 + 2s + 1} \quad \frac{\text{Volts}}{\text{Arcsecond}} \tag{22}$$

where V_2 is the seismometer output. The physical variable state equations are

$$\dot{x}_6 = 2x_1 - 2x_6 + x_7 \tag{23}$$

$$\dot{x}_7 = x_1 - x_6 \tag{24}$$

The measurement equation is

$$z_2 = x_1 - x_6 = V_2 \tag{25}$$

Process Noise Filter. The process noise represents disturbance torques from external sources, such as earth seismic activity, that are input to the platform. The process noise is modeled as a time correlated Gaussian noise plus a white noise (Ref 10). A noise shaping filter is required in order to provide noise with the desired power spectral density properties through the range of 0-20 Hz. Brunson developed a third-order approximation

for the noise shaping filter, called the process noise filter in this study (Ref 4:14). The transfer function is

$$\frac{C}{R} = \frac{1}{(s + 125)^3} \tag{26}$$

which yields the state equations

$$\dot{x}_8 = -125x_8 + x_9 \tag{27}$$

$$\dot{x}_9 = -125x_9 + x_{10} \tag{28}$$

$$\dot{x}_{10} = -125x_{10} + w_1 \tag{29}$$

where x_8 is the output from the process noise filter that is input to the platform in the form of disturbance torque, called T_w (see platform model description), and w_1 represents the white noise input to the filter.

Pneumatic Actuator Dynamics. The pneumatic actuator dynamics are associated with the control of the platform and are omitted during analysis of the Kalman filters (forced separation).

Shaker Dynamics. In the frequency range of interest (0-20 Hz), the shaker has essentially no dynamics. Figure 7 represents the frequency response of the shaker actuator. For purposes of analysis, the shaker transfer function is replaced by a constant gain.

Combined State Equations. The full set of state equations representing the truth model is

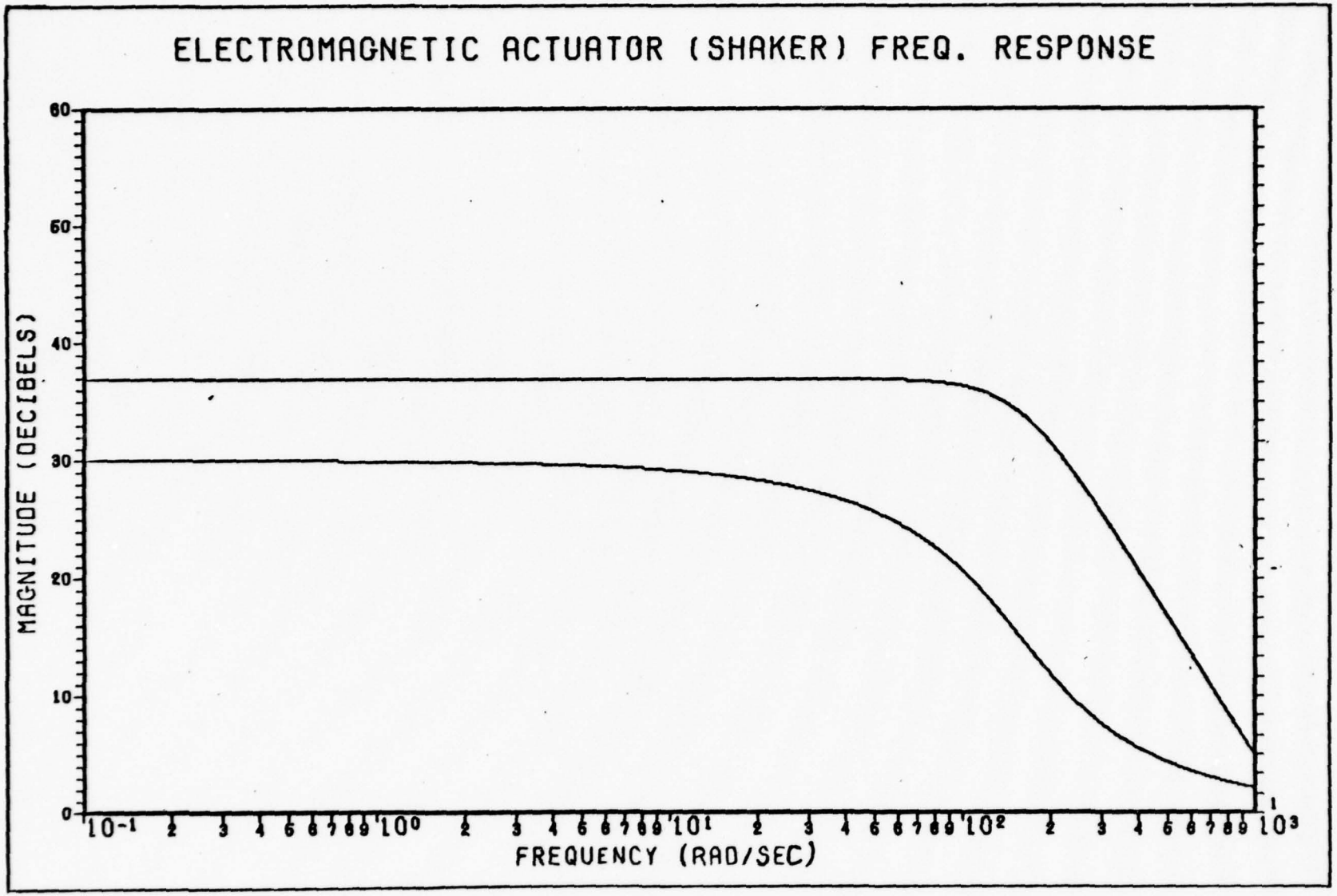

Figure 7. Frequency Response of Electromagnetic Actuator (Shaker)

$$
\begin{aligned}
\dot{x}_1 &= x_2 \\
\dot{x}_2 &= -49x_1 - 0.7x_2 + 2.156x_8 + 2.156u_p + 2.156u_s \\
\dot{x}_3 &= -3.037504x_1 - 12.56x_3 + x_4 \\
\dot{x}_4 &= -77.6x_3 + x_5 \\
\dot{x}_5 &= 19.84x_1 - 198.4x_3 \\
\dot{x}_6 &= 2x_1 - 2x_6 + x_7 \\
\dot{x}_7 &= x_1 - x_6 \\
\dot{x}_8 &= -125x_8 + x_9 \\
\dot{x}_9 &= -125x_9 + x_{10} \\
\dot{x}_{10} &= -125x_{10} + w_1
\end{aligned} \tag{30}
$$

The F matrix is

$$
F = \begin{bmatrix}
0 & 1 & 0 & 0 & 0 & 0 & 0 & 0 & 0 & 0 \\
-49 & -0.7 & 0 & 0 & 0 & 0 & 0 & 2.156 & 0 & 0 \\
-3.037504 & 0 & -12.56 & 1 & 0 & 0 & 0 & 0 & 0 & 0 \\
0 & 0 & -77.6 & 0 & 1 & 0 & 0 & 0 & 0 & 0 \\
19.84 & 0 & -198.4 & 0 & 0 & 0 & 0 & 0 & 0 & 0 \\
2 & 0 & 0 & 0 & 0 & -2 & 1 & 0 & 0 & 0 \\
1 & 0 & 0 & 0 & 0 & -1 & 0 & 0 & 0 & 0 \\
0 & 0 & 0 & 0 & 0 & 0 & 0 & -125 & 1 & 0 \\
0 & 0 & 0 & 0 & 0 & 0 & 0 & 0 & -125 & 1 \\
0 & 0 & 0 & 0 & 0 & 0 & 0 & 0 & 0 & -125
\end{bmatrix} \tag{31}
$$

and the G and L matrices are

$$G = \begin{bmatrix} 0 \\ 0 \\ 0 \\ 0 \\ 0 \\ 0 \\ 0 \\ 0 \\ 0 \\ 1 \end{bmatrix} \qquad L = \begin{bmatrix} 0 & 0 \\ 2.156 & 2.156 \\ 0 & 0 \\ 0 & 0 \\ 0 & 0 \\ 0 & 0 \\ 0 & 0 \\ 0 & 0 \\ 0 & 0 \\ 0 & 0 \end{bmatrix} \tag{32}$$

The control input is

$$\underline{u} = \begin{bmatrix} u_p \\ u_s \end{bmatrix} \tag{33}$$

The control input u_p, associated with the pneumatic actuators, is generated by a deterministic position feedback controller that is used to directly counter any torque imbalance resulting from unsymmetrical positioning of items on the platform. The control input u_s, associated with the electromagnetic shaker activators, is generated by an optimal state feedback controller. The optimal controller is used to regulate the position feedback controller and also to control the angular rate of the platform. The Kalman filter receives input from the sensors and the optimal controller (Fig 8) and the control input u_p is

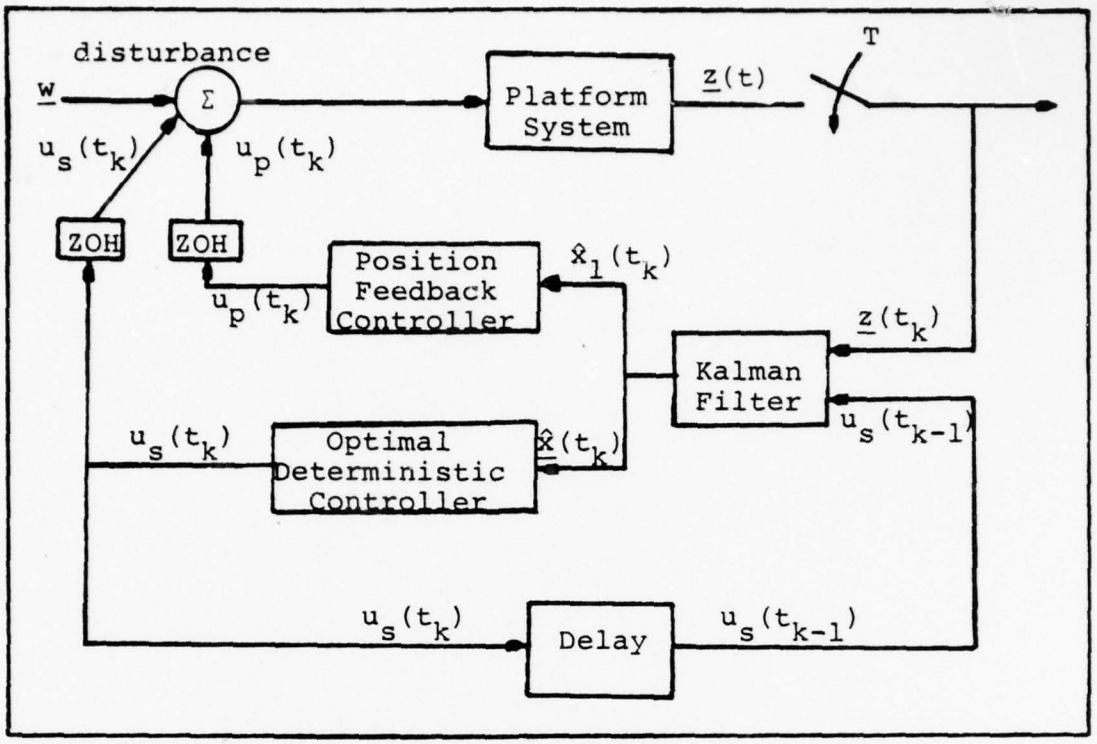

Figure 8. Filter/Controller Configuration

not considered in the design and analysis of the Kalman filter. This is addressed further in Chapter III in the discussion of the design of the controllers. Because of the "forced separation", u_s is the only control input of interest in the Kalman filter analysis, the $L\underline{u}(t)$ term becomes:

$$L\underline{u}(t) = \begin{bmatrix} 0 & 0 \\ 0 & 2.156 \\ 0 & 0 \\ 0 & 0 \\ 0 & 0 \\ 0 & 0 \\ 0 & 0 \\ 0 & 0 \\ 0 & 0 \\ 0 & 0 \end{bmatrix} \begin{bmatrix} u_p \\ u_s \end{bmatrix} = \begin{bmatrix} 0 \\ 2.156 \\ 0 \\ 0 \\ 0 \\ 0 \\ 0 \\ 0 \\ 0 \\ 0 \end{bmatrix} \begin{bmatrix} u_s \end{bmatrix} \qquad (34)$$

Finally, the system measurement matrix is

$$H = \begin{bmatrix} 0 & 0 & 1 & 0 & 0 & 0 & 0 & 0 & 0 & 0 \\ 1 & 0 & 0 & 0 & 0 & -1 & 0 & 0 & 0 & 0 \end{bmatrix} \quad (35)$$

Kalman Filter Model

A Kalman filter is a predictor-corrector type of estimator that uses a conditional probability density, conditioned on the actual measurements, to describe the probabilities of possible system states. The conditional probability density is a function of the system dynamics, initial states, and the assumed statistics of the disturbance noises. Since the conditional probability density function itself is Gaussian, it is completely described by the first and second order statistics, i.e. conditional mean and covariance. The general Kalman filter equations that represent these statistics are divided into two functions; those that propogate (predict) the conditional mean (optimal estimate) and the covariance, and those that update (correct) the optimal estimate and covariance at measurement sample times.

The propagation equations (in discrete form) are

$$\hat{\underline{x}}(t_k^-) = \Phi(t_k, t_{k-1})\hat{\underline{x}}(t_{k-1}^+) + \Gamma(t_k, t_{k-1})\underline{u}(t_{k-1}) \quad (36)$$

and

$$P(t_k^-) = \Phi(t_k, t_{k-1})P(t_{k-1}^+)\Phi^T(t_k, \tau) + \int_{t_{k-1}}^{t_k} \Phi(t_k, \tau)G(\tau)Q(\tau)G^T(\tau)\Phi^T(t_k, \tau)d\tau \quad (37)$$

where $\underline{\hat{x}}(t_k^-)$ is the predicted estimate vector, Φ is the state transition matrix (derived from the system F matrix), and $P(t_k^-)$ is the state covariance (prediction error) matrix. The superscripts - and + denote before and after a new measurement (update) is taken. The argument t_{k-1} represents the sample time of the preceding sample. The superscript T is the matrix transpose operator. Since the control input is constant between samples, the control transition matrix, Γ, is given by

$$\Gamma(t_k, t_{k-1}) = \int_{t_{k-1}}^{t_k} \Phi(t_k, \tau) L(\tau) d\tau \tag{38}$$

where L is the control distribution matrix. The disturbance distribution matrix, G, describes which states are corrupted by process noise and the matrix Q(t) is the process noise covariance matrix given by Eq (7) where $\underline{w}(t)$ is the process noise vector.

The Kalman filter update equations (in discrete form) are

$$\underline{\hat{x}}(t_k^+) = \underline{\hat{x}}(t_k^-) + K(t_k)[\underline{z}(t_k) - H\underline{\hat{x}}(t_k^-)] \tag{39}$$

$$P(t_k^+) = P(t_k^-) - K(t_k)H(t_k^-)P(t_k^-) \tag{40}$$

and

$$K(t_k) = P(t_k^-)H^T(t_k)[H(t_k)P(t_k^-)H^T(t_k) + R(t_k^-)]^{-1} \tag{41}$$

where $\underline{\hat{x}}(t_k^+)$ is the updated estimate (corrected by measurement), $P(t_k^+)$ is the updated covariance (filter error) matrix,

and $K(t_k)$ is the Kalman gain (optimal weighting) matrix. Variable $\underline{z}(t_k)$ is the sampled measurement vector, H is the measurement matrix and the superscript -1 above the bracketed term in Eq (39) is the matrix inversion operator. The matrix $R(t_k)$ is the measurement noise covariance matrix given by Eq (8) where $\underline{v}(t_k)$ is the measurement noise vector.

Figure 9 is a block diagram of a Kalman filter. The Kalman filter model contains the state transition matrix (derived from the system F matrix), the H matrix, and the G matrix, all of which have been previously derived. In addition, the noise covariance matrices are required and are derived below.

Process Noise Covariance Model. The covariance model of the white noise source driving the noise filter was determined using the variance of the output of the tiltmeter (angular position) with the platform in the uncontrolled mode. "The uncontrolled mode is defined by the platform floating on the pneumatic cylinders with no control feedback from the sensors" (Ref 4:17). The uncontrolled mode is represented by the system dynamics model (platform), the tiltmeter, and the process noise filter. The model state matrices, F_1 and G_1, are then

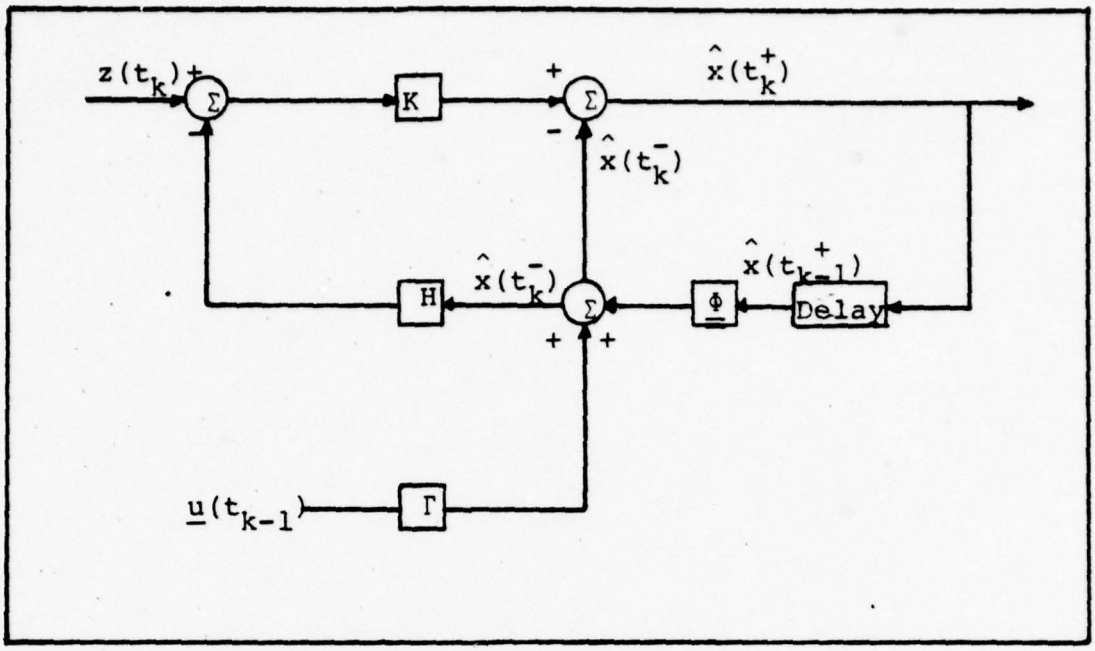

Figure 9. Kalman Filter (Ref 11:18).

$$F=\begin{bmatrix} 0 & 1 & 0 & 0 & 0 & 0 & 0 & 0 \\ -49 & -0.7 & 0 & 0 & 0 & 2.156 & 0 & 0 \\ -3.037504 & 0 & -12.56 & 1 & 0 & 0 & 0 & 0 \\ 0 & 0 & -77.6 & 0 & 1 & 0 & 0 & 0 \\ 19.84 & 0 & -198.4 & 0 & 0 & 0 & 0 & 0 \\ 0 & 0 & 0 & 0 & 0 & -125 & 1 & 0 \\ 0 & 0 & 0 & 0 & 0 & 0 & -125 & 1 \\ 0 & 0 & 0 & 0 & 0 & 0 & 0 & -125 \end{bmatrix} \quad (42)$$

and the disturbance matrix is

$$G_1 = \begin{bmatrix} 0 \\ 0 \\ 0 \\ 0 \\ 0 \\ 0 \\ 0 \\ 1 \end{bmatrix} \quad (43)$$

The RMS quiescent peak-to-peak amplitude of the controlled platform has been determind to be ±0.4 arcseconds. The RMS excursion, which can be considered to represent the standard deviation or one-sigma value, is, therefore, 0.2 arcseconds. Since the tiltmeter has a gain of 100 millivolts per arcsecond, the excursion corresponds to 0.02 volts output from the tiltmeter. The variance is found, by squaring the one-sigma value, to be 0.0004 volts.

The equivalent process noise covariance model was determined by solving for Q in the steady-state linear covariance propagation equation

$$\dot{P}(t) = 0 = F_1 P(t) + P(t) F_1^T + G_1 Q G_1^T \qquad (43)$$

where $\dot{P}(t)$ is the time derivative of the system covariance. The diagonal elements of P(t) are the variances of the states. The noise covariance matrix is a one-by-one matrix (scalar) in this model and the p_{33} element of the covariance matrix is the variance of the output of the tiltmeter (state x_3), in volts.

The process noise covariance was found by utilizing a computer program to integrate Eq (43) and by varying the value of Q until the tiltmeter variance approached the value determined for quiescent excursions. A value of 1.849×10^{N} for Q resulted in a tiltmeter variance of 0.000403. This value of Q was used in the optimal Kalman model.

Measurement Noise Covariance Model. There have been no accurate models developed for the noise characteristics

of the sensors employed in the platform control system. An estimate, however, was made by using one-half of the threshold values of the sensors as "rough" models of the one-sigma noise amplitude. The noise variances are the one-sigma values, squared. Therefore, for the tiltmeter, the threshold is 1.0×10^{-4} volts and the variance is 2.5×10^{-9} volts. The threshold of the seismometer is 1.66×10^{-3} volts and the variance is 6.889×10^{-7} (Ref 12).

Since there are two independent measurement noise sources, the measurement noise matrix, R, is the two-by-two matrix (described by Equation 8).

$$R = \begin{bmatrix} 2.5 \times 10^{-9} & 0 \\ 0 & 6.889 \times 10^{-7} \end{bmatrix} \qquad (44)$$

Analysis of Optimal Kalman Filter Performance

Kalman filter performance can be analyzed, without actually implementing the filter, by analyzing a time history of the covariance of the estimates, P^- and P^+. This is possible because the covariance update and propagation equations, as well as the associated Kalman gain equation, are not dependent on the measurement realizations or the estimates.

A program called the "General Covariance Analysis Program"(GCAP)(Ref 13) was used for the filter performance analysis (and tuning) described in this report. Essentially, this program generates a "true" covariance time history

for a filter at a given sampling rate. More specifically, the product used most for this study is the one-sigma values (square-roots of diagonal elements) for the system state estimate errors. GCAP is described in more detail in Appendix A.

The truth model represents the best available model of the real world system. The covariance analysis of the Kalman filter based on the truth model, at a given sampling rate, represents a theoretical performance bound at that sampling rate. This performance bound or "benchmark" is used to evaluate the effects of varying the analysis parameters, i.e. sampling frequency, noise levels, sensor sensitivities, and simplifying model reductions.

The time histories of the x1 state (angular position, θ) and the x2 state (angular rate, $\dot{\theta}$) estimate errors (one-sigma values), for a sampling rate of 200 Hz, are presented in Figures 10 and 11, respectively.

The shape of the plots indicate that, after an initial transient period, the one-sigma values for P^+ and P^- settle to steady state conditions. This is indeeed the case since it can be shown that stable time-invarient systems driven by stationary noises settle to constant one-sigma values, independent of the initial state uncertainties (Ref 11:II-63). For the seismic isolation platform, the noises are white Gaussian noise with noise strengths that do not vary with time (thus stationary statistics) and the system matrices are time-invariant. This result is important since it

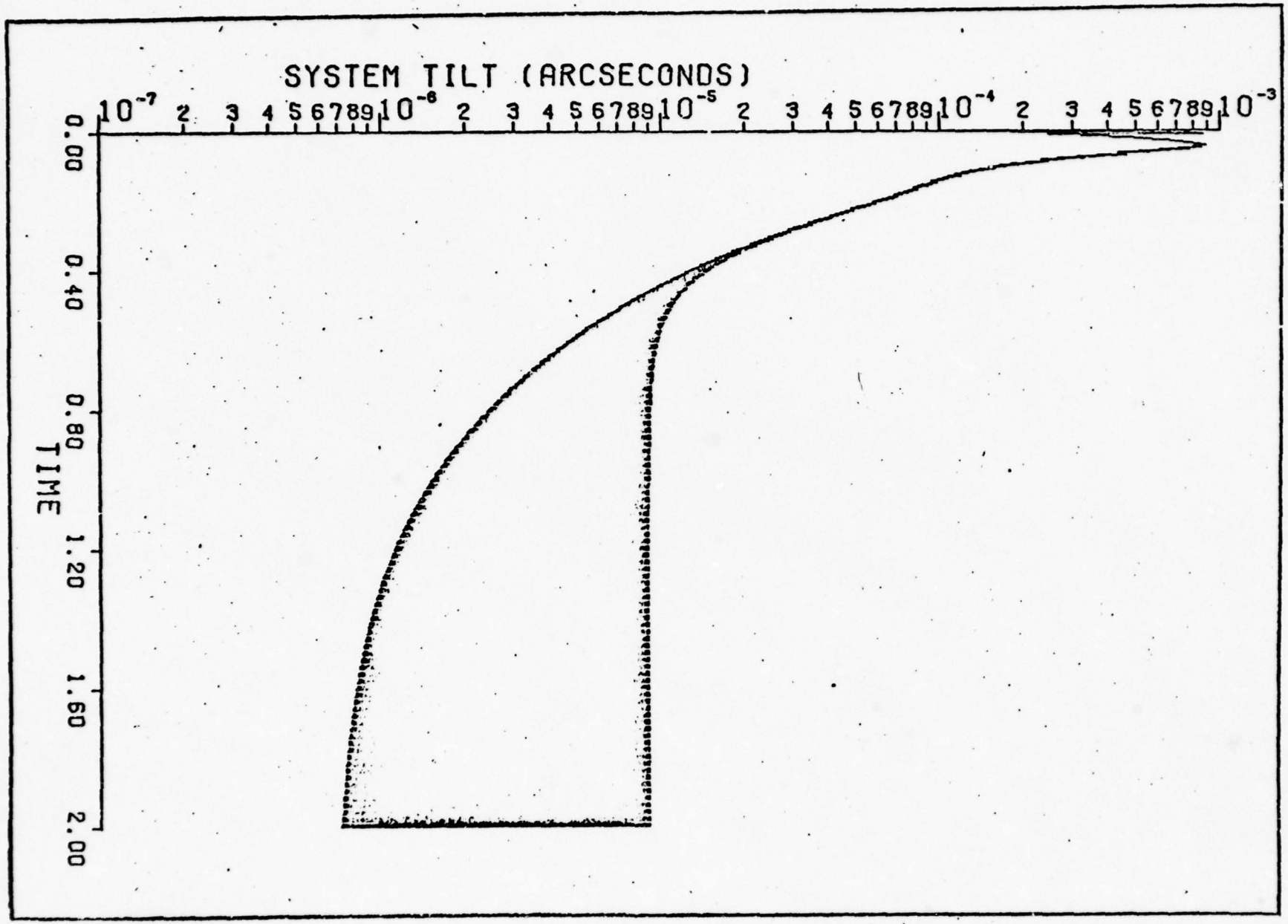

Figure 10. Platform Tilt (One-Sigma Estimate Error)
200 Hz Sample Rate

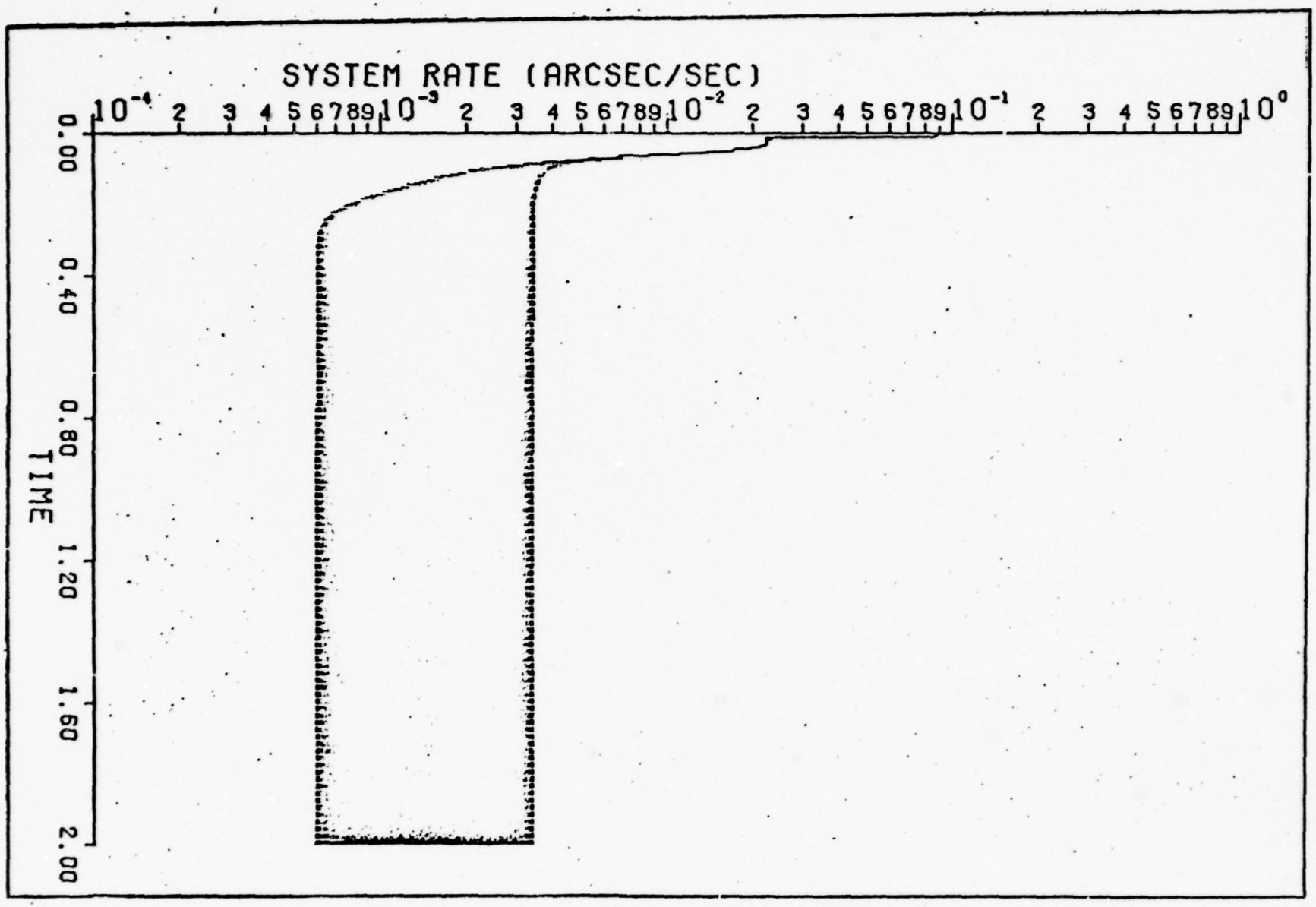

Figure 11. Platform Rate (One-Sigma Estimate Error), 200 Hz Sampling Rate

permits the implementation of an approximate Kalman filter with a constant Kalman gain

$$K = P_{\infty} H^T R^{-1} \tag{45}$$

where P_{∞} is the steady-state covariance. The Kalman filter implementation is then greatly simplified (see Chapter IV). The steady state one-sigma values are the values used for performance analysis in this study.

Since the optimal estimates generated by the Kalman filter are used as inputs of the controllers, the design criteria for acceptable performance are that the one-sigma errors in these estimates be at least as good as the required controller performance specifications, i.e. 1.0×10^{-3} arcseconds for one-sigma position error and 1.667×10^{-3} arcseconds/second for one-sigma rate errors. In addition, since the largest error occurs for values of P^- (just before measurement update), this error (prediction error) is used as the measurement of interest.

The one-sigma prediction errors for the optimal Kalman filter, with a 200 Hz sampling rate, are

$$\begin{aligned} \theta &= 9.05 \times 10^{-6} \text{ arcseconds} \\ \dot{\theta} &= 3.37 \times 10^{-3} \text{ arcseconds/second} \end{aligned} \tag{46}$$

The position (tilt) prediction error (θ) is well within specifications but the rate prediction error is more than two orders of magnitude larger than required. Since this Kalman filter is based on the "best" estimate of the

physical system, the results indicate that a Kalman filter will not provide the required accuracy with a 200 Hz sampling rate.

One postulated improvement is to sample at a higher rate since, as the sampling interval becomes shorter, the prediction error decreases. To test this postulate, time histories were generated at various sampling rates from the Nyquist frequency (40 Hz) to 200kHz. The one-sigma prediction errors obtained from this analysis are presented in Table I. The plots of the one-sigma rate prediction errors are presented in Figures 28 through 36 in Appendix B. A plot of rate prediction error versus sampling rate is presented in Figure 12.

With a three-order-of-magnitude increase in the sampling rate (from 200 Hz to 200 kHz), only slightly more than a one-order-of-magnitude decrease in the sampling rate occurs. Obviously, a 200 kHz sampling is impossible to implement and, in fact, a sampling rate that high would tend to invalidate the white noise assumptions. However, by analyzing the filter at extreme sampling rates, some insight is gained about performance bounds of the filter. Therefore, it is concluded that it is not possible to meet the rate prediction error criteria with the platform, actuators, and sensors as presently configured, at any, physically realizable sampling rate.

Since it might be possible to improve the prediction

Table I

Comparison of One-Sigma Prediction Errors at Different Sampling Rates

Sampling Rate	Angular Position Error (arcseconds)	Angular Rate Error (arcseconds/second)
40 Hz	5.7×10^{-4}	4.5×10^{-2}
50 Hz	3.1×10^{-4}	3.3×10^{-2}
100 Hz	4.4×10^{-5}	9.9×10^{-3}
200 Hz	9.05×10^{-6}	3.37×10^{-3}
2 kHz	6.7×10^{-7}	5.5×10^{-4}
20 kHz	2.5×10^{-7}	2.4×10^{-4}
200 kHz	1.4×10^{-7}	9.0×10^{-5}

error by decreasing the error (noise) sources, an analysis of the effects of decreasing the process noise or increasing the sensitivities of the sensors was performed. The results of that analysis (in the form of one-sigma prediction errors) are presented in Table II. The plots of the one-sigma rate prediction error time history are presented in Figures 28 through 36 in Appendix B.

As expected, the prediction error is most sensitive to changes in the noise asscciated with the angular acceleration measurement (the seismometer sensitivity), but a one-order-of-magnitude increase in sensitivity (reduction in measurement noise) does not significantly reduce

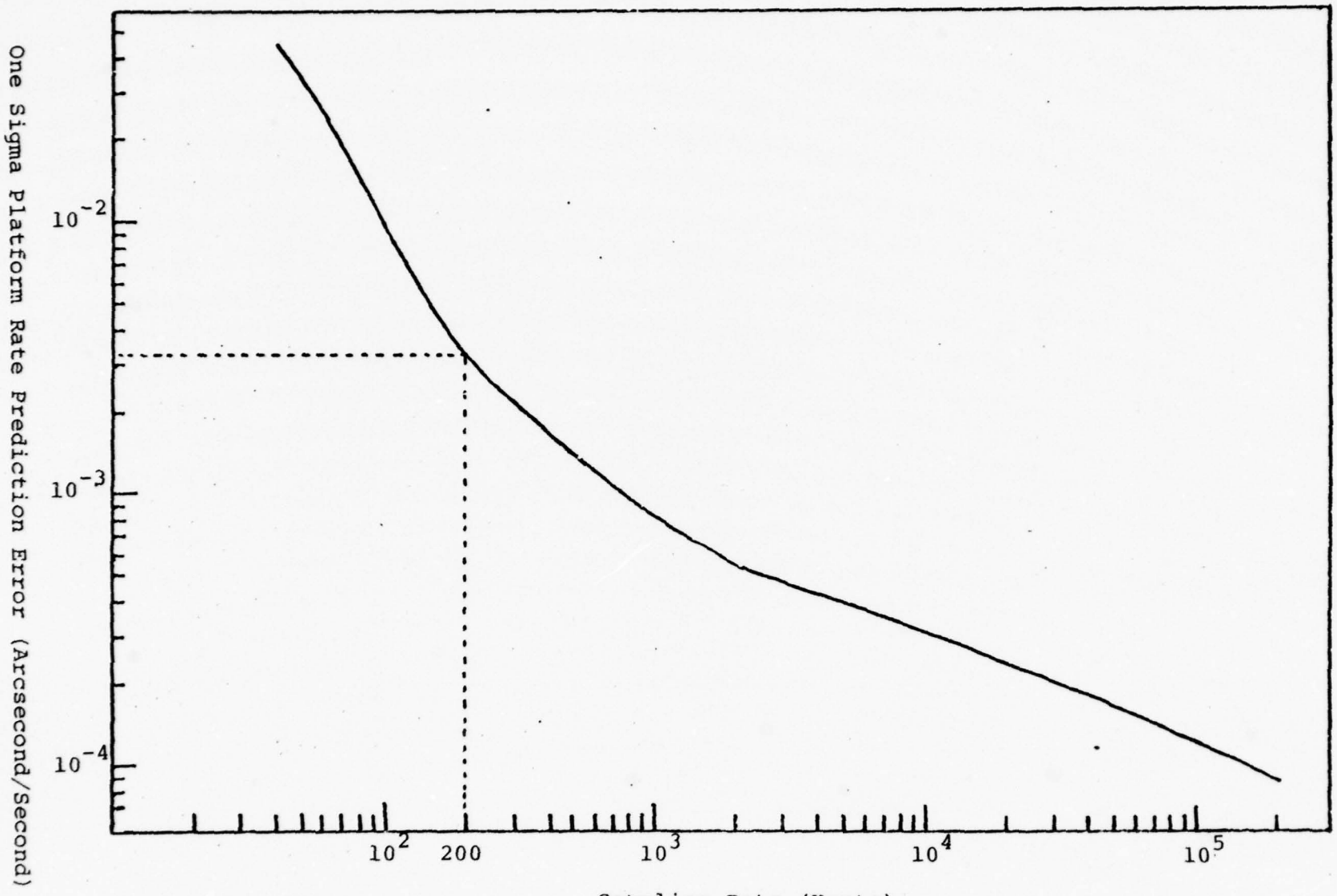

Figure 12. Platform Rate Prediction Error Versus Sampling Rate

Table II

Effects of Decreasing the Error Sources (noise) at 200 Hz

Case	Type of Improvement	One-Sigma Tilt Error (arc-seconds)	One-Sigma Rate Error (arcseconds/seconds)
1	No Change	9.05×10^{-6}	3.37×10^{-3}
2	One-order-of-magnitude reduction of process noise	4.9×10^{-6}	1.6×10^{-3}
3	One-order-of-magnitude increase in seismometer sensitivity	6.5×10^{-6}	2.8×10^{-3}
4	One-order-of-magnitude increase in tiltmeter sensitivity	8.4×10^{-6}	3.1×10^{-3}
5	Both Case 3 and Case 4	4.1×10^{-6}	1.9×10^{-3}

the prediction error. Even with the sensitivities of both sensors improved by one order of magnitude, the prediction error is far above the specification. It is concluded, then, that improvements in the sensors, in the present configuration, will not bring the filter rate prediction error down significantly!

The error is due, primarily, to the fact that the rate estimate is based on a position measurement and an acceleration measurement. With a direct measurement of

the angular rate, it is possible that the Kalman filter would provide estimates for the rate that are accurate within the specified levels.

Since it has been concluded that the optimal Kalman filter will not meet the performance criteria, with the system as presently configured, and, since this study is constrained to the analysis of the system as it presently exists, two approaches for further analysis were considered. The first approach is to neglect the angular rate specification and design the simplest Kalman filter that will meet the angular position specification. This is the approach taken by Brunson (Ref 4). The second approach is to design the Kalman filter that meets or exceeds the angular position specification and, in addition, provides the smallest angular rate prediction error. It is the latter approach that was taken in this study.

The analysis completed to this point has not considered the effects that accrue from the implementation of the Kalman filter on a small, relatively slow, computer (PDP-11/03). The analysis has been completed using a very fast, 60-bit wordlength machine and the final implementation is done on a slower, 16-kit wordlength machine. The filter performance is degraded further due to the limitations of the smaller machine. These degradations are discussed as part of the algorithm design and implementation considerations (Chapter IV).

As noted previously, the Kalman filters in this in-

vestigation can be modeled as constant Kalman gain filters. This is a result of the fact that the covariances (both propagated and updated) reach steady state values, for all of the system states, after an initial transient period. The transient period is short, compared to the time the platform is in use and, therefore, after an initial "warm-up" time for the filter (equal to the transient time for the covariances to reach steady state), a constant Kalman gain filter can be used. The constant Kalman gain implementation greatly reduces the computation time required by the filter algorithm because the covariance equations and the Kalman gain equation (Equations 37, 40 and 41), which are the most time consuming computations in the filter algorithm, are not computed as a part of the real-time filter. The constant Kalman gain matrix is stored, in memory, in the computer for use in the estimate update equation (Equation 39). In addition, a constant Kalman gain implementation eliminates the, often severe, numeric difficulties caused by the covariance update equation (Equation 40) that, normally, drive the wordlength requirements. The numeric difficulties often drive the implementation of the Kalman filter to some type of square-root form, e.g. U-D Factorization, to overcome the large wordlength requirements. Since the covariance update equation does not drive the wordlength considerations in this investigation, an eigenvalue test was used to determine

wordlength requirements.

In order to determine what wordlength is required to implement the optimal Kalman filter, the effects of quantization on the system eigenvalues were examined. A program called STM (modified version of program described in Ref 4) determines the normalized eigenvalue shifts caused by quantizing the system to a finite wordlength. A listing of STM is presented in Appendix C. The eigenvalues of the state transition matrix are the roots of the system characteristic equation (in discrete form). The computer program STM computes the state transition matrix for the system and computes the true eigenvalues associated with this state transition matrix. Next, STM quantizes the state transition matrix for various wordlengths and computes the eigenvalues associated with the quantized state transition matrices. The program computes the distance from the true eigenvalues to the unit circle and the distance (shift) between the true eigenvalues and the quantized eigenvalues for each wordlength. The criteria for accepting a given wordlength for implementation are that the system remains stable after quantization (roots inside unit circle on z-plane) and that the normalized eigenvalue shift is less than 10 percent for each eigenvalue at that wordlength. The normalized shift, S_n, is defined as

$$S_n = \left| \frac{D_q}{D_c} \right| \tag{47}$$

where $|D_q|$ is the magnitude of the distance (shift) between the true eigenvalue and the quantized eigenvalue and $|D_c|$ is the magnitude of the distance from the true eigenvalue to the unit circle. The wordlength is acceptable only if the 10 percent criterion (Ref 4:35) is met by each eigenvalue. In Figure 13, the maximum normalized eigenvalue shift is plotted for wordlengths from 10 bits to 20 bits. The wordlength where all the eigenvalue shifts are less than 10 percent, and thus the minimum acceptable wordlength is shown to be 13 bits. The fact that the PDP-11/03 minicomputer has more bits than required (it is a 16-bit machine) allows more flexibility in scaling and lessens the effects of overflow due to arithmetic operations.

Reduced Order Kalman Filter

Since the optimal Kalman filter is based on a ten-state model, the number of computations required to implement the filter limits the range of possible sampling rates and it is possible that a reduced order model (sub-optimal Kalman filter) might provide a smaller prediction error since a higher sampling rate could be employed.

In order to investigate this possibility, four sub-optimal Kalman filter models are developed below. The state matrices associated with the reduced models are presented in Appendix D.

Noise Filter Reduction. The frequency response of the process noise filter is shown in Figure 14. The noise

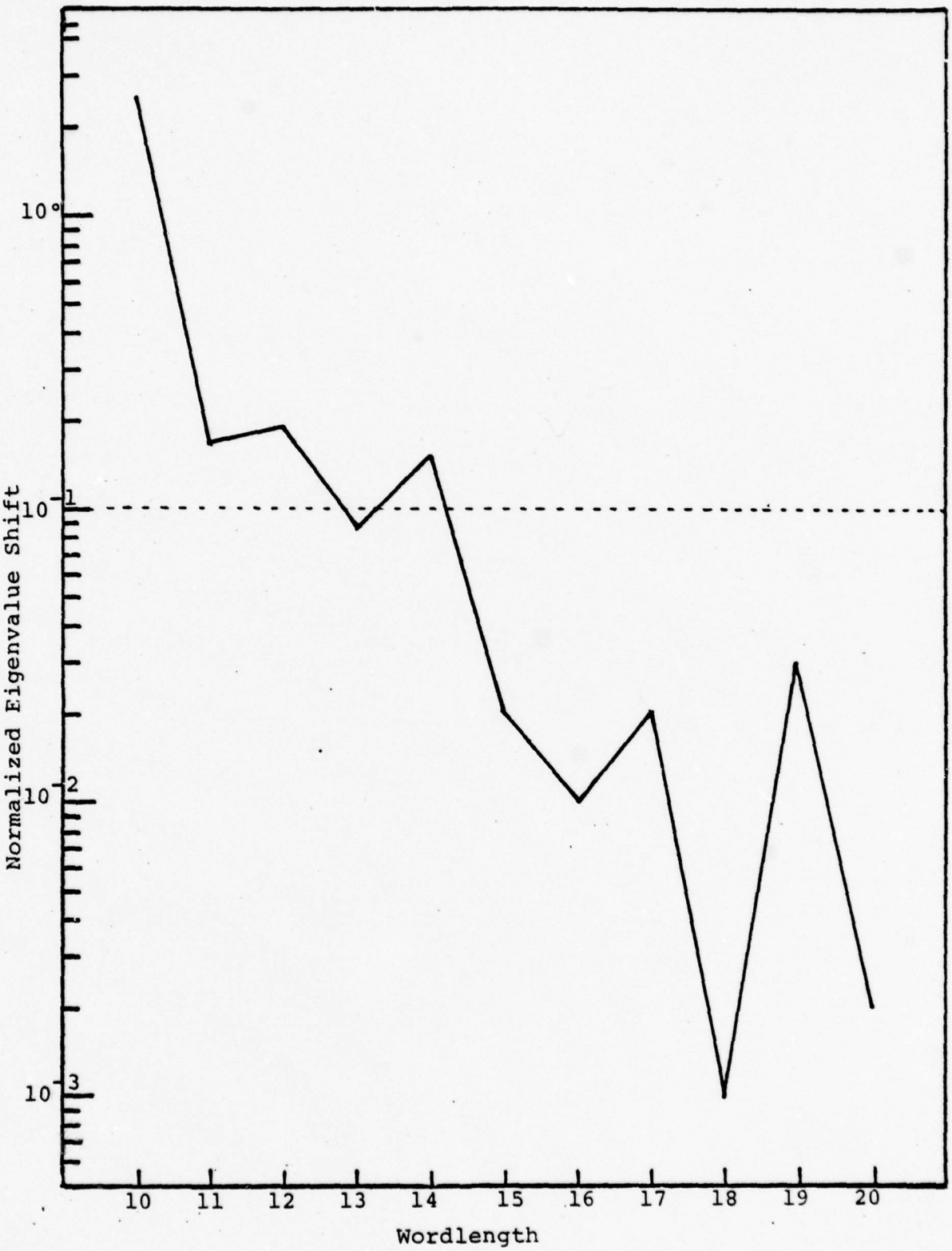

Figure 13. Optimal Filter Wordlength Effects

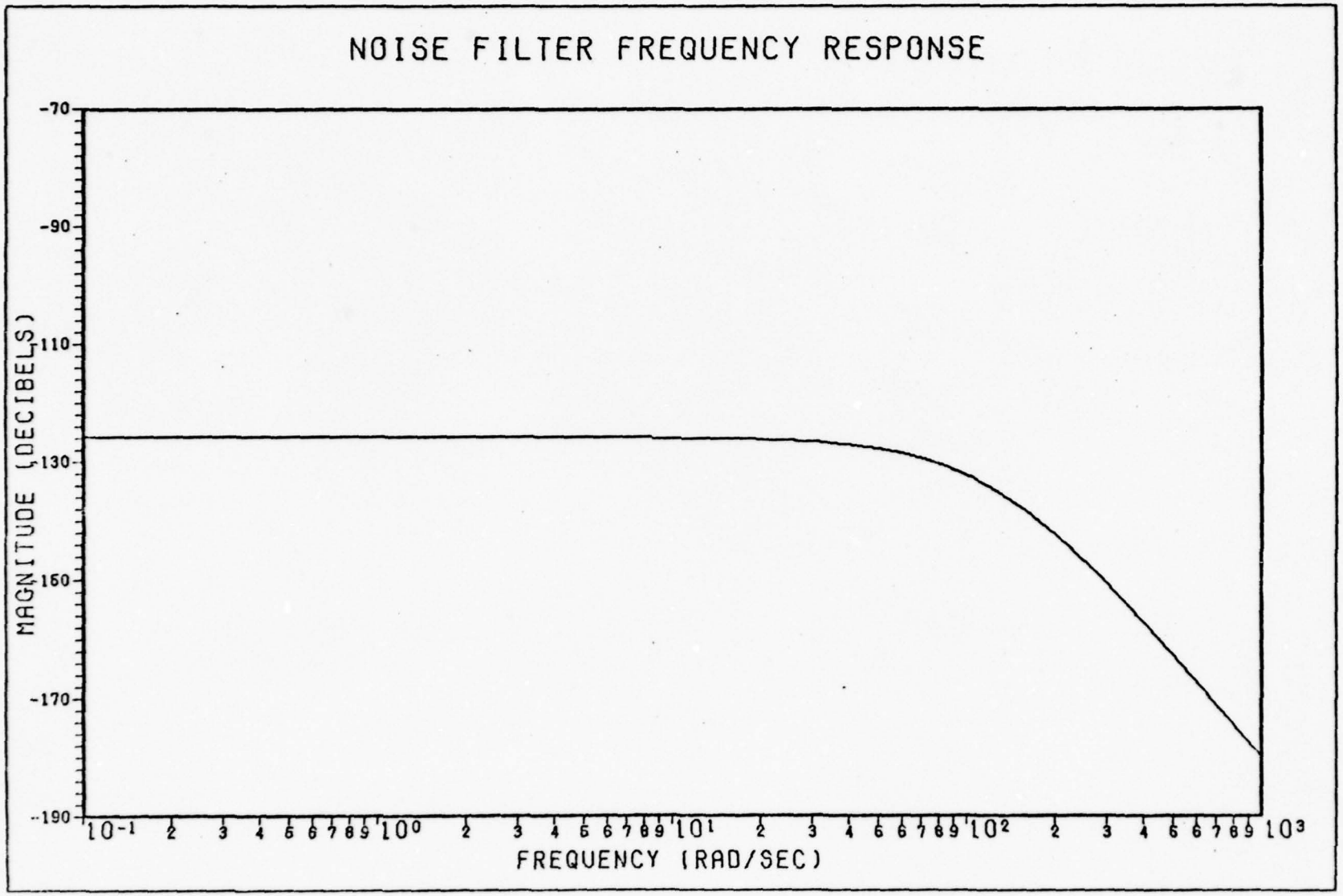

Figure 14. Process Noise Filter Frequency Response.

filter provides a sharp cutoff for frequencies above approximately 20 Hz (125 radians/second, see Equation 24). Since the 20 Hz bandwidth of the noise from the process noise filter (exponentially correlated) is much greater than the 1.3 Hz natural frequency of the platform, the noise is assumed to be white (limited bandwidth system driven by relatively broadband noise). This simplifying assumption results in a reduced (approximate) model composed of seven states. Since, as indicated by the frequency response, the process noise filter attenuated the process noise by approximately 125 dB, a rough estimate of the equivalent white noise for the reduced model is

$$Q_{eq} \approx 10^{-13} Q_{Ts} \approx 1.849 \times 10^{-1} \tag{48}$$

where Q_{eq} is the estimated equivalent white noise strength and Q_{Ts} is the process noise covariance used in the truth model for the system.

Tiltmeter Model Reduction. In order to reduce the tiltmeter model, a second-order approximation was developed that has approximately the same frequency response as the tiltmeter truth model (Ref 4:26). The form of this approximation is

$$\frac{C}{R} = \frac{4.9(1 - 0.55s)}{s^2 + 8s + 49} \quad \frac{\text{Volts}}{\text{Arcsecond}} \tag{49}$$

A comparison of the frequency responses of the truth model and reduced model is presented in Figure 15. As indicated by the plot, the frequency response of the

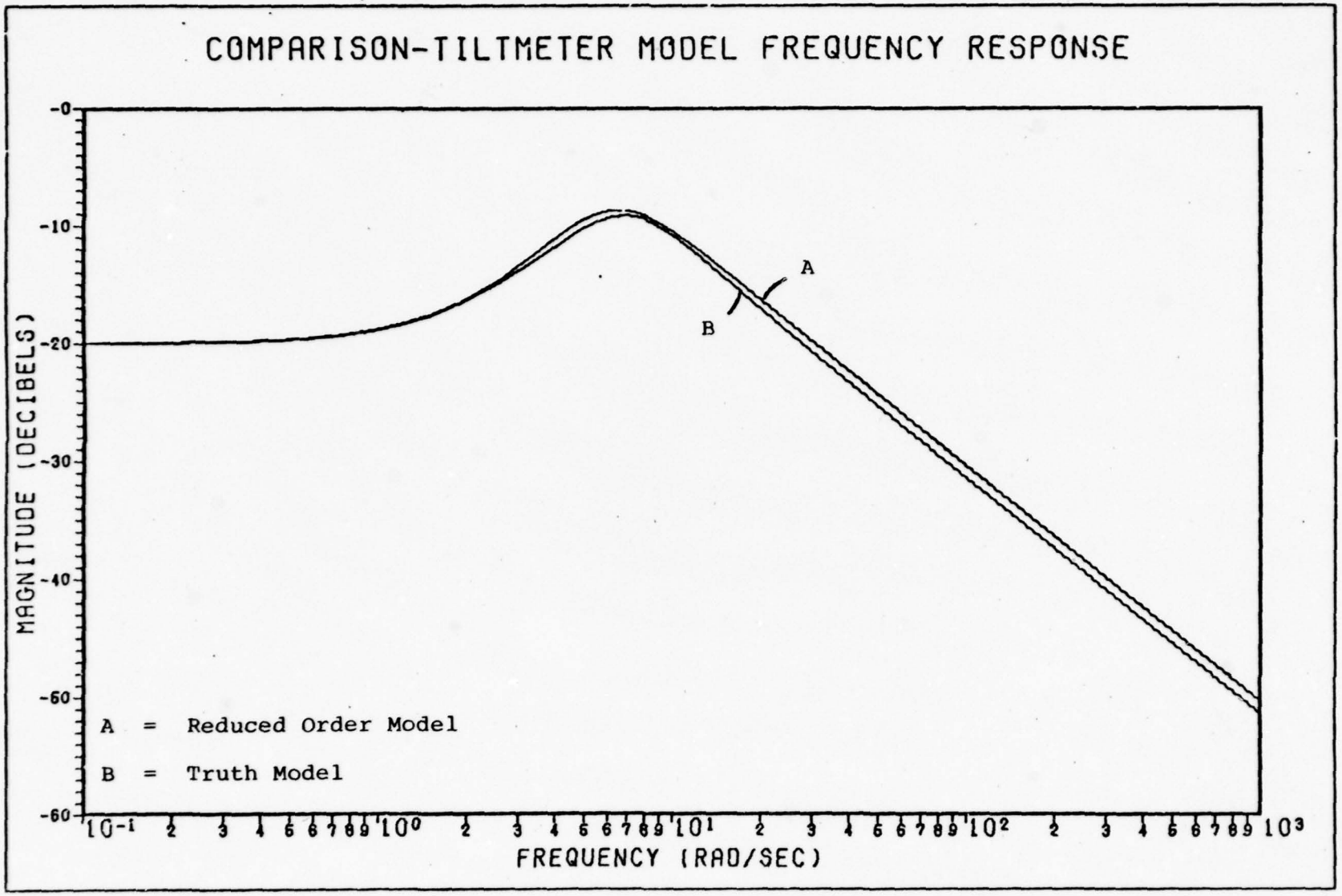

Figure 15. Comparison of Tiltmeter Model Frequency Responses

reduced-order model has the same general shape as the true model. The responses appear to be identical at very low frequencies (up to approximately 2.5 Hz) and differ by, at most, 1 dB (beyond 20 Hz). Figure 16 is a plot of the phase response of the tiltmeter models. The general shape of the plots are the same but the phase response of the true model lags the response of reduced-order model. The lag is a maximum of approximately 20 degrees (at 2 Hz) and is generally much less than 10 degrees. Since the measurement from the tiltmeter is considered most accurate in the 0-1 Hz range, the reduced-order model is an adequate representation. However, the reduced-order model will inject additional inaccuracies (noise) into the system.

Seismometer Model Reduction. The frequency response of the seismometer is depicted in Figure 17. The seismometer exhibits essentially no dynamics in the 0-20 Hz frequency band and is, therefore, approximated by a constant gain of one. This simplifying assumption reduces the system by two states. Two reduced models were developed using this approximation. First, in order to investigate the effects of the seismometer reduction in combination with the true tiltmeter model, a five state model was developed. The five state model consists of the platform dynamics model (two states), the true tiltmeter model (three states), the reduced-order seismometer model (constant gain of 1), and the reduced-order noise filter model

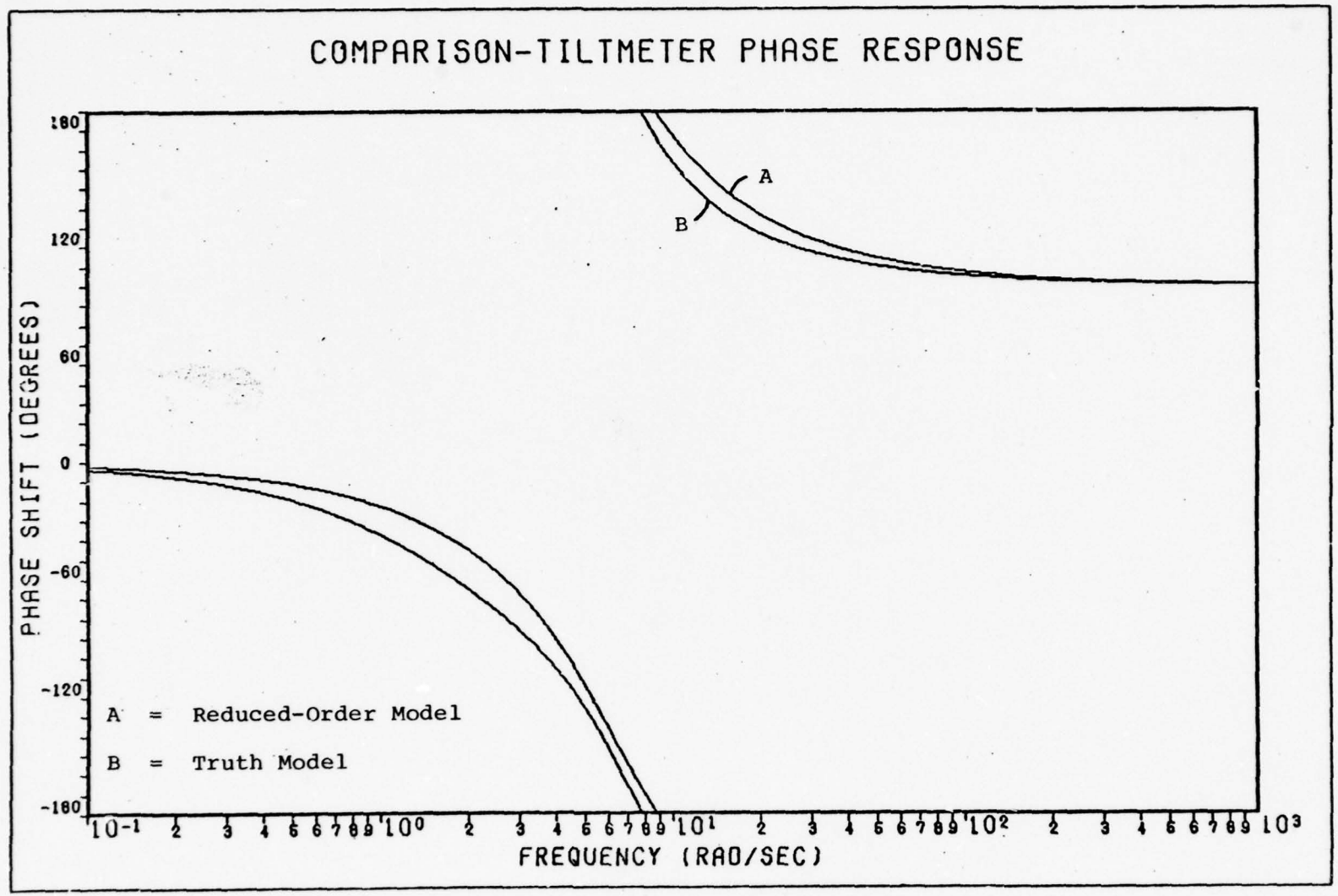

Figure 16. Comparison of Tiltmeter Model Phase Response

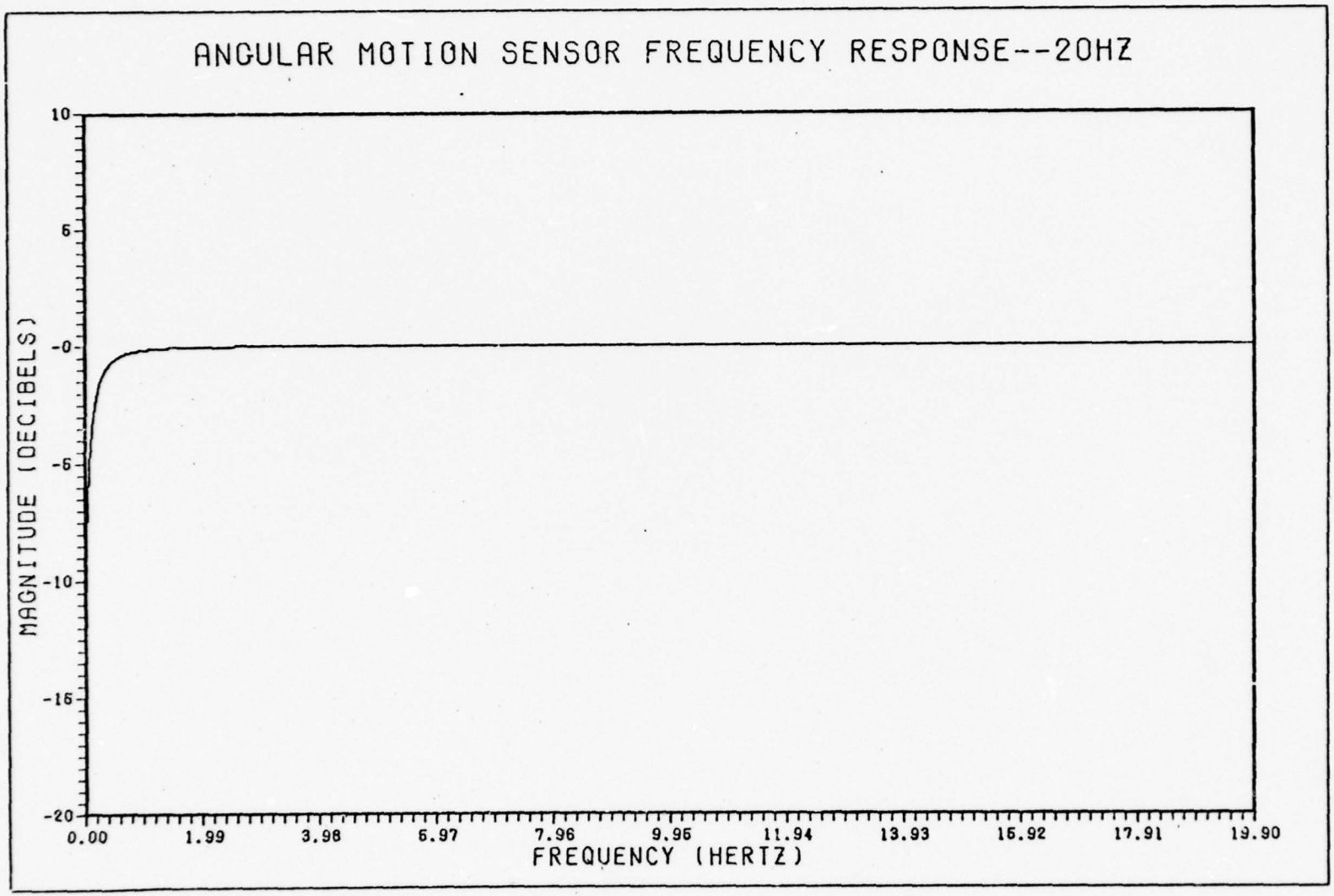

Figure 17. Seismometer Frequency Response

(constant strength white noise). Second, in order to investigate the effects of the combination of the reduced-order models, a four state model was developed. The four state model consists of the platform dynamics (2 states), the reduced-order tiltmeter model (2 states), the reduced-order seismometer model (constant gain of 1), and the reduced-order noise filter model (constant strength white noise).

In Chapter IV, each filter model (in combination with the optimal controller) is analyzed at an appropriate sampling rate, determined by the number of calculations involved in that filter/controller implementation.

Summary

It has been shown that, with the seismic isolation platform as presently configured, optimal estimation by Kalman filter techniques will not reduce the uncertainties inherent in the system to levels low enough to meet the minimum accuracy required for successful optimal control. In addition, neither decreases in process noise, nor increases in sensor sensitivities significantly improve the performance of the Kalman filter. Possible significant improvement can be achieved by augmenting the system with a direct measurement of the angular rate of the platform.

Since the angular rate specification (1.667×10^{-5} arcseconds/second) cannot be met (the angular position specification is surpassed by more than two orders of magnitude), the approach followed in this thesis is to

design for the best possible angular rate performance that can be expected for this system configuration. In addition to the optimal Kalman filter model, four sub-optimal models were developed for performance comparisons. The approach is to select and implement the filter model that provides the best rate prediction performance (smallest error). The selected Kalman filter is combined with the optimal controller developed in Chapter III.

III. Controller Development

The development of the controller segment is based on discrete models of the platform and the actuators (pneumatic cylinders and shakers). A control segment model was proposed by Burkhart (Ref 1). The model was developed for a sampling rate of 200 Hz and tested with a 1.25 foot-pound step input. This chapter contains a brief discussion of the models and techniques employed in the development of the controller segment. In addition, pertinent results stated by Burkhart are included as background information. In Chapter IV, a control segment is developed, in general form, based on the sampling rate dictated by the analysis of the various filter/controller combinations.

Separation of Controller Segment

The design of the controller segment was divided into two tasks (Fig 8). Each control task is associated with one of the two types of actuators used in controlling the angular motion about the horizontal axis. The justification for the separation of the controller segment is based, primarily, on the dynamic characteristics of the actuators. The pneumatic actuators are slow (time constant of 20 seconds) and are actually part of the platform support system. Due to the pneumatic actuators' dynamic response, they are employed in a position feedback loop to counter any torque imbalances resulting from unsymmetrical loading

of the platform. The shakers have a much faster dynamic response (natural frequency is 26 Hz) and are employed in an optimal state-feedback control (optimal regulator) loop, to regulate the effects of the environmental disturbances. In both cases, the control loops were developed with the assumption that they are receiving perfect information about the system states from the Kalman filter, i.e. exact knowledge of the entire state.

The optimal regulator is designed to regulate the pneumatic loop. The states associated with the pneumatic actuator are the contents of registers in the computer (derived from the pneumatic loop compensator algorithm) and are known exactly. These states are incorporated into the optimal control problem through the use of an augmented state space model that is used in deriving the control law. Assuming the exact values of the states (from the Kalman filter and from the pneumatic loop), the deterministic discrete-time optimal controller will minimize the discrete performance index given in Eq (3)(Ref 15:502). This is, again, based on the "forced separation" concept described in Chapter I.

Continuous System Models

The development of the controllers is based on the models of those components used in controlling angular motion about the horizontal axis. The sensor models are not included in the controller segment development since

they are part of the estimator problem ("forced separation"). The models required include the seismic isolation platform model, the pneumatic actuator model, the shaker actuator model, and a model of the environmental disturbances (process noise).

Seismic Isolation Platform. The transfer function for the seismic isolation platform was presented in Eqs (7) and (8) (Chapter II).

Pneumatic Actuator. The pneumatic actuator transfer function is (Ref 1:17)

$$H_p(s) = \frac{1}{s + .05} \quad \frac{\text{Foot-pound}}{\text{Volt}} \tag{50}$$

Shaker Actuator. The shaker actuator transfer function is (Ref 1:18)

$$H_s(s) = \frac{k_s \omega_s^2}{s^2 + 2\zeta_s \omega_s s + \omega_s^2} \quad \frac{\text{Foot-pounds}}{\text{Amps}} \tag{51}$$

where

$\zeta_s = 0.7$

$\omega_s = 157$ radians/second

and $k_s = 70$ foot-pounds/amp

Environmental Disturbance (Noise) Model. To evaluate the performance of the controller, a deterministic model of the environmental disturbance (called process noise in Chapter II) was developed. A torque step function, $u_t(t)$, directly applied to the top surface of the concrete block was selected since it is readily modeled in both the z-domain

and the s-domain. There is some question as to the weight of the step-input that more closely represents the process noise. The peak overshoot of the time response of the platform model, to a step input, approximates the average excursion of the uncontrolled platform due to the environmental disturbances. Burkhart's model is based on an average excursion of 0.1 arcseconds, derived from Reference 12:2. The average excursion used to determine the process noise model for the Kalman filter was 0.2 arcseconds (Ref 8). Since no estimate of the quiescent platform oscillatory excursion appears to be more acceptable than the others, the "worst case" model (0.2 arcseconds) is used in this investigation. However, for the purpose of describing the results of Burkhart's work, the 0.1 arcsecond excursion model is employed.

Using the computer program TOTAL, the weight of the representative step input was determined to be 1.25 foot-pounds. As seen in Figure 18, a 1.25 foot-pound step input produces a peak overshoot of 0.102 arcseconds.

Figure 18 illustrates the relationships of the torques and transfer function associated with the actuators and the process noise.

Discrete System Models

Two discrete models were derived from the continuous system transfer functions. A z-domain function, $\theta(z)$, of angular position of the platform, with a step input, was

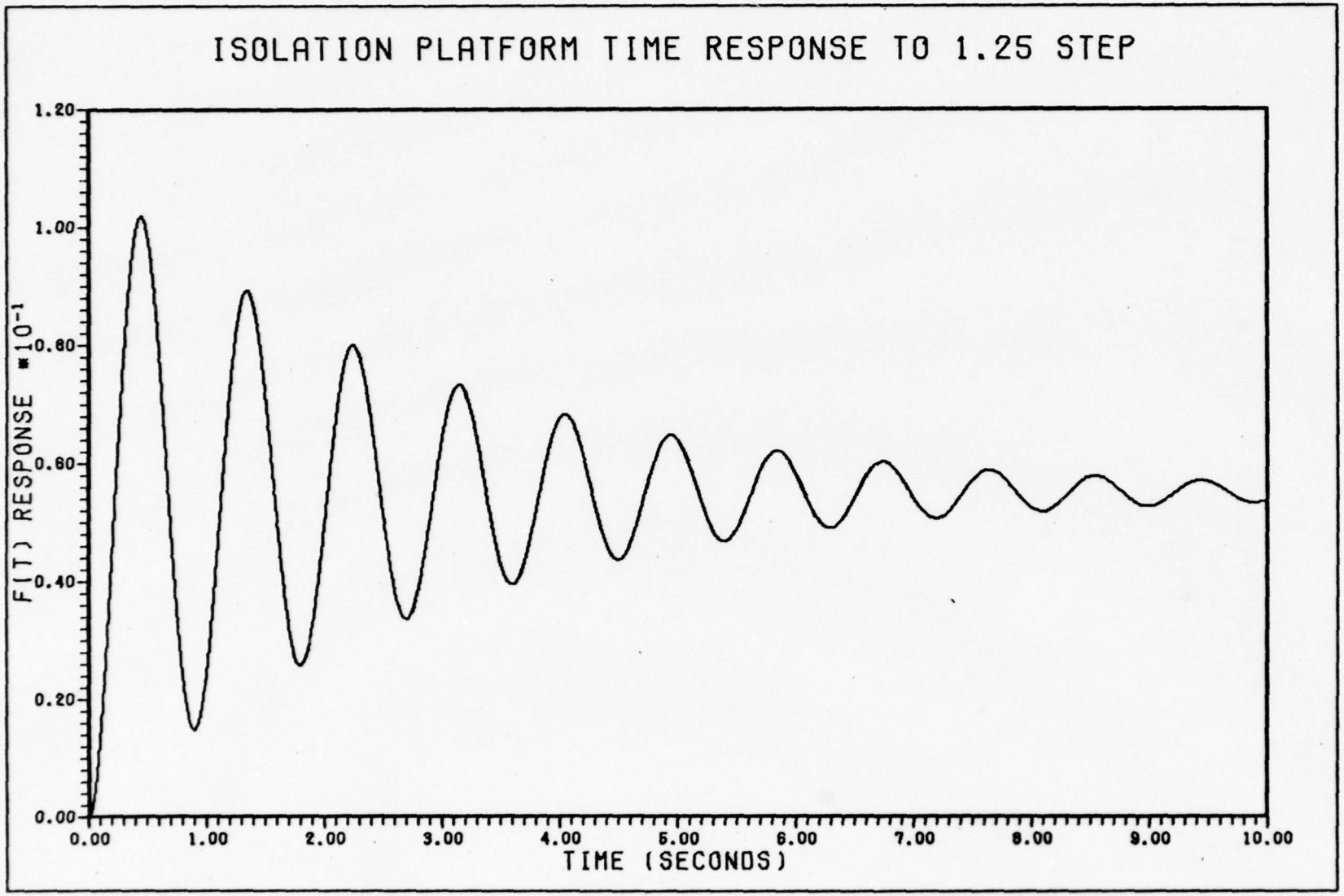

Figure 18. Isolation Platform Time Response to 1.25 Foot-Pound Step Input

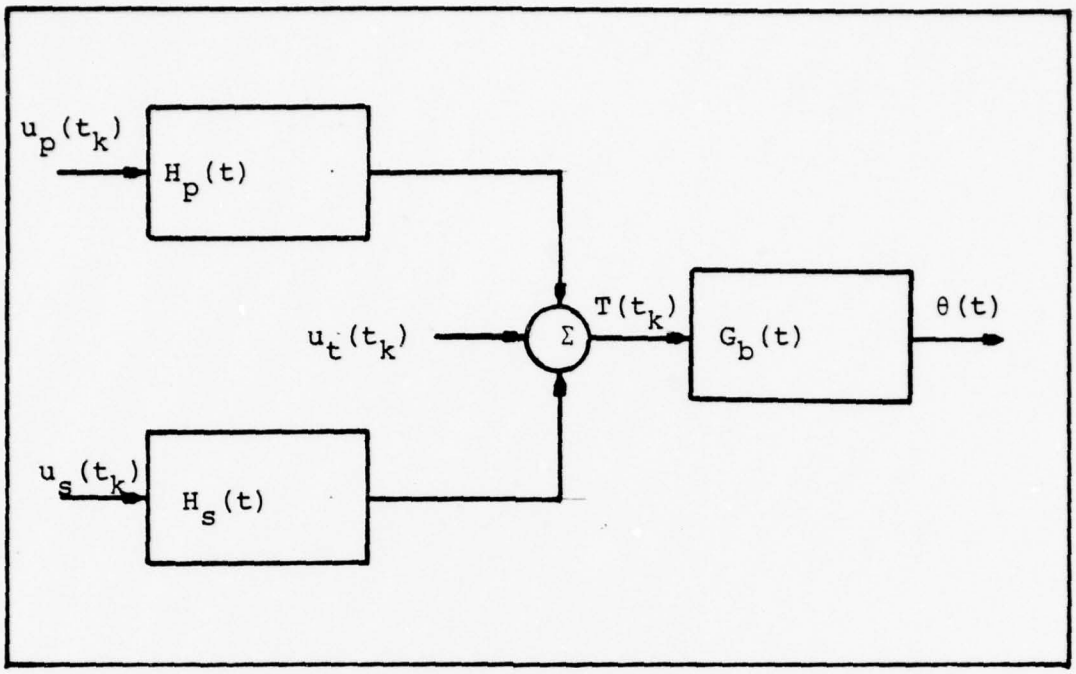

Figure 19. Block Diagram of Platform and Actuators (Ref 1:21)

derived for use in designing the controller for the pneumatic control loop. A discrete state representation of the platform and the actuators was developed for use in the designing of the optimal controller in the regulator loop.

Position Feedback Loop. A block diagram of the pneumatic loop is shown in Figure 20.

The pneumatic loop includes, along with the platform ($G_b(s)$) and the pneumatic actuator ($H_p(s)$), an impulse sampler, a computer algorithm D(z) and a digital-to-analog converter (DAC). The impulse sampler in the model prepresents the estimation process completed by the Kalman filter (denoted $\theta^*(s)$). The DAC is represented by a zero-order hold (ZOH), $H_o(s)$. The ZOH holds the output of the DAC constant

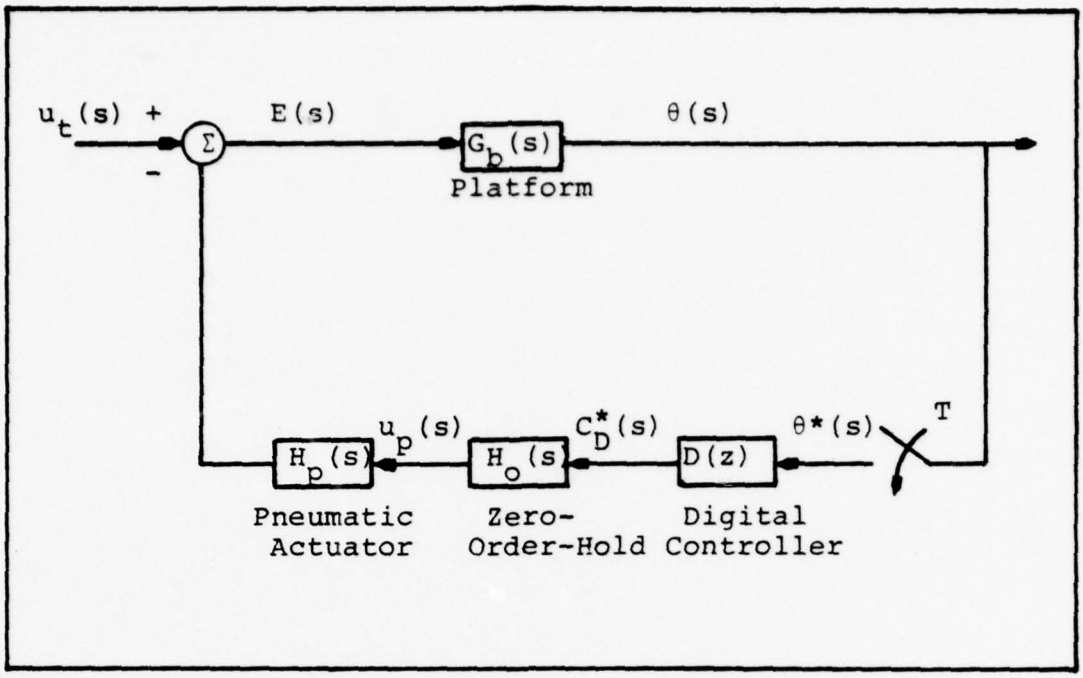

Figure 20. Block Diagram of Pneumatic Loop (Ref 1:22)

between samples and has the transfer function

$$H_o(s) = \frac{1 - e^{-Ts}}{s} \tag{52}$$

where T is the sampling period.

The computer algorithm, D(z), is a digital computer program (digital controller or compensator) that receives the estimated angular position from the Kalman filter and produces a control signal, $C_D^*(s)$, that is, in turn, sent to the DAC and converted to analog form for input to the pneumatic actuator.

The location of the computer in the feedback loop prohibits the reduction of the block diagram to the z-domain transfer function $\theta(z)/u_t(z)$. Instead, the approach is to solve for an expression of $\theta(z)$. First

$$E(s) = u_t(s) - H_p(s)H_o(s)C_D^*(s) \tag{53}$$

So

$$\theta(s) = u_t(s)G_b(s) - G_b(s)H_p(s)H_o(s)C_D^*(s) \tag{54}$$

And taking the z-transform

$$\theta(z) = u_tG_b(z) - G_bH_pH_o(z)C_D(z) \tag{55}$$

Since

$$C_D(z) = D(z)\theta(z) \tag{56}$$

Then

$$\theta(z) = \frac{u_tG_b(z)}{1 + G_bH_pH_o(z)D(z)} \tag{57}$$

The z-transforms $u_tG_b(z)$ and $G_bH_pH_o(z)$ must be determined. Since the design objective is to meet the specified response characteristics for a step input $u_t(s)G_b(s)$ is evaluated with

$$u_t(s) = 1/s \tag{58}$$

And

$$Z[u_t(s)G_b(s)] = \frac{Bz^2 + Cz}{(z-1)(z^2+\beta z+\varepsilon)} \tag{59}$$

where

$$\alpha = Ae^{-aT}\sin(bT - \emptyset) \tag{60}$$

$$\beta = -2e^{-aT}\cos(bT) \tag{61}$$

$$\varepsilon = e^{-2aT} \tag{62}$$

$$B = k_b(\beta - \alpha + 1) \tag{63}$$

$$C = k_b(\alpha + \varepsilon) \tag{64}$$

The coefficients, evaluated at T = 5 msec, are

$$B = 2.6915839 \times 10^{-5}$$

$$C = 2.6884453 \times 10^{-5}$$

$$\beta = 1.9952834$$

$$\varepsilon = 0.99650612$$

The z-transform for $G_b(s)H_p(s)H_o(s)$, since $H_o(s)$ is a zero-order hold, is

$$G_b H_p H_o(z) = \frac{z-1}{z} Z\left[\frac{G_b(s)H_p(s)}{s}\right] \tag{65}$$

Now

$$Z\left[\frac{G_b(s)H_p(s)}{s}\right] = \frac{Jz^4 + Lz^3 + Mz^2 + Nz}{(z-1)(z-\delta)(z^2+\beta z+\varepsilon)} \tag{66}$$

where

$$J = G + k_b - E \tag{67}$$

$$L = \beta k_b - \beta E + E - \delta k_b + H - \delta G - G \tag{68}$$

$$M = \varepsilon k_b - \varepsilon E + \delta\beta k_b + E\beta + \delta G - H\delta + H \tag{69}$$

$$N = \delta\varepsilon k_b + \varepsilon E + \delta G \tag{70}$$

The coefficients, calculated at T = 5 msec are

$$J = 2.1439340 \times 10^{-17}$$

$$L = 2.2435920 \times 10^{-9}$$

$$M = 8.9654109 \times 10^{-9}$$

$$N = 2.2393891 \times 10^{-9}$$

$$\delta = 0.99975003$$

To verify the discrete models, an initial value verification was employed. For verification, the initial values of the continuous time functions were compared to the initial values for the corresponding discrete-time functions. All

the functions had initial values of zero except the discrete function $G_bH_p(z)$ which had an initial value equal to the value of the coefficient J. Since J is several orders-of-magnitude smaller than the other coefficients, the term involving J, i.e., the z^4 term, was deleted. This deletion is justified since, with single-precision 16-bit wordlength computations, J is too small to be represented and would, therefore, be rounded to zero. The resulting function is

$$Z\left[\frac{G_b(s)H_p(s)}{s}\right] = \frac{Lz^3 + Mz^2 + Nz}{(z-1)(z-\delta)(z^2-\beta z+\varepsilon)} \qquad (61)$$

To obtain $G_bH_pH_o(z)$, Equation 71 is substituted in Equation 65 to yield

$$G_bH_pH_o(z) = \frac{Lz^2 + Mz + N}{(z-\delta)(z^2-\beta z+\varepsilon)} \qquad (72)$$

Finally, substituting Equations 72 and 59 into Equation 57 yields

$$\theta(z) = \frac{\dfrac{Bz^2 + Cz}{(z-1)(z^2+\beta z+\delta)}}{1 + \dfrac{Lz^2+Mz+N}{(z-\delta)(z^2+\beta z+\varepsilon)}\, D(z)} \qquad (73)$$

Discrete State Space Model. Since the zero-order hold device maintains the control inputs constant over the sampling period, the continuous state space model is transformed to a discrete state space model by the following transformation:

$$\Phi = e^{FT} \qquad (74)$$

and

$$\Gamma = \int_0^T e^{(T-\tau)} B d\tau \tag{75}$$

where Φ is the discrete state transition matrix, F is the continuous plant matrix, T is the sampling interval, Γ is the control transition matrix (discrete control matrix), and B is the continuous control matrix. The continuous state equation is

$$\dot{\underline{x}}(t) = F\underline{x}(t) + L\underline{u}(t) \tag{76}$$

with $\underline{u}(t)$ for $t\varepsilon[kT, (k+1)T]$ and the discrete state equation is

$$x(k+1) = \Phi\underline{x}(k) + \Gamma u(k) \tag{77}$$

Using phase variable form state equations to represent the individual transfer functions, the resulting state matrices are

$$F = \begin{bmatrix} 0 & 1 & 0 & 0 & 0 \\ -49 & -.7 & 1 & 1725430 & 0 \\ 0 & 0 & -.05 & 0 & 0 \\ 0 & 0 & 0 & 0 & 1 \\ 0 & 0 & 0 & -24649 & -219.8 \end{bmatrix} \tag{78}$$

and

$$L = \begin{bmatrix} 0 & 0 & 0 \\ 0 & 0 & 0 \\ .05 & 0 & 0 \\ 0 & 0 & 0 \\ 0 & 1 & 0 \end{bmatrix} \tag{79}$$

where

$$\theta = 2.156x_1(t) \tag{80}$$

$$\dot{\theta} = 2.156x_2(t) \tag{81}$$

and

$$\underline{u}(t) = \begin{bmatrix} u_p(t) \\ u_s(t) \\ u_t(t) \end{bmatrix} \tag{82}$$

The general form of the transition matrices is

$$\Phi = \begin{bmatrix} \Phi_{11} & \Phi_{12} & \Phi_{13} & \Phi_{14} & \Phi_{15} \\ \Phi_{21} & \Phi_{22} & \Phi_{23} & \Phi_{24} & \Phi_{25} \\ 0 & 0 & \Phi_{33} & 0 & 0 \\ 0 & 0 & \Phi_{43} & \Phi_{44} & \Phi_{45} \\ 0 & 0 & \Phi_{53} & \Phi_{54} & \Phi_{55} \end{bmatrix} \tag{83}$$

and

$$\Gamma = \begin{bmatrix} \Gamma_{11} & \Gamma_{12} & \Gamma_{13} \\ \Gamma_{21} & \Gamma_{22} & \Gamma_{23} \\ \Gamma_{31} & 0 & 0 \\ 0 & \Gamma & 0 \\ 0 & \Gamma & 0 \end{bmatrix} \tag{84}$$

The numerical values of the elements of the matrices is determined by the relationships described in Equations 74 and 75 and is a function of the sampling interval, T.

Pneumatic Controller (Compensator), D(z)

The criteria used in designing the pneumatic loop com-

magnitude), the approach followed in this

pensator, D(z), are that the system remains stable with D(z) in the feedback loop, that D(z) drives the platform to zero steady-state angular position, and that the transient response (peak overshoot and settling time), to a 1.25 foot-pound input, of the controlled platform is better than that of the uncontrolled platform (depicted in Figure 17).

The steady state response of $\theta(z)$ was analyzed by letting

$$D(z) = \frac{N_D(z)}{D_D(z)} \tag{85}$$

in Equation 73 and employing the final value theorem

$$(t\to\infty) = \lim_{z-1}(z-1)\left[\frac{z(Az+B)(z-\delta)D_D(z)}{(z-1)P(z)}\right] \tag{86}$$

where

$$P(z) = D_D(z)[z^3 + (\beta + \delta)z^2 + (\varepsilon - \delta\beta)z - \delta\varepsilon] + (Lz^2 + Mz + N)N_D(z) \tag{87}$$

To insure that the steady state value of $\theta(z)$ goes to zero, D(z) must have a factor (z-1) in the denominator (Ref 16:290).

Root locus techniques were used to examine the stability and transient response of various compensators having a factor of (z-1) in their denominators. Using the root loci of the expression, $D(z)G_bH_pH_o(t)$ (Equation 58), for various D(z)'s the characteristic values of the pneumatic loop were determined. By varying the gain and the location

and number of poles and zeros in the compensator, a form for D(z) was chosen that produces a stable system and a fast transient response. The selected form for the discrete controller for the pneumatic loop was

$$D(z) = \frac{7500(z-0.99900)(z^2-2.0150z+1.0158)}{(z-1.0)(z^2-0.9752)} \qquad (88)$$

The response of the system, with the compensator, was determined by evaluating the difference equation (transformed from $\theta(z)$, Equation 73) with the above D(z) in the feedback loop (Ref 1:52). As depicted in Figure 21, the steady-state response for the controlled system is zero (versus 0.055 arcseconds for the uncontrolled platform, Figure 17) and the peak overshoot is slightly less than that for the uncontrolled platform (0.097 arcseconds versus 0.102 arcseconds). However, the settling time is slightly greater for the compensated system (approximately 11 seconds versus 10.86 seconds). The D(z) described above was designed based on a sampling rate of 200 Hz. It is assumed, for analysis purposes, that the general form of D(z)(Equation 88) is maintained through the change in sampling rate. This assumption is based on the fact that changes in the sampling rate will cause changes in the locations of the roots of the discrete system models (platform and pneumatic actuator), but will not change the order of these models. Therefore, the general form of the compensator that is used in Chapter IV for determining the approximate sampling rate is

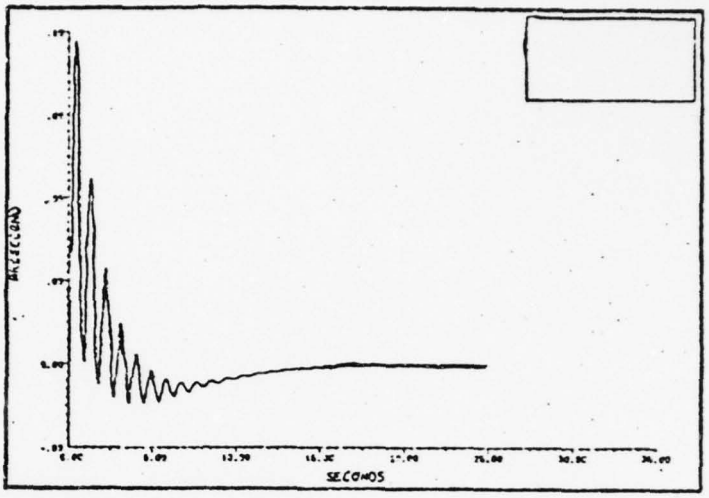

Figure 21. Graph of Difference Equation for $\theta(kT)$ (Ref 1:53)

$$D(z) = \frac{k_D(z-a)(z^2-bz+c)}{(z-1.0)(z^2-dz)} \tag{89}$$

Burkhart determined that, with the form of D(z) in Equation 88, the time responses (to a 1.25 ft-lb step-input) for the discrete compensator and for a thirteen-bit digitized version of the compensator agreed within three significant digits after 25 seconds. It was concluded that the thirteen bit controller shows no significant degradation of performance (Ref 1:57).

Regulator Loop. The regulator (shaker) loop is used to provide further damping of the pneumatic loop and also to provide control of the angular rate of the platform. The shaker receives its control input from a state feedback control law (optimal controller) that is based on an augmented system state model consisting of the discrete state space model of the inertial instrument test platform and

actuators (Equations 83 and 84) combined with a discrete state space model of the pneumatic compensator.

A state space model of the pneumatic actuator is derived by factoring Equation 88 into

$$D(z) = \frac{C(z)}{\theta(z)} = 7500 \quad \frac{z-0.999}{z} \quad \frac{z^2-2.015z+1.0158}{(z-1.0)(z-0.975)} \qquad (90)$$

and forming a state space representation for each term using partial fraction expansion. After combining the state representations for each term, the state space model of D(z) is (see Figure 19)

$$\underline{x}_D(k+1) = \begin{bmatrix} 0 & 0 & 0 \\ -0.999 & 1.0 & 0 \\ -0.999 & 0 & 0.975 \end{bmatrix} \underline{x}_D(k) + \begin{bmatrix} 1 \\ 1 \\ 1 \end{bmatrix} \theta(k) \qquad (91)$$

$$C_D(k) = 7500\{[-0.999 \quad 3.36324\text{x}10^{-2} \quad -7.36324\text{x}10^{-2}]\ \underline{x}_D(k) + \theta(k)\} \qquad (92)$$

After augmenting the system model (Equations 83 and 84) with the compensator model (Equation 91 and 92), the discrete pneumatic loop state space model becomes (in general form)

$$\Phi_P = \begin{bmatrix} \Phi_{P11} & \Phi_{P12} & \Phi_{P13} & \Phi_{P14} & \Phi_{P15} & \Phi_{P16} & \Phi_{P17} & \Phi_{P18} \\ \Phi_{P21} & \Phi_{P22} & \Phi_{P23} & \Phi_{P24} & \Phi_{P25} & \Phi_{P26} & \Phi_{P27} & \Phi_{P28} \\ \Phi_{P31} & 0 & \Phi_{P33} & 0 & 0 & \Phi_{P36} & \Phi_{P37} & \Phi_{P38} \\ 0 & 0 & 0 & \Phi_{P44} & \Phi_{P45} & 0 & 0 & 0 \\ 0 & 0 & 0 & \Phi_{P54} & \Phi_{P55} & 0 & 0 & 0 \\ \Phi_{P61} & 0 & 0 & 0 & 0 & 0 & 0 & 0 \\ \Phi_{P71} & 0 & 0 & 0 & 0 & \Phi_{P76} & 1.0 & 0 \\ \Phi_{P81} & 0 & 0 & 0 & 0 & \Phi_{P86} & 0 & \Phi_{P88} \end{bmatrix} \qquad (93)$$

and

$$\Gamma_P = \begin{bmatrix} \Gamma_{P11} \\ \Gamma_{P21} \\ 0 \\ \Gamma_{P31} \\ \Gamma_{P41} \\ 0 \\ 0 \\ 0 \end{bmatrix} \tag{94}$$

where Φ_P is the pneumatic loop state transition matrix and Γ_P is the pneumatic loop control transition matrix.

The objective of the deterministic discrete optimal controller is described by Equations 3 and 4 in Chapter I except that, due to the forced separation, $\hat{\underline{x}}(t_k)$ (the state estimate from the Kalman filter) is replaced by $\underline{x}(t_k)$ for design purposes. Thus, the design of the control law, $C(t_k)$ is assumed independent of the stochastic properties of the system.

The quadratic performance index, J (in Equation 4), can be interpreted as "system error plus control effort" measure of performance that uses a tradeoff between system error, represented by quadratic term involving the V matrix, and control effort, represented by the quadratic control "intensity" term involving the U matrix (Ref 17: 326).

The procedure used to solve for $C(t_k)$ was adapted from Linear Optimal Control Systems (Ref 15:502) and consists

of solving the equations

$$C(t_k) = \{U + \Gamma_P^T[V + P(k+1)]\Gamma\}^{-1}\Gamma^T[V + P(k+1)]\Phi \quad (95)$$

and

$$P(k) = \Phi^T[V + P(k+1)][\Phi - \Gamma C(k)] \quad (96)$$

backward in time from the terminal condition

$$P(n) = V_f \quad (97)$$

It has been demonstrated that the solution of Equations 95 through 97 results in a steady-state solution for $C(t_k)$ that is independent of the terminal condition. The resulting control law is time invariant and asymptotically stable (Ref 1:62).

The solution of the optimal control law does not guarantee that the design specifications will be met (Ref 1:61). The optimal control law must be solved by the iterative process of selecting various values for the weighting matrices V, V_f, and U, and evaluating the resulting control law to determine if it meets the design specifications. The resulting control law vector, in general form, is

$$C = \begin{bmatrix} C_{11} \\ C_{12} \\ C_{13} \\ C_{14} \\ C_{15} \\ C_{16} \\ C_{17} \\ C_{18} \end{bmatrix}^T \quad (98)$$

The results of Burkhart's analysis (Fig 21) indicate that, for the control law based on a sampling rate of 200 Hz, the angular rate specification is not met, although the system does settle to within the design specification (1.667×10^{-5} arcseconds/second) within 0.08 seconds. It was concluded that the angular rate specification could not be met, at any physically realizable sampling rate, by the designed optimal controller, due to the fact that the angular rate of the inertial test platform was already three orders-of-magnitude greater than the design specification at the end of the first sample period (0.05 seconds) (Ref 1:68). The optimal controller controlled the angular position to less than 2.9×10^{-4} arcseconds (much better than the design specification of 1×10^{-3} arcseconds).

Summary

In this chapter, the general forms of the control equations are developed. The pneumatic loop controller uses angular position feedback to generate the control signal to the pneumatic actuator. The matrix form of the controllers are converted to scalar equation form to alleviate the inefficiency of matrix operations with sparse matrices and also to allow more flexibility in the ordering of the computations. The resulting pneumatic controller scalar equations are (from Equation 91 and 92).

$$x_6(k+1) = 2.156\, x_1(k) \tag{99}$$

$$u_p = C_D(k) = k_D[u_p'(k) + x_6(k+1)] \quad (100)$$

$$x_7(k+1) = -0.999\ x_6(k) + x_7(k) + x_6(k+1) \quad (101)$$

$$x_8(k+1) = -0.999\ x_6(k) + 0.975\ x_8(k) + x_6(k+1) \quad (102)$$

$$u_p'(k+1) = 0.999\ x_6(k+1) + 3.36\times10^{-2} x_7(k+1) - 7.36\times10^{-2} x_8(k+1) \quad (103)$$

The optimal regulator uses state feedback to derive a control law that produces the control signals to the shaker actuator. The scalar equations representing the optimal regulator algorithm are (from Equations 3 and 98)

$$u_s(k) = c_{11}x_1(k) + c_{21}x_2(k) + c_{31}x_3(k) + c_{41}x_4(k) + c_{51}x_5(k) + u_s'(k) \quad (104)$$

$$u_s'(k+1) = c_{61}x_6(k+1) + c_{71}x_7(k+1) + c_{81}x_8(k+1) \quad (105)$$

In Chapter IV, these scalar equations are used to determine a rough estimate of the computation times involved in the implementation of various filter/controller pairs. Although the results of Burkharts investigation indicate that the angular rate specification cannot be met, even when the input from the cascaded Kalman filter is assumed to be within design specifications, the angular rate specification is not neglected in the remainder of this investigation. As mentioned in Chapter II, the design approach is to provide improved angular rate control and to meet or exceed the angular position design specification.

Based on the results of Burkhart's investigation, the optimal control approach warrants further investigation as a method of isolating the inertial instrument test platform at FJSRL.

IV. Selection of Kalman Filter Model

All of the model development in the previous chapters was based on a sampling rate of 200 Hz. The selection of this sampling rate was based on engineering judgement i.e., it is five times the Nyquist frequency. In reality, since the computations involved in executing the optimal estimation and control algorithm take a finite length of time, the sampling rate will be limited by the instruction execution (arithmetic, store, shift, etc.) times of the PDP-11/03 Minicomputer. In this chapter, the Kalman filter models developed in Chapter II are combined, in turn, with the general model of the controllers developed in Chapter III to determine the approximate maximum sampling rate for each combination. Each filter is then tuned, using the General Covariance Analysis Program (GCAP), to determine an expected performance bound for that filter. The tuned filter performances are compared and a "best cut" filter model is selected as a baseline for future implementation. In addition, some implementation considerations are presented as background for possible "follow-on" investigation.

General Form of the Algorithm

The implementation of the optimal estimation and control algorithm, developed in this investigation, is separated into five tasks:

- Input
- Output

- Supervisor
- Pneumatic Control Loop
- Optimal Regulator Loop
- Kalman Filter

Input. The input task is to move the current measurement from the Analog-to-Digital Converter (ADC) to a storage register within the computer. Assuming the use of the PDP-11/03 compatable ADC (Model ADV-11-A), the measurement enters the computer, after conversion, in offset binary form. The input routine checks for overflow or underflow and the measurement data is converted to two's complement form since the arithmetic operations used by this algorithm are computed using two's complement arithmetic.

Output. The output routine is essentially the mirror image of the input routine. After all computations on control data are complete, the output routine converts the data from two's complement form to offset binary form, checks for overflow or underflow, and moves the data from a storage register to the Digital-to-Analog Converter (DAC).

Supervisor. The supervisor routine is used to control the sequencing of the other tasks. In addition, various "housekeeping" tasks (i.e., scaling, error checking, etc) can be accomplished in this routine.

The controllers and the Kalman filter are implemented in the remaining subroutines and are discussed in more detail below.

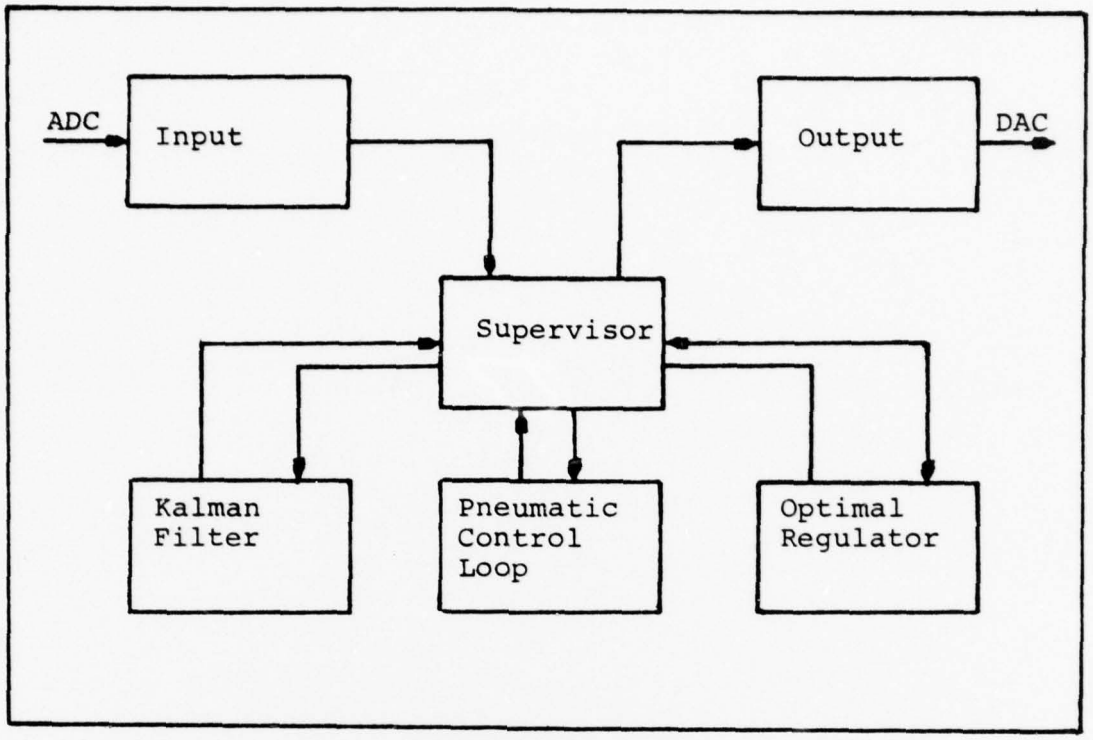

Figure 22. Implementation Tasks for Optimal Estimation and Control Algorithm.

Figure 22 is a block diagram representation of the tasks involved in the optimal estimation and control algorithm.

Computation Times

Based on the general form of the algorithm described above, the total computation time for the optimal estimation and control algorithm can be described as

$$T_C = ((T_I + T_O + T_P + T_R + T_K)*1.1) \qquad (106)$$

where

T_C = total computation time

T_I = input computation time

T_O = output computation time

T_P = pneumatic control loop computation time

T_R = optimal regulator computation time

T_K = Kalman filter computation time

The 1.1 multiplier represents a 10% overhead that is added to represent the supervisory operations.

Since there are actually two optimal estimation and control systems involved in isolating the platform (two horizontal axes through the center of the platform), the total approximate computation time, T_{AC}, will be

$$T_{AC} = 2T_C \tag{107}$$

For purposes of evaluating the sampling rates for the various Kalman filter models, the computation times for the input, output, pneumatic controller, and optimal regulator are considered to be the same for each filter case.

The instruction execution times, for the PDP-11/03 Minicomputer, for the instructions employed in the optimal estimation and control algorithm are presented in Table III (Ref 18)

All arithmetic operations are assumed to be single-precision fixed-point operations. Floating-point and/or double precision arithmetic operations would provide more accuracy for representing the terms, but it is felt that the increases in computation times involved more than offset the benefits derived. All coefficients are normalized

Table III

PDP-11/03 Instruction Execution Times

Instruction	Assembly Language Code	Execution Time (microseconds)
Move	MOV	3.5
Compare	CMP	6.65
Fixed-Point Subtraction	SUB	7.7
Fixed-Point Addition	ADD	7.7
Fixed-Point Multiply	MUL	64.0
Arithmetic Shift Combined	ASHC	15.0

(by scaling) so that they are represented as fractions. In this way, the multiplication operation will always result in a fraction and, therefore, multiplication overflows will be avoided. To illustrate the result, the following simple example is presented

$$\begin{array}{rcl} .1_2 & & .5_{10} \\ \times\ \underline{.1_2} & = & \underline{.5_{10}} \\ .01_2 & & .25_{10} \end{array} \qquad (108)$$

where $.1_2$ is the binary representation of .5 (decimal). The PDP-11/03 multiplication operation will result in the following product

$$\begin{array}{r} .1_2 \\ \times\ \underline{.1_2} \\ .1_2 \end{array} \qquad (109)$$

which is obviously an incorrect result. In order to correct the result, an Arithmetic Shift Combined (AHSC) instruction is used to shift the result right by one position (with a zero fill), resulting in a correct representation of the product. An AHSC instruction is provided with each multiplication instruction in this investigation. As indicated in Table III, this will increase the multiplication computation time by 15 microseconds for each operation, resulting in a total multiplication time of 79 microseconds.

Input/Output Computation Times. The input routine consists of one move instruction, two compare instructions (checking for overflow/underflow), and one fixed-point subtraction instruction (to convert from offset-binary to two's complement form) and results in a total computation time of approximately 24.5 microseconds. The output routine is essentially the mirror image of the input routine (except one fixed-point addition instead of subtraction to convert from two's complement to offset binary form) and also results in a total computation time of approximately 24.5 microseconds. The analog-to-digital and digital-to-analog conversion times are not included in the calculation of the I/O computation times since it is assumed that an interrupt scheme will be used for controlling the ADC, thus permitting simultaneous conversion and filter/controller algorithm execution, and it is also assumed that the DAC can complete its conversion process without interferring (based on Model

ADV-11-A Converter) with filter/controller algorithm execution.

Pneumatic Control Loop Algorithm. The pneumatic control loop algorithm is represented by Equations 99 through 103 in Chapter III.. The algorithm consists of a series of multiplications and additions. It is assumed that the common (constant) gain operation, K_D, in Equation 100, is accomplished using an external analog amplifer. An example of the steps involved in the execution of the algorithm is (using Equation 101)

MOV	TERM1,R2	(Move -0.999 into Register 2)
MUL	x6,R2	(Multiply $x_6(k)$ by -0.999 and store the product in Registers 2 and 3)
MOV	TERM2,R4	(Move 0.975 into Register 4)
MULT	x_8,R4	(Multiply $x_8(k)$ by 0.975 and store the product in Register 4)
ADD	R4,R2	(Add the products and store result in Register 2)
ADD	$x_6(k+1)$,R2	(Add $x_6(k+1)$ to previous sum, store result in Register 2)
MOV	R2,$x_8(k+1)$	(Move the result to memory location of $x_8(k+1)$)

The total pneumatic control algorithm requires 13 move instructions, 6 fixed-point additions, and 5 fixed-point multiplications, resulting in a total computation time of approximately 565.4 microseconds.

Optimal Regulator Algorithm. The optimal regulator algorithm is represented by Equations 104 and 105. In

a manner similar to the precedure used for the pneumatic control algorithm, the computation time for the optimal regulator loop was determined to be approximately 694.4 microseconds.

The total computation time for the input, output, and controllers is approximately 1308.8 microseconds. This computation time is assumed constant for all filter/controller combinations.

Kalman Filter Algorithms. The Kalman filter algorithms are represented by Equations 34 and 38. In order to allow for control inputs, each Kalman filter model is augmented with the state associated with the pneumatic actuator. The augmented state represents the output torque generated by the pneumatic actuators. Although the augmented models are not used during the covariance analysis to determine filter performance ("forced separation"), they are included in the implemented algorithm and do, therefore, affect the computation time for each filter. Therefore, the state matrices referred to in the Kalman filter computation time determination are the state matrices associated with the augmented filter models. These models are presented in Appendix E. To determine the computation times for the estimate propagation equation (Equation 34) for each filter, the general form of the state transition matrix (Φ) and the discrete control matrix (Γ) was derived (using the STM program with a sampling rate of 200 Hz) for each filter

AD-A064 179 AIR FORCE INST OF TECH WRIGHT-PATTERSON AFB OHIO SCH--ETC F/G 8/11
ANALYSIS AND IMPLEMENTATION OF OPTIMAL ESTIMATION AND CONTROL F--ETC(U)
DEC 78 P L TOLER

UNCLASSIFIED AFIT/GE/EE/78D-45 NL

2 OF 2
AD
A064 179

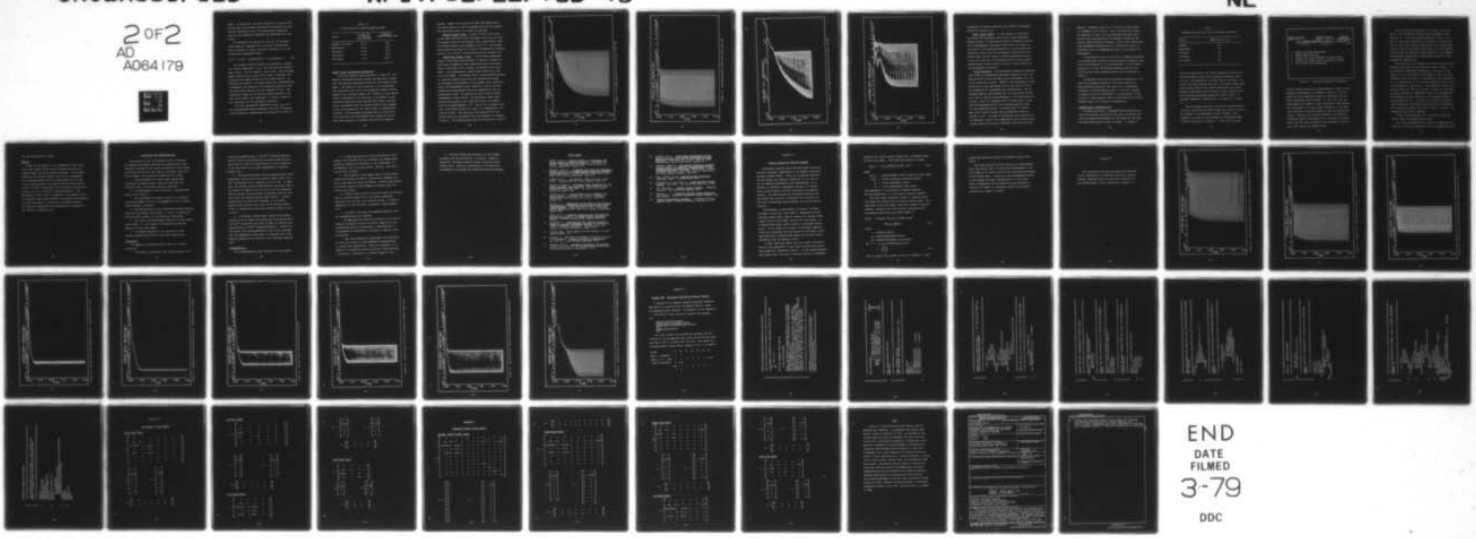

END
DATE
FILMED
3-79
DDC

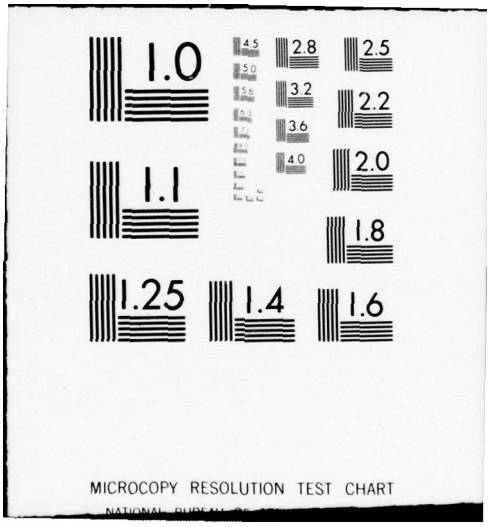
1.0
1.1
1.25
1.4
1.6
1.8
2.0
2.2
2.5
2.8
3.2
3.6
4.0
4.5
5.0
5.6
6.3
7.1
8.0
9.0
MICROCOPY RESOLUTION TEST CHART

model. By converting the matrix equations to scalar form, and applying the procedure employed for determing the controller computation times, the approximate computation time for the propagation equation was determined for each filter.

To determine the computation time for the estimate update equation (Equation 38), the matrix equation was again converted to scalar form which resulted in the set of equations represented below.

$$\hat{x}_i(t_k^+) = \hat{x}_i(t_k^-) + k_{i1}[\text{Residual 1}] + k_{i2}[\text{Residual 2}] \qquad (110)$$

The residual terms represent the difference between the current measurement, $z(t_k)$, and the predicted measurement, $H\hat{x}(t_k^-)$, and are common to each scalar, state estimate update equation for a given filter model, therefore, the residuals are computed once for each sample period. As mentioned previously, a constant Kalman gain implementation is employed, and therefore, the covariance equations and the Kalman gain equation are not computed on-line. The computation times for the estimate update equation, for each filter model, was determined in a manner similar to that described for the propagation equation.

The total approximate computation times, T_{AC}, and the corresponding maximum sampling rates for the various filter/controller combinations are presented in Table IV.

Table IV

Filter/Controller Maximum Sampling Rates

Filter	T_{AC} (Eqs 106 and 107) (milliseconds)	Maximum Sampling Rate (Hz)
Optimal (10 state)	22.17	45.1
Seven-state	15.63	64.0
Six-state	12.04	83.0
Five-state	10.95	91.4
Four-state	9.46	105.7

Kalman Filter Performance Evaluations

Using the sampling rates indicated in Table III, the General Covariance Analysis Program was employed to determine the expected performance bound for each Kalman filter model. The object of this evaluation is to investigate the possibility that one of the suboptimal Kalman filters, based on the increased sample rate (relative to the optimal filter) permitted by the reduction in the number of computations required by that reduced-order model, provides better performance than the optimal Kalman filter sampled at the rate dictated by the large number of computations involved. The performance measures used as criteria for this evaluation are the platform rate prediction errors which are produced as an output from the GCAP computer

program. Again, the criteria are that the angular position specification is met or exceeded and that the angular rate prediction error is as small as possible.

Optimal Kalman Filter. Figures 23 and 24 are plots of the time histories of the one-sigma errors for the platform angular position and angular rate, respectively, from the optimal Kalman filter sampled at 45.1 Hz. The steady-state prediction errors are 2.53×10^{-4} Arcseconds for angular position and 2.92×10^{-2} Arcseconds/Second for angular rate.

Seven-State Kalman Filter. A seven-state suboptimal Kalman filter model was developed in Chapter II based on a simplifying assumption which approximated the third-order noise filter model with a roughly equivalent white noise model. This approximation inserts more uncertainty into the filter model. The Kalman filter tuning process consists of inserting pseudo-noise into the reduced-order model, by increasing the strengths of the process noise (matrix Q) and/or the measurement noises (matrix R), until the true system error approximates the error generated by the reduced-order filter. By varying the white noise strength represented by the Q matrix, the equivalent white noise driving the platform, that tuned the filter, was determined to be approximately 3.25. This is not a unique solution, since other values for Q and R (in combination) will tune the filter. The resulting time histories for the angular position and angular rate are presented in Figures 25 and 26. The steady-state prediction errors are 3.34×10^{-4}

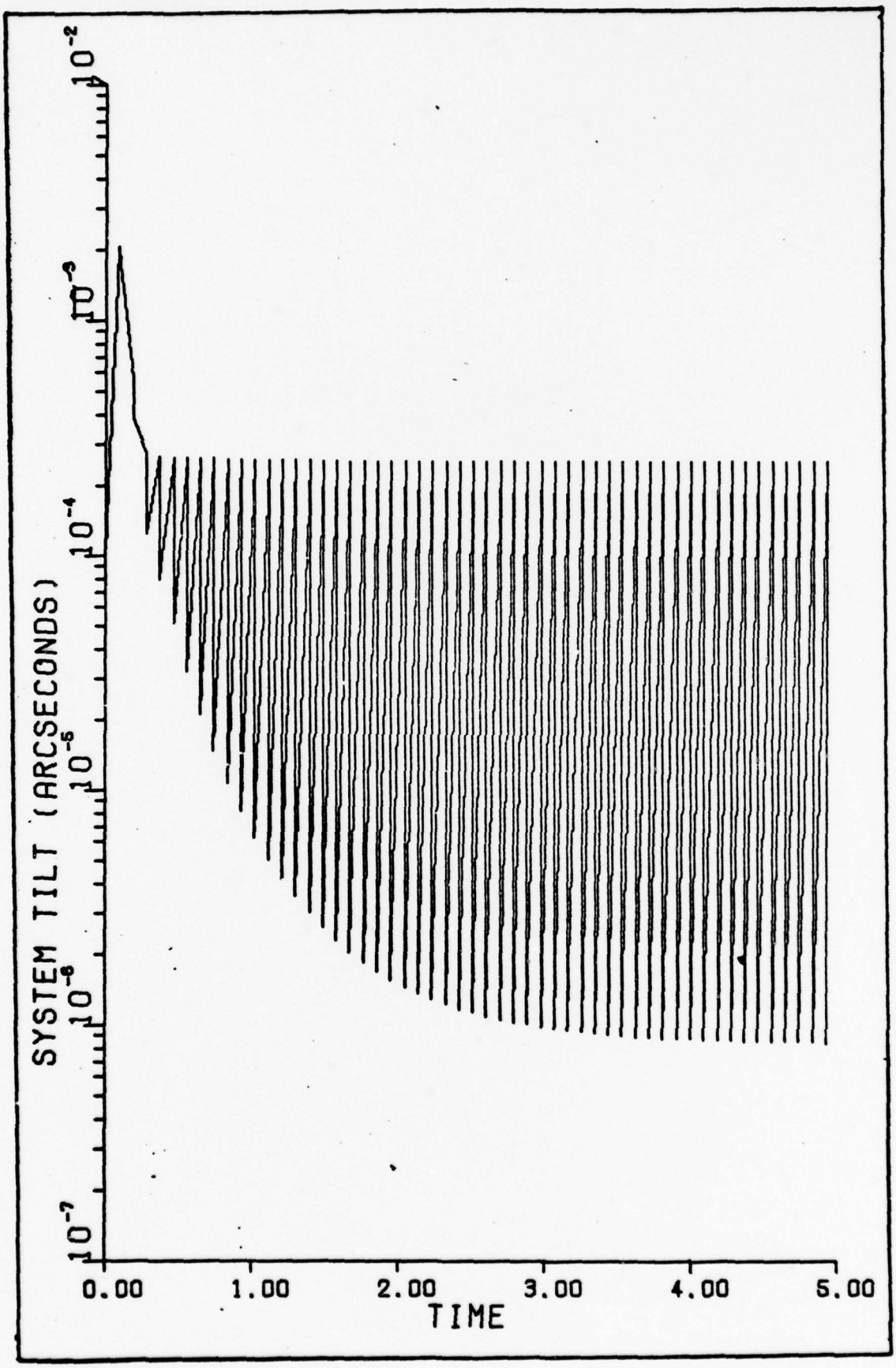

Figure 23. One-Sigma Optimal Filter Tilt Error (45.1 Hz)

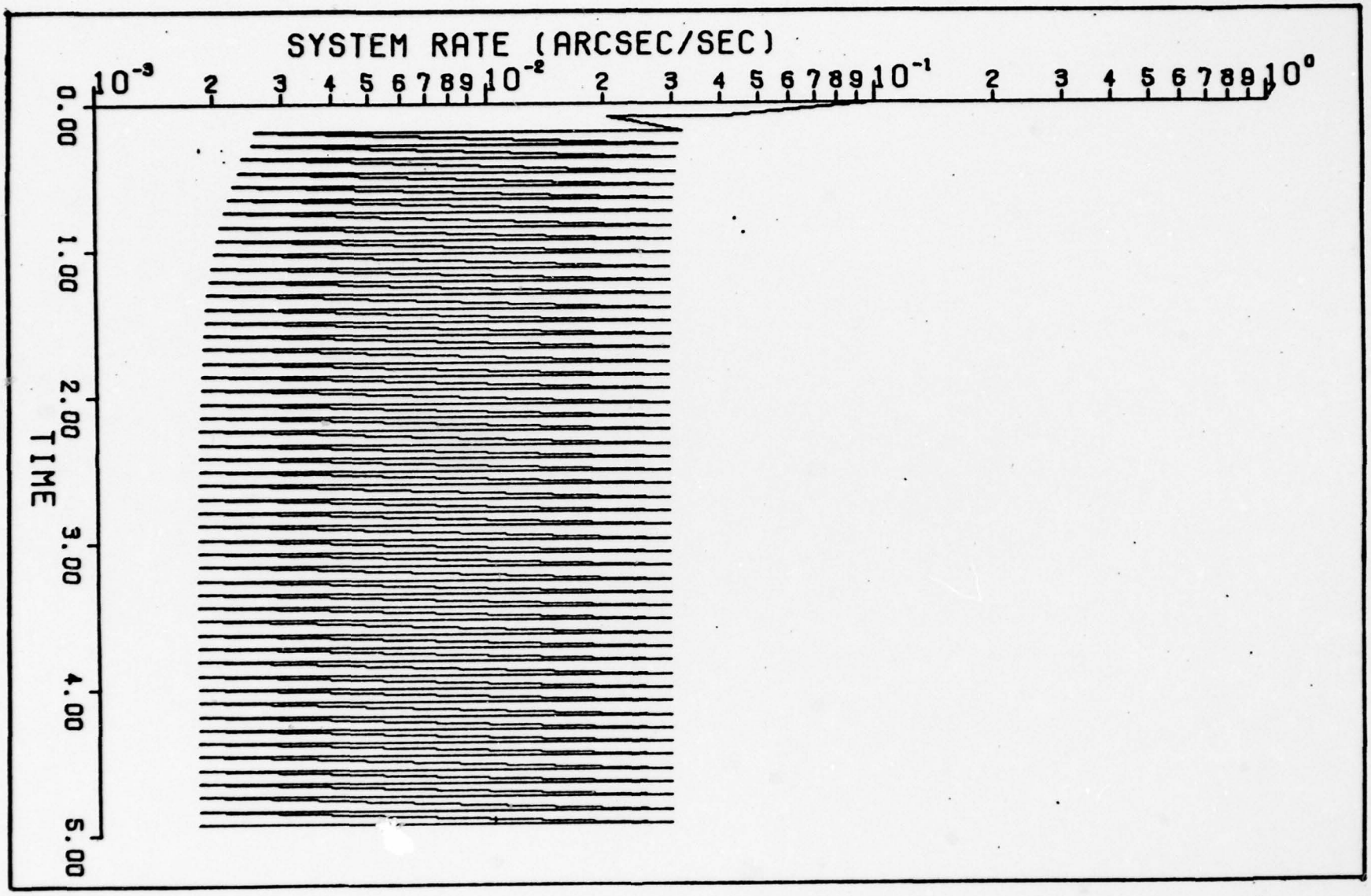

Figure 24. One-sigma Optimal Filter Rate Error (45.1 Hz)

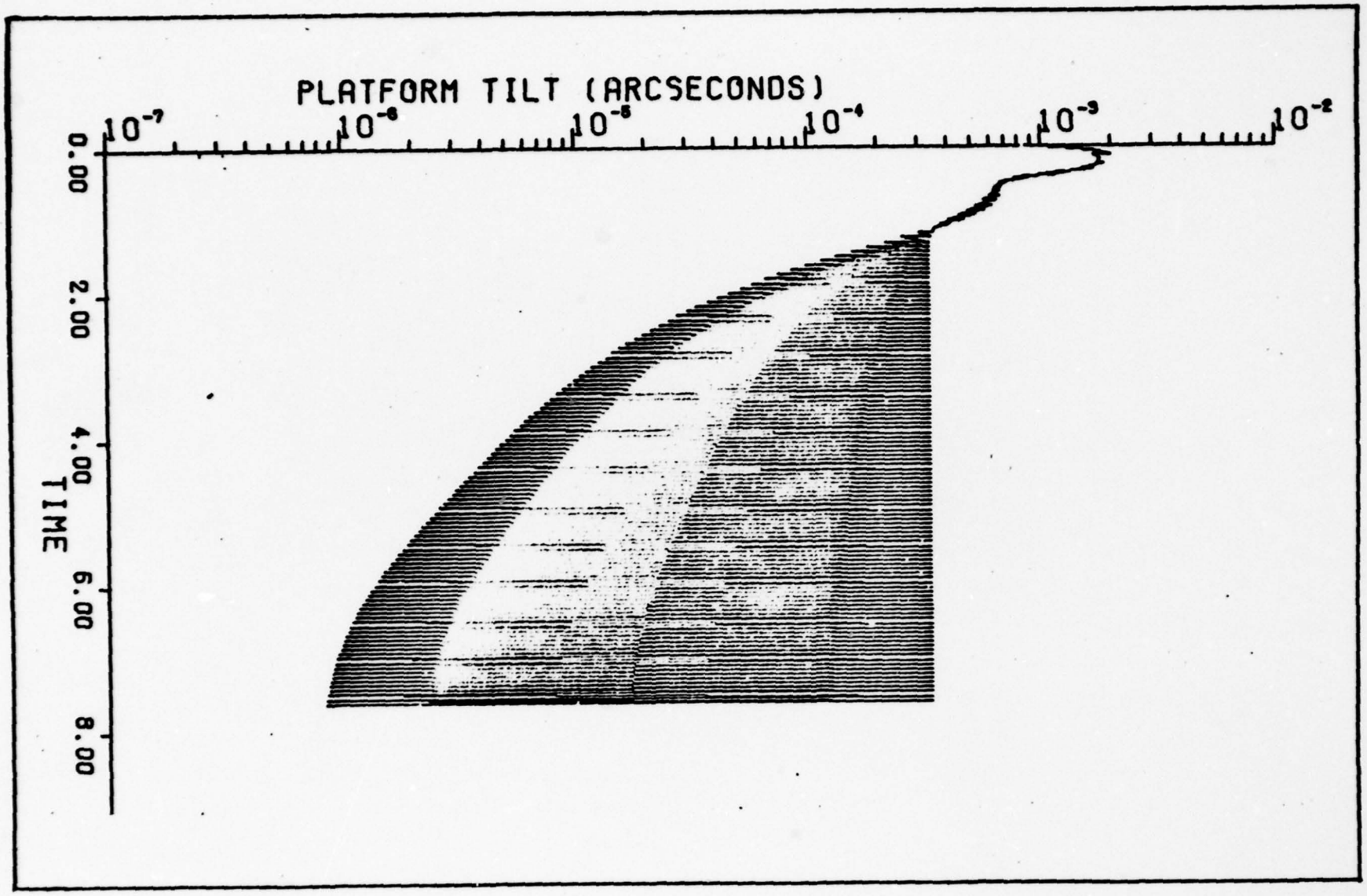

Figure 25. One-Sigma Seven-State Filter Tilt Error (64 Hz)

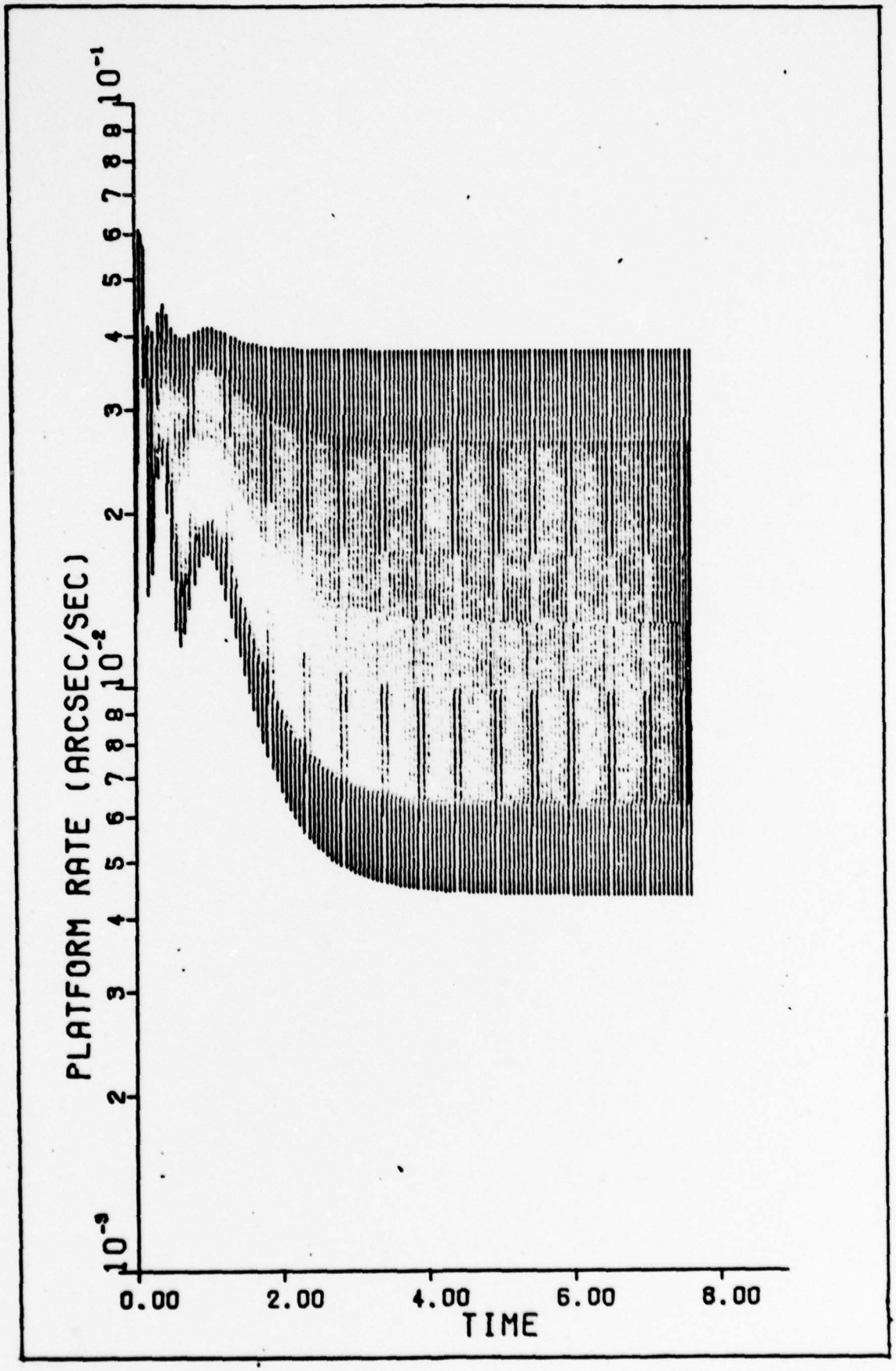

Figure 26. One-Sigma Seven-State Filter Rate Error (64 Hz)

Arcseconds for angular position and 3.78×10^{-2} Arcseconds/Second for angular rate.

Other Filter Models. In the process of tuning the six-state, the five-state, and the four-state suboptimal Kalman filters, the preliminary results indicated that the error performances from those filters were far worse (on the order of 200 Arcseconds/Second for the one-sigma rate prediction error) than the performance indicated for the higher-order filters. Based on these preliminary results, it was felt that the time-consuming task of tuning these reduced-order filters would be little, if any, benefit to the performance evaluation.

Filter Selection. The performance evaluation indicated that, based on the maximum permissible sampling rates, the optimal Kalman filter provides better performance than any of the suboptimal filters. However, the performance of the seven-state filter approaches that of the optimal filter and should not be eliminated from consideration. The increased sampling rate possible for the seven-state filter will tend to improve the performance of the associated controllers, and it is possible that the improvement in controller performance due to the increased sampling rate, for the suboptimal filter, is greater than the improvement due to better Kalman filter performance from the optimal filter. In order to investigate this possibility, two pneumatic control loop compensators and two associated optimal regulators would be designed, one controller pair

based on a sampling rate of 45.1 Hz and the other based on a sampling rate of 64 Hz. Each controller pair would be combined, in turn, with the associated Kalman filter and the total performance of the optimal estimation and control system would be evaluated. Due to time constraints, this performance analysis was not undertaken in this investigation but is recommended as part of a follow-on investigation.

A mulitarized version of the LSI-11 hardware multiplier is available that reduces the multiplication execution time from 64 microseconds to 12.2 microseconds. If the faster multiplier is used, the maximum sampling rates for the various filter model implementations are as indicated in Table IV.

As expected, since the multiplication operation is the most time consuming operation, the large reduction is multiplication execution time results in a significant increase in maximum sampling rates. Since the increase in sampling rates is significant, a re-evaluation of the filters at these sampling rates is warranted and is recommended as part of a follow-on investigation.

Implementation Considerations

Of prime importance in implementing the optimal estimation and control algorithm is the time lag between the time the sampled measurements are performed and the time the associated control signal is output. In order to

Table V

Maximum Sampling Rates Using High-Speed Multiplier

Filter	Sampling Rate (Hz)
Optimal	111
Seven-state	147
Six-state	218
Five-state	237
Four-state	239

reduce the magnitude of the state propagation (prediction) error generated by the state propagation equation (Equation 34), the computation lag time should be minimal. To ensure the least possible lag time, only those computations that actually require the updated measurement and those directly associated with the control output should be computed between measurement update and control output. A proposed sequence of computations is presented in Figure 27.

The two optimal estimation and control systems associated with the horizontal axes through the center of gravity are assumed to be independent control systems. This assumption is based on the assumption of decoupled modes of motion mentioned in Chapter I. Since each of these

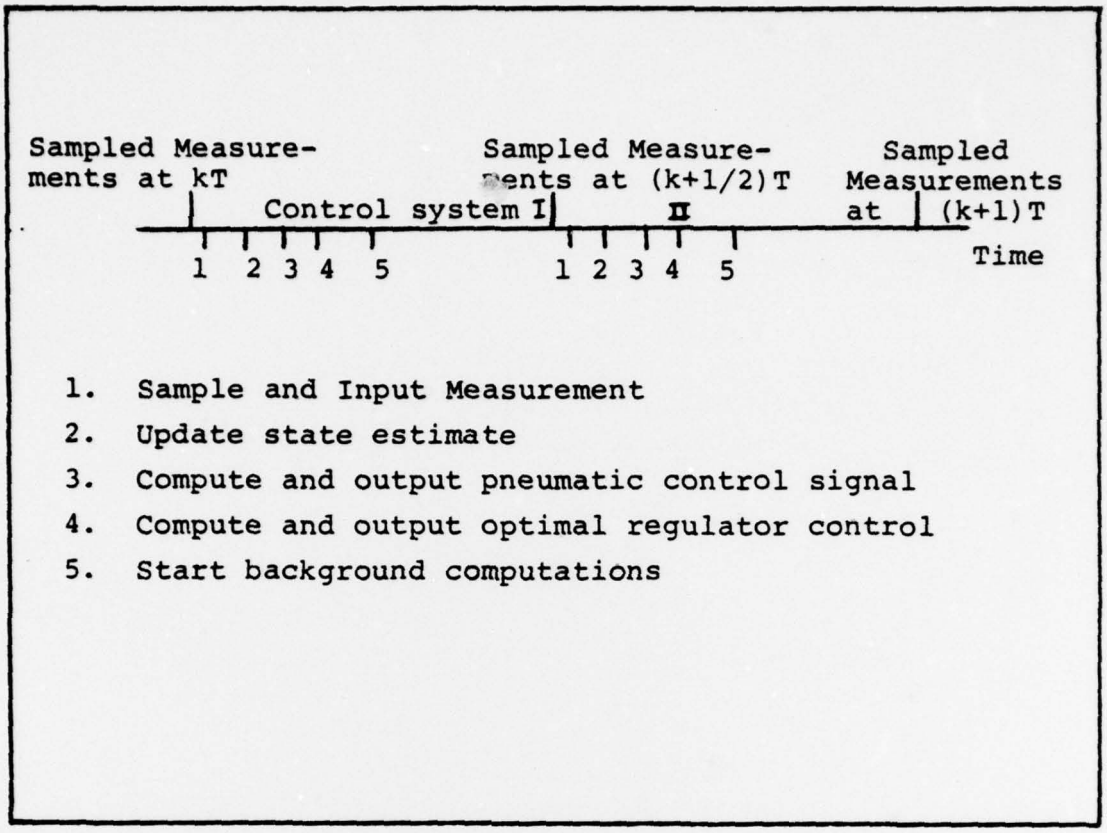

Figure 27. Algorithm Computations Sequence

control systems requires two measurements (a total of four separate measurements) per sampling interval, it is proposed that each sampling interval be separated into two equal independent sub-intervals. In this way, only two measurements are needed in each subinterval, thus reducing the measurement to control output lag while, at the same time, maintaining the same sampling rate for each control system. Further gain could be achieved if an additonal processing system (minicomputer) was available that would permit the two control systems to be executed in parallel and, thus, double the sampling rate.

After the sampled measurements are input, the next step is to determine the updated state estimates using Equation 38. Using the forced separation concept, since some of the states estimated by the Kalman filter are not used in the control output computations, only those states that are used in the control algorithm need to be updated at this time, the remaining state updates will be computed as background computations, immediately before the state propagation computations.

The next step is to compute and output the new control signals, beginning with the pneumatic control signal. In the pneumatic compensator development discussed in this thesis, the state variables were chosen so that the state associated with the input to the pneumatic loop compensator (x_6) is proportional to the platform angular position (x_1) as represented in Equation 80. By choosing the state variables so that the state x_6 is equal to state x_1, the multiplication required in Equation 99 would be eliminated and the pneumatic control signal could be computed simply by solving Equation 100. In addition, by using an external analog amplifier to perform the multiplication associated with the term K_D (after the control signal is output), the computation lag time is reduced.

Finally, using Equation 104, the optimal regulator control signal is generated and output.

The remaining equations are solved as background computations in the time remaining until the samples are taken

for the second control system.

Summary

Based on the results of the computation time evaluations, the optimal Kalman filter provides the best performance among the filter models developed. It was determined that the optimal Kalman filter can be implemented with a maximum sampling rate of approximately 45 Hz and, at this sampling rate, the angular position specification is met (2.53×10^{-4} Arcseconds) but the angular rate specification is not met (2.92×10^{-2} Arcseconds/Second). The performance of the filter is improved if the sampling rate is increased, and various methods of increasing the sampling rate were discussed. In addition, a proposed sequence for algorithm computation was presented for consideration for follow-on investigations.

V. Conclusions and Recommendations

The purpose of this investigation was to determine the expected performance derived from implementing linear stochastic estimation and control techniques to the problem of actively controlling the inertial instrument test platform at FJSRL. The study was divided into six areas:

1. The development of a state space system model from which an optimal Kalman filter was developed and evaluated using a covariance analysis tehcnique.

2. The development of four suboptimal (reduced-order) Kalman filter models.

3. The development of general models for a pneumatic (position-feedback) control loop compensator and an optimal (state-feedback) regulator.

4. The determination of the approximate maximum sampling rates for each Kalman filter model, in turn, in combination with the general models of the controller algorithms.

5. The tuning and performance evaluation of each Kalman filter model, in turn, based on the appropriate maximum sampling rate for that model.

6. A proposed sequence for the execution of the optimal estimation and control algorithm computations.

Conclusions

The specific conclusions derived from this investigation are:

1. As presently configured, the platform angular rate

uncertainty specification (1.667×10^{-5} Arcseconds/Second) cannot be met at any physically realizable sampling rate. The failure to meet this specification is due, primarily, to the fact there is no direct measurement of platform angular rate.

2. The platform angular position specification (1×10^{-3} Arcseconds) can be met by the optimal Kalman filter (2.53×10^{-4} Arcseconds) with a sampling rate of 45 Hz. In addition, the angular position specification can be met (Ref 1: 75) based on a sampling rate of 200 Hz and the assumption that the Kalman filter provides estimations that are accurate within the angular positon specification. Further investigation is required to determine if the angular position specification can be met by the optimal Kalman filter in cascade with controllers based on sampling rate of 45 Hz.

3. A suboptimal (seven-state) Kalman filter model, sampled at 64 Hz, meets the angular position specification (3.34×10^{-4} Arcseconds) but fails to meet the angular rate specification (3.78×10^{-2} Arcseconds/Second). Further investigation into the performance of this filter cascaded with the appropriate controllers is warranted due to the possible benefits to be derived by the increased sampling rate.

Recommendations

Five recommendations have resulted from this study:

1. A covariance analysis of the performance of the system, with the addition of an angular rate sensor model, should be completed to determine if the improvement in performance, due to the rate sensor, warrants the inclusion of such a sensor.

2. The stochastic noise models used in this investigation were primarily based on engineering judgement and not on any realistic empirical models. Further study should be directed toward the development of process noise and sensor error models.

3. Further study should be directed toward the development of accurate models of all the system components, especially the inertial test platform (center of gravity, homogeneity of the structure, resonances, bending modes, etc.).

4. In order to increase the maximum sampling rates, two recommendations are proposed:

- By employing the militarized version of the LSI-11 hardware multiplier the multiplication computation time is decreased from 64 microseconds to approximately 12 microseconds and substantial increases in sampling rates are derived.

- Even more substantial improvement can be derived by utilizing several microprogrammable microprocessors to perform the computations. With this approach, it is possible to accomplish several operations simultaneously (in parallel), resulting in increased sampling rates.

5. Further testing and evaluation of the optimal estimator and the controllers (in cascade), based on physically realizable sampling rates, should be accomplished using digitally implemented (on the PDP-11/03 minicomputer) algorithms and simulated noise disturbances.

Bibliography

1. Lamont, Gary B. Digital Control of a Pneumatic Isolation System for Inertial Testing. AIAA Paper No. 73-830. Key Biscaynce, Florida: AIAA Guidance and Control Conference, August 1973.

2. Burkhart, Martin J. A Digital Controller for Horizontal Angular Motion of the FJSRL Seismic Isolation Platform. Unpublished thesis. Wright-Patterson AFB, Ohio: Air Force Institute of Technology, June 1976.

3. Simmons, Bill J. Lab Sponsor, FJSRL (personal interview). United States Air Force Academy, June 1978.

4. Brunson, Richard L. An Optimal State Estimator for the FJSRL Instrument Test Platform. Unpublished thesis. Wright-Patterson AFB, Ohio: Air Force Institute of Technology, March 1976.

5. Lorenzini, D. A. Active Control of a Pneumatic Isolation System. AIAA Paper No. 72-843. Stanford, California: AIAA Guidance and Control Conference, August 1972.

6. Wittry, J. P. Description of an Inertial Test Facility Incorporating a Passively Isolated and Actively Stabilized Platform. AIAA Paper No. 69-863. Princeton: AIAA Guidance, Control, and Flight Dynamics Conference, August 1969.

7. Wynne, M. W. A Classical Analysis into the Stability and Control of the F. J. Seiler Seismic Isolation System. Software Sciences Corp. Paper, March 1973.

8. Broderson, E. Stabilization of a Seismic Isolation Block for Inertial Instrument Testing. AIAA Paper No. 74-857. Anahiem, California: AIAA Mechanics and Control of Flight Conference, August 1974.

9. Grimes, Gary. FJSRL Report Contract #F05611-76-90203, Kappa Systems, Inc.

10. Lorrain, P. "Low Natural Frequency Vibration Isolator or Seismograph," Review of Scientific Instruments, Vol. 45, No. 2, pp. 198-202, February 1974.

11. Maybeck, Peter S. Stochastic Estimation and Control. Course Notes from EE 7.12, Wright-Patterson AFB, Ohio: Air Force Institute of Technology, 1975.

12. Simmons, Bill J. Multi-Sensor Measurement of the Motion Stability of an Active Controlled Isolation Test Pad. AIAA Paper No. 75-181. Boston: AIAA Guidance and Control Conference, August 1975.

13. Hamilton, Edward L. The General Covariance Analysis Program (GCAP), An Efficient Implementation of the Covariance Analysis Equations. Users Guide. Wright-Patterson AFB, Ohio: Air Force Avionics Laboratory, Air Force Systems Command, June 1976.

14. Gelb, Arthur, et al. Applied Optimal Estimation. Cambridge, Mass.: The MIT Press, 1974.

15. Kwakernaak, H. and Sivan, R. Linear Optimal Control Systems. New York: John Wiley and Sons, Inc., 1972.

16. Kuo, Benjamin C. Digital Control Systems. Champaign, Illinois: SRL Publishing Company, 1977.

17. Meditch, J. S. Stochastic Optimal Linear Estimation and Control. New York: McGraw-Hill Book Company, 1969.

18. Digital Microcomputer Handbook. Information Manual. Maynard, Mass.: Digital Equipment Corporation, 1977.

Appendix A

General Covariance Analysis Program

Performance analyses were performed using covariance analysis techniques implemented on the General Covariance Analysis Program (GCAP). Since the covariance equations and the Kalman gain equation (equations 35, 39, and 40) can be computed independent of any measurements, it is possible to perform a performance analysis of a Kalman filter design without actually simulating the sampling process. The GCAP employs the covariance equations and the Kalman gain equation to generate the statistics (in the form of one-sigma time histories) of a filter design, directly.

Two mathematic system models are used by the GCAP. One model, called the "truth model", represents the best available system model (used to develop the optimal Kalman filter) and the other model, called the filter model, is a reduced-order model used to develop a suboptimal Kalman filter. As the order of the model is decreased, modeling errors are introduced into the design and the Kalman filter based upon such a reduced-order model will provide poorer performance than the optimal filter.

In GCAP, both truth model and filter model covariance matrices are propagated in time using a fourth-order Runge-Kutta numerical integration formula. At each sample measurement update time, the filter covariance update is performed

(Equation 39) and an optimal Kalman gain is computed based on the filter model. The Kalman gain equation becomes

$$K_F(t_k) = P_F(t_k)H_F^T[H_F P_F^-(t_k)H_F^T + R_F]^{-1} \quad (111)$$

where

$K_F(t_k)$ = Optimal Kalman filter (based on filter model)

$P(\bar{t}_k)$ = Filter covariance prediction matrix

H_F = Filter measurement matrix

R_F = Filter measurement noise matrix

the superscript T is the matrix transpose operator, and the superscript -1 is the matrix inversion operator.

The truth model covariance update is computed using the Kalman gain matrix derived from the filter model. The magnitude of the truth model covariance elements (diagonal elements) represent the "true system" one-sigma errors. The equation describing the system update is

$$P_S^+(t_k) = (I-MK_F(t_k)\ H_S)P_S^-(t_k)(I-MK_F(t_k)H_S)^T + MK_F(t_k)R_S K_F^T(t_k) \quad (112)$$

where

I = Identity matrix

H_S = System measurement matrix

R_S = System measurement noise matrix

and M = is the transformation matrix

$$M = \begin{bmatrix} I \\ \underline{1} \\ 0 \end{bmatrix} \quad (113)$$

used to augment the K_F matrix with null elements in order

to make the matrices conform for arithmetic matrix operations.

The tuning process involves varying the tuning parameters (Q_F and R_F) until the covariance performance of the truth model is at least a good as the covariance performance of the filter model. Varying the tuning parameters refers to the process of adding "pseudo-noise" to the filter model to compensate for the modeling errors produced by reducing the amount of information known by the system (reducing the number of states).

Appendix B

The following plots are one-sigma error time histories, generated by the General Covariance Analysis Program, resulting from the sensitivity analysis of the optimal Kalman filter, performed in Chapter II.

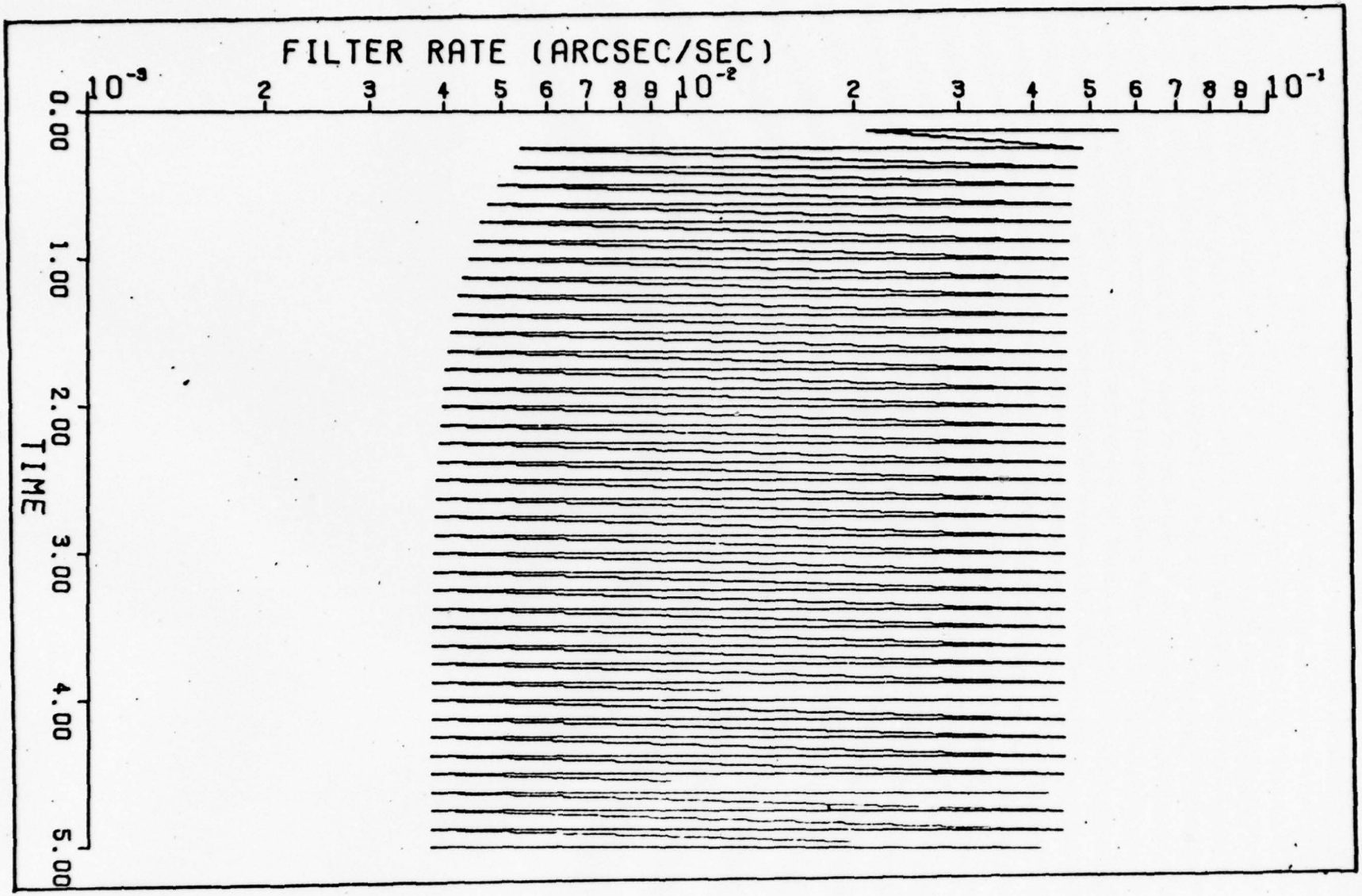

Figure 28. Optimal Filter Rate Prediction Error: Sampling Rate is 40 Hz.

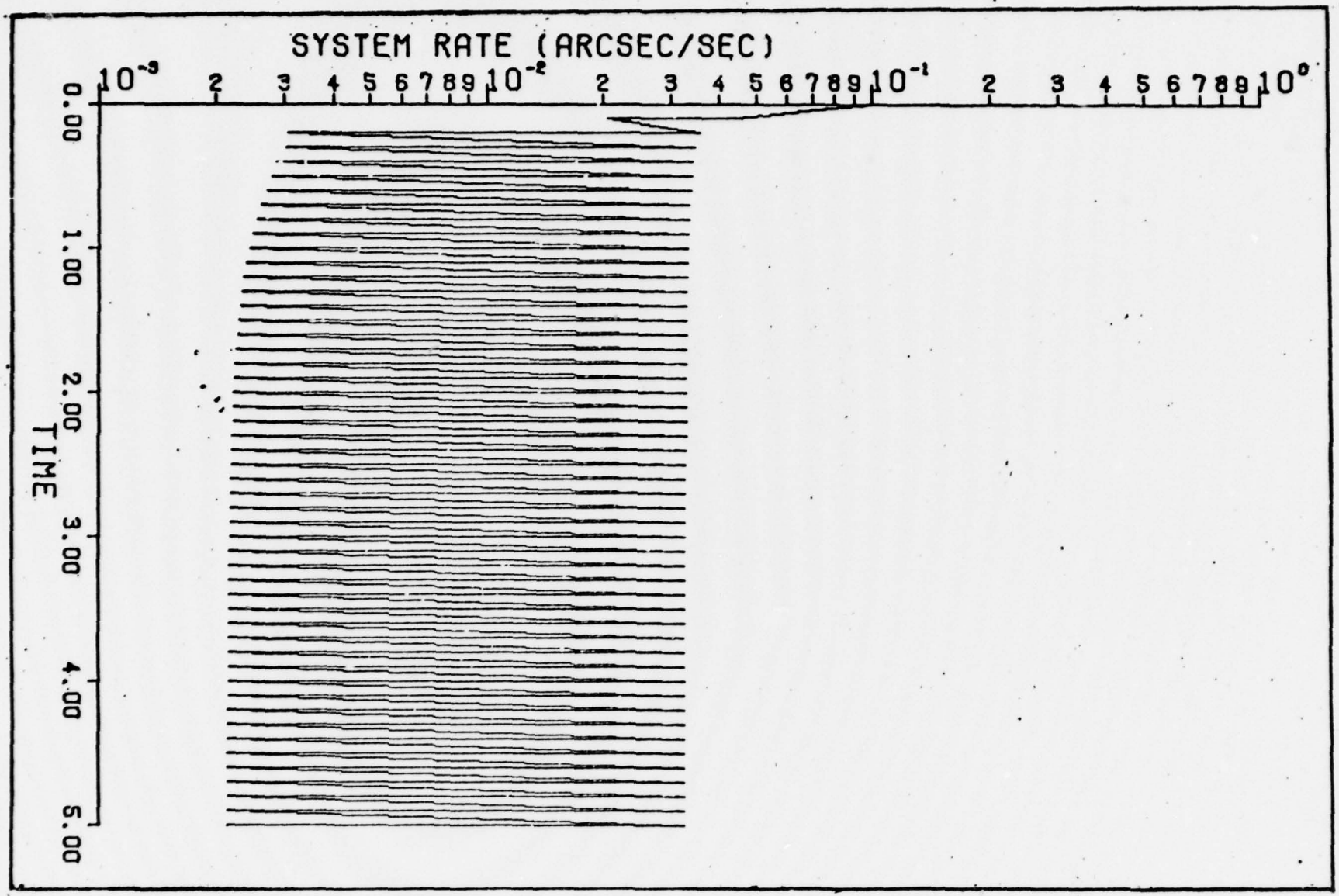

Figure 29. Optimal Filter Rate Prediction Error: Sampling Rate is 50 Hz.

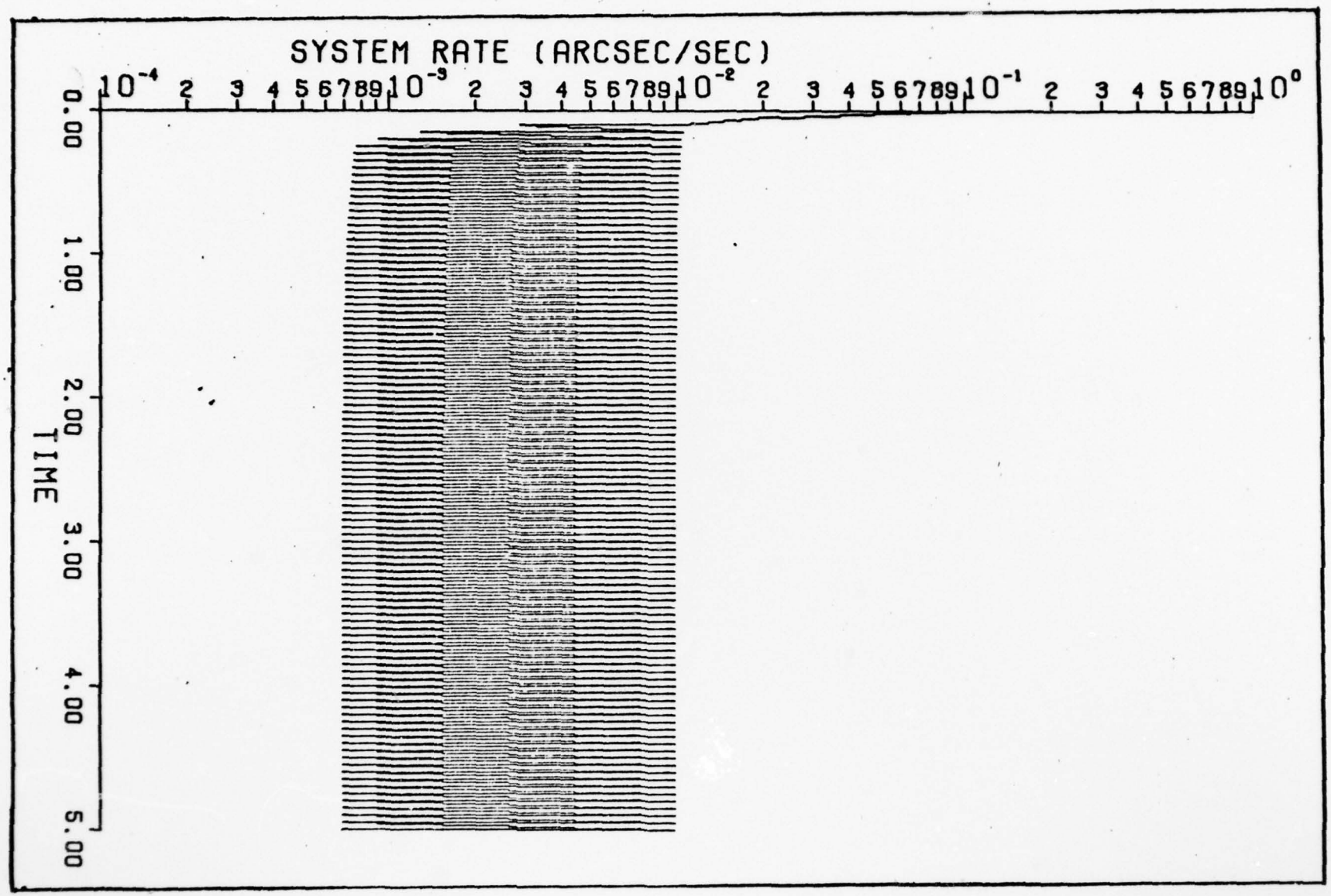

Figure 30. Optimal Filter Rate Prediction Error: Sampling Rate is 100 Hz.

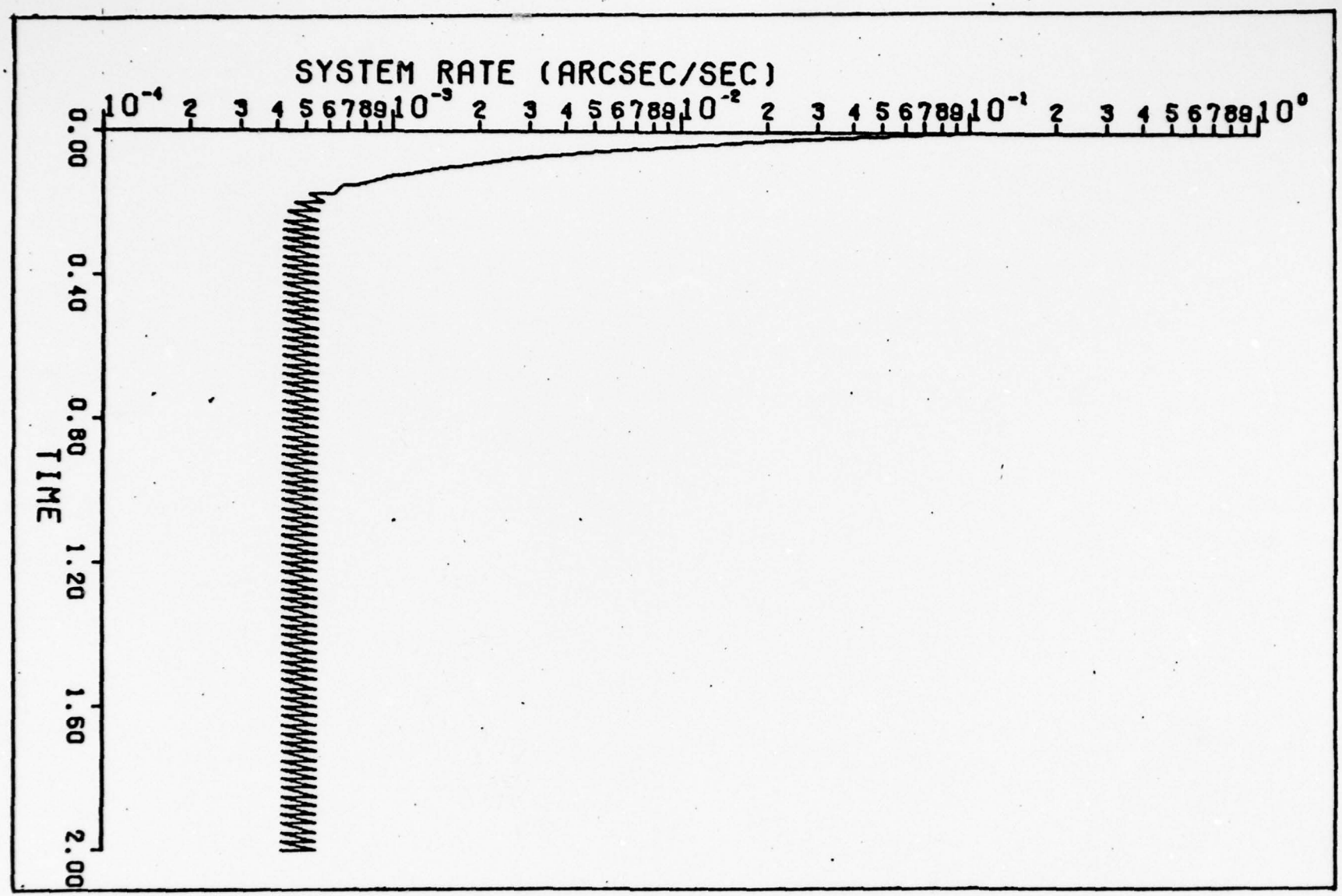

Figure 31. Optimal Filter Rate Prediction Error: Sampling Rate is 2 kHz.

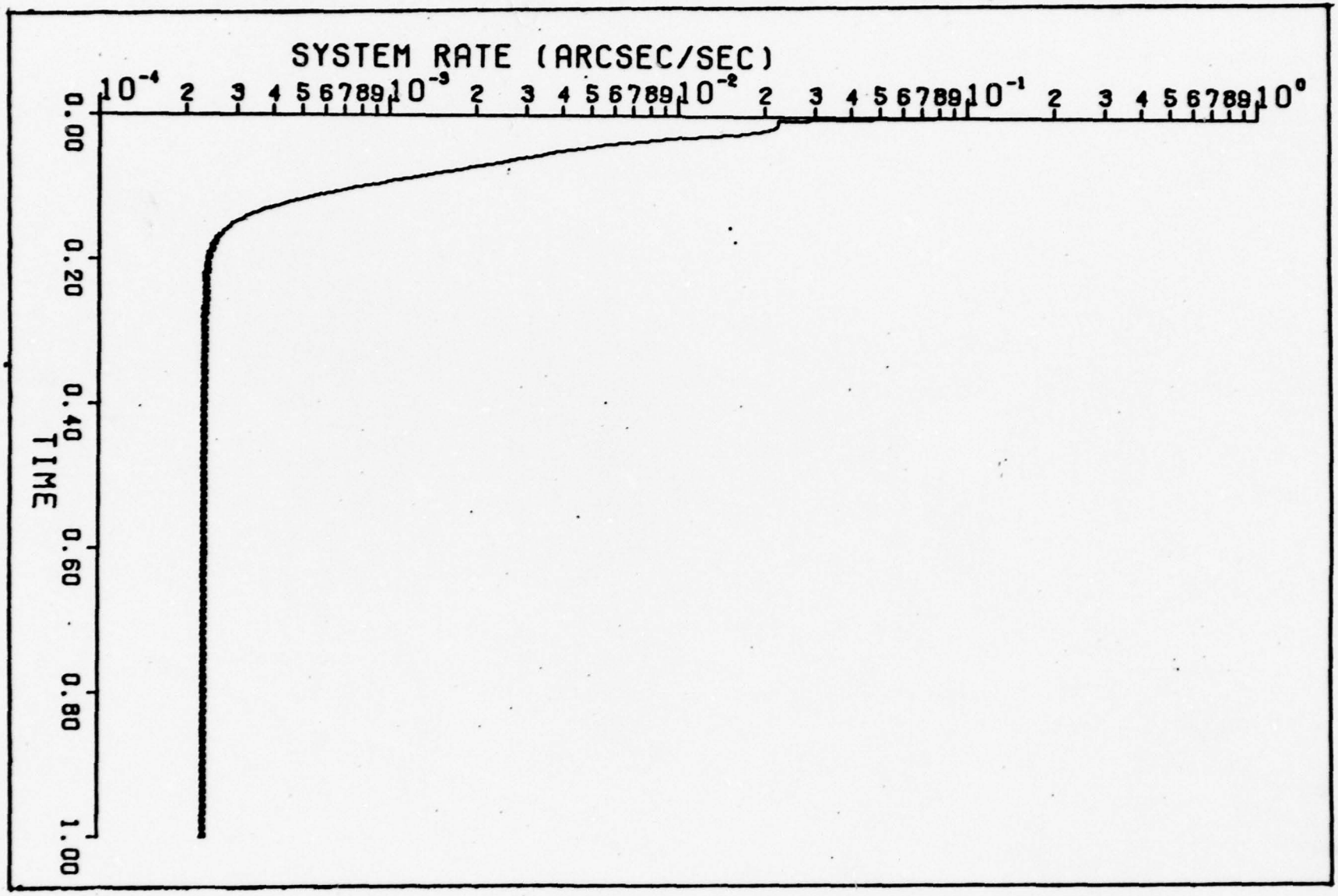

Figure 32. Optimal Filter Rate Prediction Error: Sampling Rate is 20 kHz.

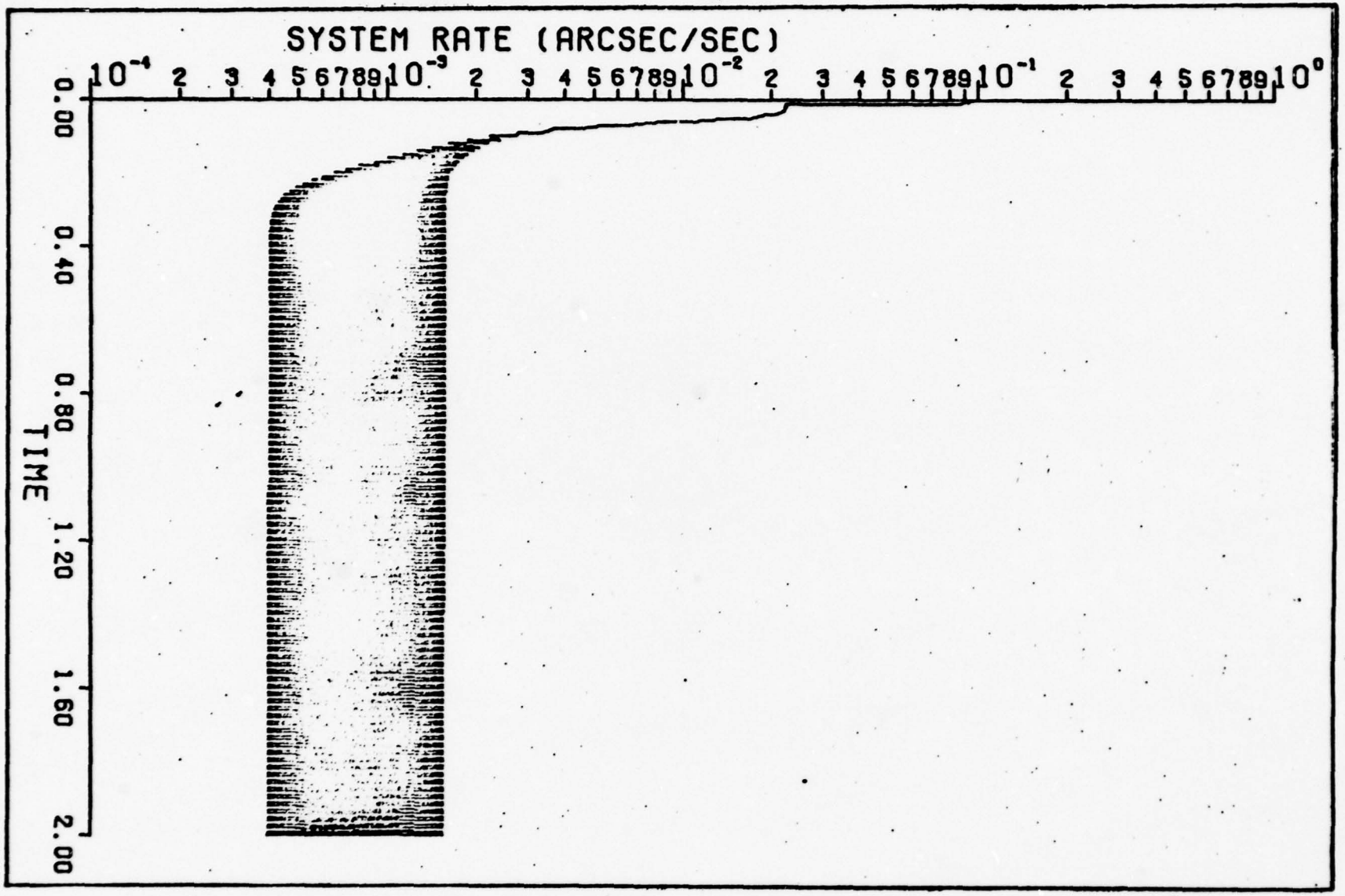

Figure 33. Optimal Filter (200 Hz) Low Process Noise

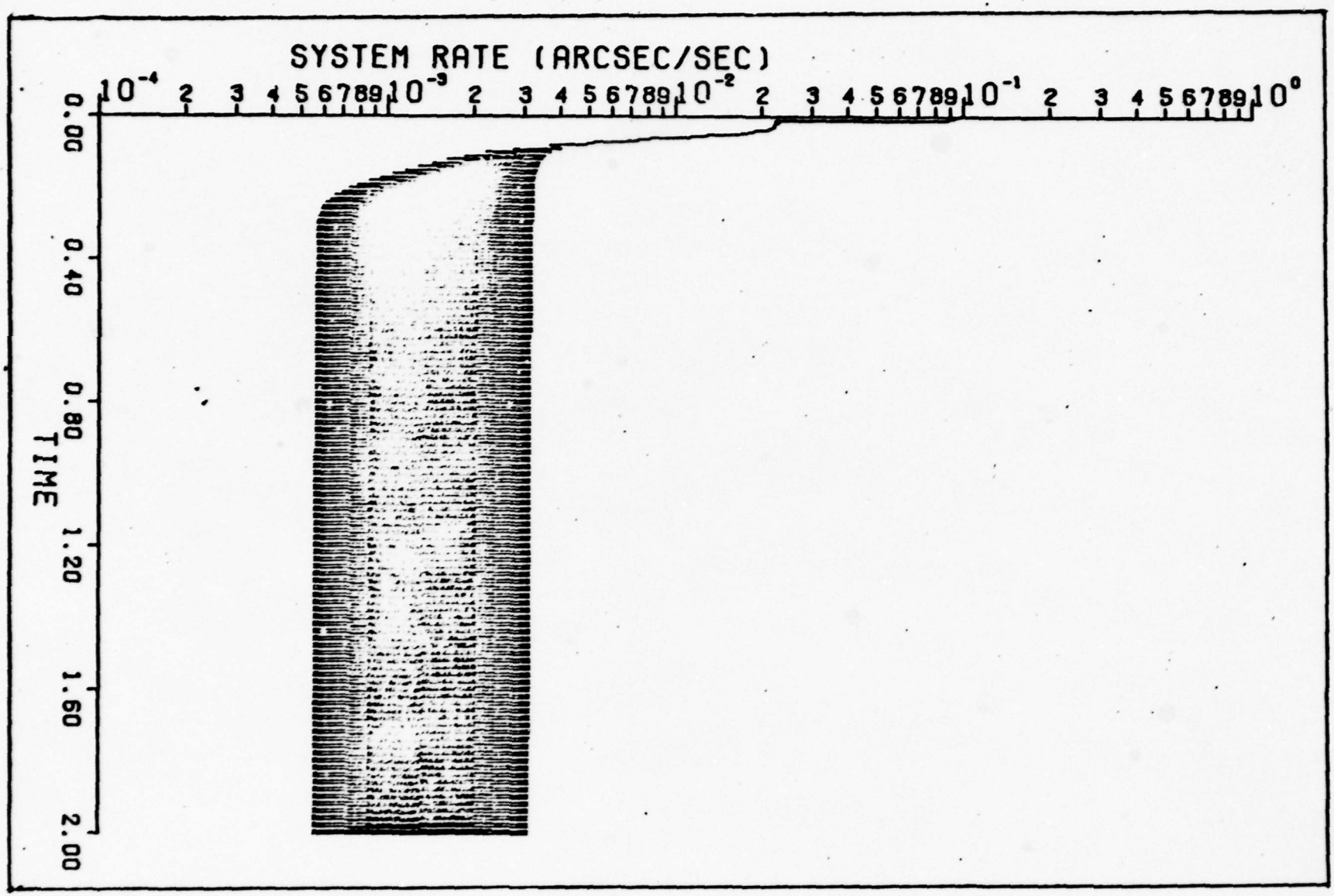

Figure 34. Optimal Filter (200 Hz) Increased Tiltmeter Sensitivity.

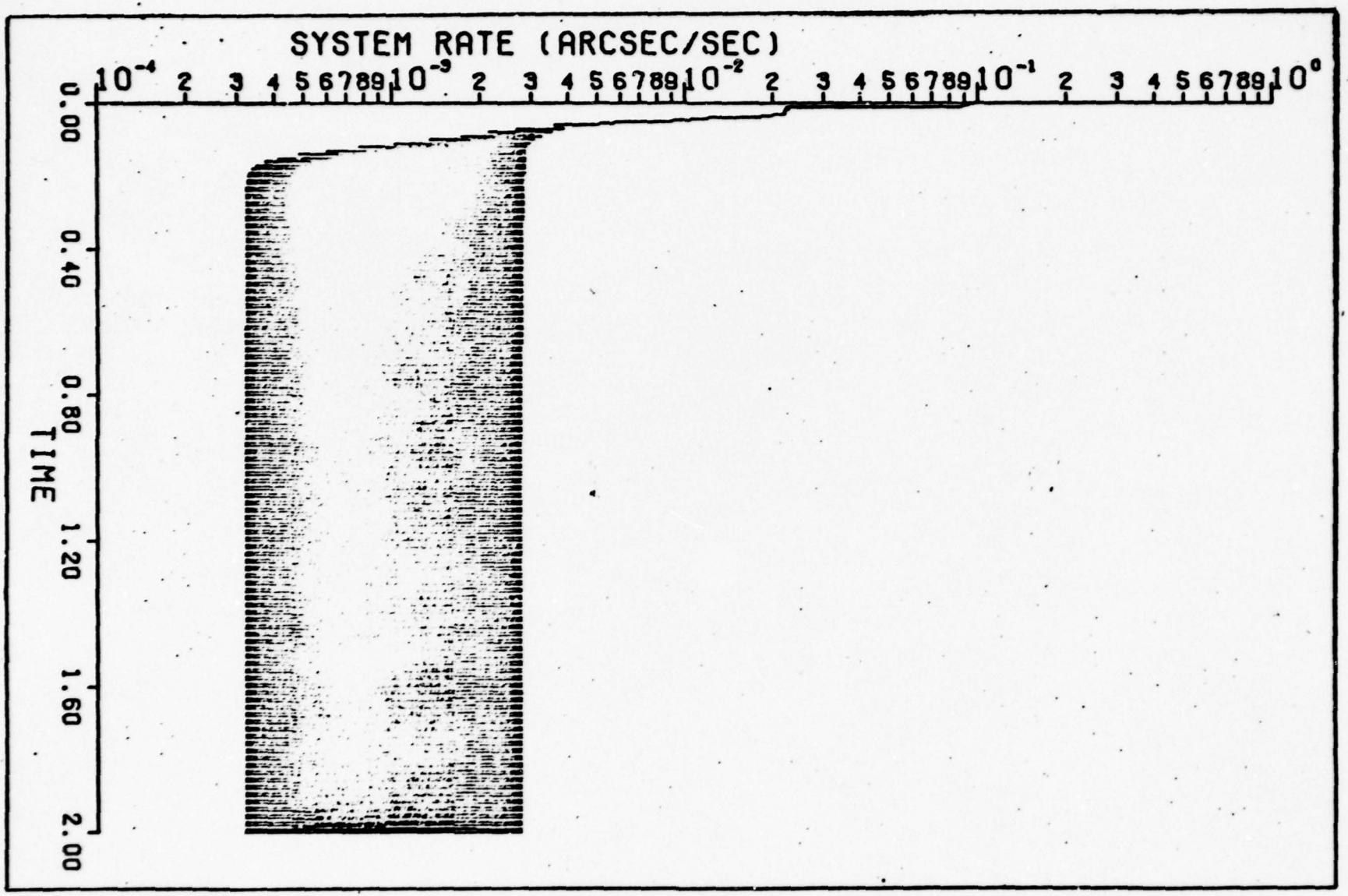

Figure 35. Optimal Filter (200 Hz) Increased Seismometer Sensitivity.

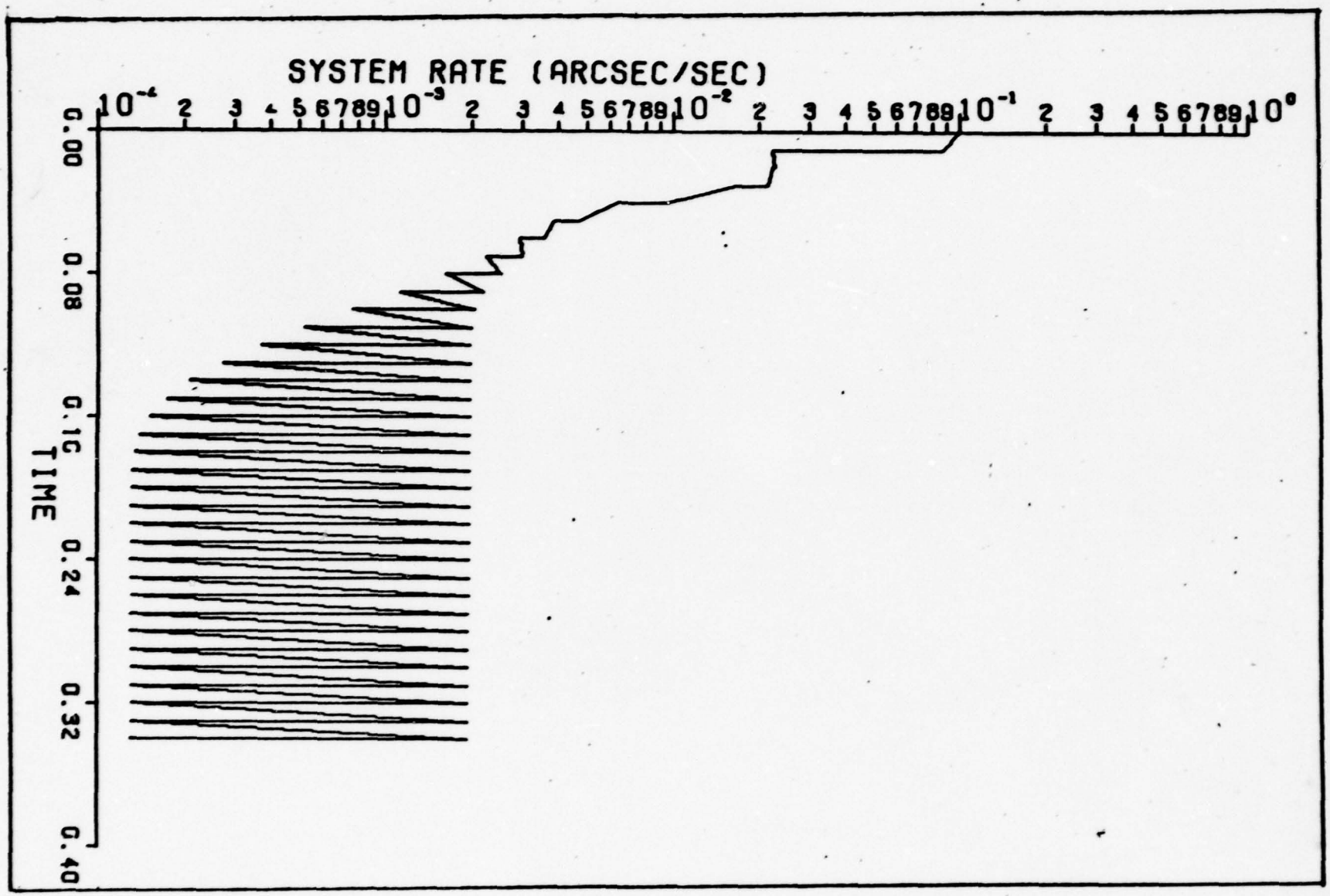

Figure 36. Optimal Filter (200 Hz) Increased Tiltmeter and Seismometer Sensitivity.

Appendix C

Program STM - Quantized Eigenvalue Analyses Program

A listing of the computer program developed (modified from Ref 3) to analyze finite wordlength effects, based on eigenvalue shift criteria, is presented in this appendix.

The control cards required to execute the program are

```
ATTACH,A,M371SUB,10=AFIT.
ATTACH,BIMSL,10=LIBRARY,SN=ASD.
ATTACH,AFIT,AFITSUBROUTINES,ID=AFIT.
FTN.
LDSET(LIB=A/B/AFIT).
LGO.
```

The input record file consists of the data card described in the program and input cards containing the state matrices F and L (in that order) by rows. The format for the data cards is shown below (example is for 2 x 9 matrix)

Column	10	20	30	40	50	60	70
Card 1 - Dimension	2	9					
Cards 2 to 5 - Data	0	1	0	0	0	0	2.156
(Right Justified)	0	2.56					
	-49	0	1	2	4	5	6
	7	8					

```
      PROGRAM STM(INPUT,OUTPUT,TAPE5=INPUT,TAPE6=OUTPUT)
C
C     ******************************************************************
C
C     THIS PROGRAM DISCRETIZES A CONTINUOUS SYSTEM OF THE FORM
C        DX
C        -- = F*X + L*U
C        DT
C
C     INTO THE DISCRETE FORM GIVEN BY
C
C        X(N+1)=A*X(N)+B*U(N)
C
C     WHERE A IS THE STATE TRANSITION MATRIX AND B IS THE CONTROL
C     TRANSITION MATRIX. THE EXACT EIGENVALUES ARE THEN COMPUTED
C     FOR THE DISCRETE SYSTEM.
C     THE STATE TRANSITION MATRIX IS QUANTIZED FOR WORDLENGTHS
C     BETWEEN NBITS1 AND NBITS2 (SPECIFIED BY THE USER). AT EACH
C     WORDLENGTH, THE QUANTIZED EIGENVALUES, THE EIGENVALUE SHIFT
C     (FROM THE EXACT EIGENVALUES), AND THE NORMALIZED SHIFT (QUANTIZED
C     EIGENVALUE SHIFT DIVIDED BY THE DISTANCE FROM THE EXACT
C     EIGENVALUE TO THE UNIT CIRCLE) IS COMPUTED AND PRINTED.
C
C     ******************************************************************
C
      DIMENSION F(15,15),FN(15,15),C(15,15),ETDAT(15,15),
     1 G(15,15),BD(15,15),WK(50),ADIG(15,15),B(15,15),
     2 EM(15),DE(15),A(15),RM(20)
      COMPLEX W(15),Z(15,15),TL(15),W1(15),Z1(15,15),SH(15)
```

```
C
C     ****************************************************************
C
C     READ PARAMETERS--                                          FORMAT
C                 K = ORDER OF THE SYSTEM                         I5
C                 M = NUMBER OF COLUMNS IN L                      I5
C            NBITS1 = SMALLEST WORDLENGTH OF INTEREST             I5
C            NBITS2 = LARGEST WORDLENGTH OF INTEREST              I5
C                DT = SAMPLING INTERVAL (IN SECONDS)             F10.5
C
C     ****************************************************************
C
      READ 100,K,M,NBITS1,NBITS2,DT
      PRINT 106
C
C     ****************************************************************
C
C     PRINT SAMPLING INTERVAL
C     READ AND PRINT CONTINUOUS SYSTEM MATRICES F AND L
C
C     ****************************************************************
C
      PRINT 105,DT
      PRINT*," "
      PRINT*," "
      PRINT*," "
      CALL MREAD(F,K,K,15,5)
      CALL MPRINT(F,K,K,15,6,"   F MATRIX")
      CALL MREAD(G,K,M,15,5)
      CALL MPRINT(G,K,M,15,6,"   G MATRIX")
C
```

```
C     ***********************************************************
C
C     COMPUTE STATE TRANSITION MATRIX , A , BY SOLVING FOR FIRST 100
C     TERMS OF TAYLOR SERIES EXAPNSION
C
C     ***********************************************************
C
      DO 1 I=1,K
      DO 1 J=1,K
      FN(I,J)=F(I,J)
      ETOAT(I,J)=0.0
1     ETOAT(I,I)=1.0
      FACT=DT
      DO 2 I=1,K
      DO 2 J=1,K
2     ETOAT(I,J)=ETOAT(I,J)+F(I,J)*DT
      DO 3 II=2,100
      FACT=FACT*DT/II
      CALL MMPY(C,FN,F,K,K,K,15)
      DO 3 I=1,K
      DO 3 J=1,K
      ETOAT(I,J)=ETOAT(I,J)+C(I,J)*FACT
C
C     ***********************************************************
C
C     PRINT AND SAVE A SINCE IT IS DESTROYED BY IMSL ROUTINE EIGRF
C
C     ***********************************************************
C
      B(I,J)=ETOAT(I,J)
3     FN(I,J)=C(I,J)
      CALL MPRINT(ETOAT,K,K,15,6,"   A MATRIX")
C
```

```
C     ************************************************************
C
C     COMPUTE AND PRINT EIGENVALUES OF DISCRETE MATRIX
C
C     ************************************************************
C
      CALL EIGRF(ETOAT,K,K,1,W,Z,K,WK,IER)
      PRINT*, "    EXACT EIGENVALUES"
           DO 1003 I=1,K
1003       PRINT 103,W(I)
C
C     ************************************************************
C
C     COMPUTE AND PRINT MAGNITUDES OF THE EIGENVALUES OF DISCRETE
C     MATRIX
C
C     ************************************************************
      PRINT*,"   EXACT EIGENVALUE MAGNITUDE"
      DO 14 I=1,K
      EM(I)=CABS(W(I))
14    PRINT 101,EM(I)
C
C     ************************************************************
C
C     COMPUTE AND PRINT DISTANCE FROM UNIT CIRCLE TO EIGENVALUES OF
C     DISCRETE MATRIX
C
C     ************************************************************
C
      PRINT*,"   DISTANCE FROM UNIT CIRCLE"
      DO 15 I=1,K
      DE(I)=1.0-EM(I)
15    PRINT 101,DE(I)
           DO 4 I=1,K
4          TL(I)=W(I)
C
```

```
C     ***************************************************************
C
C     FIND SCALE FACTOR THAT MAKES ALL STATE TRANSITION MATRIX ELEMENTS
C     LESS THAN ONE
C
C     ***************************************************************
      SCALE=1.
           DO 6 I=1,K
                DO 6 J=1,K
5               IF(ABS(B(I,J)/SCALE).LT.1.) GO TO 6
                SCALE=SCALE*10
                GO TO 5
6          CONTINUE
C
C     ***************************************************************
C
C     QUANTIZE STATE TRANSITION MATRIX FOR WORDLENGTHS FROM NBITS1 TO
C     NBITS2
C
C     ***************************************************************
C
          DO 17 N=NBITS1,NBITS2
               DO 7 I=1,K
                    DO 7 J=1,K
                    VAL=ABS(B(I,J)/SCALE)
                    CALL QUANT(N,VAL,VALDIG)
                    VALDIG=SIGN(VALDIG,B(I,J))
7              ADIG(I,J)=VALDIG*SCALE
C
C     PRINT WORDLENGTH
C
      PRINT 104,N
C
```

```
C     ***********************************************************************
C
      PRINT*,"   QUANTIZED MATRIX"
C
C     ***********************************************************************
C
           DO 1004 I=1,K
1004       PRINT 103,(ADIG(I,J),J=1,K)
C
C     ***********************************************************************
C
C     COMPUTE AND PRINT EIGENVALUES OF QUANTIZED STATE TRANSITION
C     MATRIX
C
C     ***********************************************************************
C
      DO 20 I=1,K
      W1(I)=0.0
      DO 20 J=1,K
      Z1(I,J)=0.0
   20 CONTINUE
      CALL EIGRF(ADIG,K,15,0,W1,Z1,15,WK,IER)
           PRINT*,"           EIGENVALUES"
                DO 1005 I=1,K
1005       PRINT 101,W1(I)
   17 CONTINUE
C
```

```
C     ***********************************************************************
C
C     COMPUTE AND PRINT DISCRETE CONTROL MATRIX (CONTROL TRANSITION
C     MATRIX), B.
C
C     ***********************************************************************
C
      DO 10 I=1,K
           DO 10 J=1,K
           FN(I,J)=F(I,J)
           B(I,J)=0.
10    B(I,I)=1.
      FACT=DT/2.
      DO 11 I=1,K
           DO 11 J=1,K
11    B(I,J)=B(I,J)+F(I,J)*FACT
      DO 12 II=3,100
      FACT=FACT*DT/II
      CALL MMPY(C,FN,F,K,K,K,15)
           DO 12 I=1,K
                DO 12 J=1,K
                B(I,J)=B(I,J)+C(I,J)*FACT
12    FN(I,J)=C(I,J)
      DO 13 I=1,K
           DO 13 J=1,K
13    B(I,J)=B(I,J)*DT
      CALL MMPY(BD,B,G,K,K,M,15)
      CALL MPRINT(BD,K,M,15,6,"   B MATRIX")
100   FORMAT(4I5,F10.5)
101   FORMAT(5F15.5)
103   FORMAT(10G10.4)
104   FORMAT("     NUMBER OF BITS =",I4)
  105 FORMAT(10X,"SAMPLING INTERVAL IS",F10.5,"   SECONDS")
  106 FORMAT(1H1)
      END
```

```
      SUBROUTINE QUANT(N,VAL,VALDIG)
C
C     ****************************************************************
C
C     THIS ROUTINE QUANTIZES THE VARIABLE, VAL, TO NBITS AND
C     PASSES THE RESULT BACK TO THE CALLING PROGRAM, STM.
C
C     ****************************************************************
C
      IBITS=1
1     VALD1=1./(2**IBITS)
      IBITS=IBITS+1
      IF(IBITS.GT.N)GO TO 4
      IF(VALD1.LE.VAL)GO TO 2
      GO TO 1
2     IF(VALD1.EQ.VAL)GO TO 5
      N1=N-1
           DO 3 I=IBITS,N1
           VALDIG=VALD1+1./(2.**I)
           IF(ABS(VALD1-VAL).LT.ABS(VALDIG-VAL))VALDIG=VALD1
3          IF(VALDIG.LT.VAL)VALD1=VALDIG
      RETURN
4     VALDIG=0.
      RETURN
5     VALDIG=VALD1
      RETURN
      END
```

Appendix D

Sub-Optimal Filter Models

Seven-State Model

$$F = \begin{bmatrix} 0 & 1 & 0 & 0 & 0 & 0 & 0 \\ -49 & -0.7 & 0 & 0 & 0 & 0 & 0 \\ -3.037504 & 0 & -12.56 & 1 & 0 & 0 & 0 \\ 0 & 0 & -77.6 & 0 & 1 & 0 & 0 \\ 19.84 & 0 & -198.4 & 0 & 0 & 0 & 0 \\ 2 & 0 & 0 & 0 & 0 & -2 & 1 \\ 1 & 0 & 0 & 0 & 0 & 1 & 0 \end{bmatrix}$$

$$G = \begin{bmatrix} 0 \\ 2.156 \\ 0 \\ 0 \\ 0 \\ 0 \\ 0 \end{bmatrix} \qquad L = \begin{bmatrix} 0 \\ 2.156 \\ 0 \\ 0 \\ 0 \\ 0 \\ 0 \end{bmatrix}$$

$$H = \begin{bmatrix} 0 & 0 & 1 & 0 & 0 & 0 & 0 \\ 1 & 0 & 0 & 0 & 0 & -1 & 0 \end{bmatrix}$$

Six-State Model

$$F = \begin{bmatrix} 0 & 1 & 0 & 0 & 0 & 0 \\ -49 & -.7 & 0 & 0 & 0 & 0 \\ -2.695 & 0 & -8 & 1 & 0 & 0 \\ 4.9 & 0 & -49 & 0 & 0 & 0 \\ 2 & 0 & 0 & 0 & -2 & 1 \\ 1 & 0 & 0 & 0 & -1 & 0 \end{bmatrix}$$

$$G = \begin{bmatrix} 0 \\ 2.156 \\ 0 \\ 0 \\ 0 \\ 0 \end{bmatrix} \qquad L = \begin{bmatrix} 0 \\ 2.156 \\ 0 \\ 0 \\ 0 \\ 0 \end{bmatrix}$$

$$H = \begin{bmatrix} 0 & 0 & 1 & 0 & 0 & 0 \\ 1 & 0 & 0 & 0 & -1 & 0 \end{bmatrix}$$

Five-State Model

$$F = \begin{bmatrix} 0 & 1 & 0 & 0 & 0 \\ -49 & -.7 & 0 & 0 & 0 \\ -3.037504 & 0 & -12.56 & 1 & 0 \\ 0 & 0 & -77.6 & 0 & 1 \\ 19.84 & 0 & -198.4 & 0 & 0 \end{bmatrix}$$

$$G = \begin{bmatrix} 0 \\ 2.156 \\ 0 \\ 0 \\ 0 \end{bmatrix} \qquad L = \begin{bmatrix} 0 \\ 2.156 \\ 0 \\ 0 \\ 0 \end{bmatrix}$$

$$H = \begin{bmatrix} 0 & 0 & 1 & 0 & 0 \\ 1 & 0 & 0 & 0 & 0 \end{bmatrix}$$

Four-State Model

$$F = \begin{bmatrix} 0 & 1 & 0 & 0 \\ -49 & -.7 & 0 & 0 \\ -2.695 & 0 & -8 & 1 \\ 4.9 & 0 & -49 & 0 \end{bmatrix}$$

$$G = \begin{bmatrix} 0 \\ 2.156 \\ 0 \\ 0 \end{bmatrix} \qquad L = \begin{bmatrix} 0 \\ 2.156 \\ 0 \\ 0 \end{bmatrix}$$

$$H = \begin{bmatrix} 0 & 0 & 1 & 0 \\ 1 & 0 & 0 & 0 \end{bmatrix}$$

Appendix E

Augmented Kalman Filter Models

Optimal (Eleven-State) Model

$$K = \begin{bmatrix}
0 & 1 & 0 & 0 & 0 & 0 & 0 & 0 & 0 & 0 & 0 \\
-49 & -0.7 & 0 & 0 & 0 & 0 & 0 & 2.156 & 0 & 0 & 2.156 \\
-3.037504 & 0 & -12.56 & 1 & 0 & 0 & 0 & 0 & 0 & 0 & 0 \\
0 & 0 & -77.6 & 0 & 1 & 0 & 0 & 0 & 0 & 0 & 0 \\
19.84 & 0 & -198.4 & 0 & 0 & 0 & 0 & 0 & 0 & 0 & 0 \\
2 & 0 & 0 & 0 & 0 & -2 & 1 & 0 & 0 & 0 & 0 \\
1 & 0 & 0 & 0 & 0 & -1 & 0 & 0 & 0 & 0 & 0 \\
0 & 0 & 0 & 0 & 0 & 0 & 0 & -125 & 1 & 0 & 0 \\
0 & 0 & 0 & 0 & 0 & 0 & 0 & 0 & -125 & 1 & 0 \\
0 & 0 & 0 & 0 & 0 & 0 & 0 & 0 & 0 & -125 & 0 \\
0 & 0 & 0 & 0 & 0 & 0 & 0 & 0 & 0 & 0 & -0.5
\end{bmatrix}$$

$$G = \begin{bmatrix} 0 \\ 0 \\ 0 \\ 0 \\ 0 \\ 0 \\ 0 \\ 0 \\ 0 \\ 1 \\ 0 \end{bmatrix} \qquad L = \begin{bmatrix} 0 & 0 \\ 0 & 2.56 \\ 0 & 0 \\ 0 & 0 \\ 0 & 0 \\ 0 & 0 \\ 0 & 0 \\ 0 & 0 \\ 0 & 0 \\ 0 & 0 \\ 1 & 0 \end{bmatrix}$$

$$H = \begin{bmatrix} 0 & 0 & 1 & 0 & 0 & 0 & 0 & 0 & 0 & 0 & 0 \\ 1 & 0 & 0 & 0 & 0 & -1 & 0 & 0 & 0 & 0 & 0 \end{bmatrix}$$

Eight-State Model

$$F = \begin{bmatrix} 0 & 1 & 0 & 0 & 0 & 0 & 0 & 0 \\ -49 & -0.7 & 0 & 0 & 0 & 0 & 0 & 2.156 \\ -3.037504 & 0 & -12.56 & 1 & 0 & 0 & 0 & 0 \\ 0 & 0 & -77.6 & 0 & 1 & 0 & 0 & 0 \\ 19.84 & 0 & -19.84 & 0 & 0 & 0 & 0 & 0 \\ 2 & 0 & 0 & 0 & 0 & -2 & 1 & 0 \\ 1 & 0 & 0 & 0 & 0 & -1 & 0 & 0 \\ 0 & 0 & 0 & 0 & 0 & 0 & 0 & 1 \end{bmatrix}$$

$$G = \begin{bmatrix} 0 \\ 2.156 \\ 0 \\ 0 \\ 0 \\ 0 \\ 0 \\ 0 \end{bmatrix} \qquad L = \begin{bmatrix} 0 & 0 \\ 0 & 2.156 \\ 0 & 0 \\ 0 & 0 \\ 0 & 0 \\ 0 & 0 \\ 0 & 0 \\ 0 & 0 \\ 1 & 0 \end{bmatrix}$$

$$H = \begin{bmatrix} 0 & 0 & 1 & 0 & 0 & 0 & 0 & 0 \\ 1 & 0 & 0 & 0 & 0 & -1 & 0 & 0 \end{bmatrix}$$

Seven-State Model

$$F = \begin{bmatrix} 0 & 1 & 0 & 0 & 0 & 0 & 0 \\ -49 & -0.7 & 0 & 0 & 0 & 0 & 2.156 \\ -2.695 & 0 & -8 & 1 & 0 & 0 & 0 \\ 4.9 & 0 & -49 & 0 & 0 & 0 & 0 \\ 2 & 0 & 0 & 0 & -2 & 1 & 0 \\ 1 & 0 & 0 & 0 & -1 & 0 & 0 \\ 0 & 0 & 0 & 0 & 0 & 0 & 1 \end{bmatrix}$$

$$G = \begin{bmatrix} 0 \\ 2.156 \\ 0 \\ 0 \\ 0 \\ 0 \\ 0 \end{bmatrix} \qquad L = \begin{bmatrix} 0 & 0 \\ 0 & 2.156 \\ 0 & 0 \\ 0 & 0 \\ 0 & 0 \\ 0 & 0 \\ 1 & 0 \end{bmatrix}$$

$$H = \begin{bmatrix} 0 & 0 & 1 & 0 & 0 & 0 & 0 \\ 1 & 0 & 0 & 0 & -1 & 0 & 0 \end{bmatrix}$$

Six-State Model

$$F = \begin{bmatrix} 0 & 1 & 0 & 0 & 0 & 0 \\ -49 & -0.7 & 0 & 0 & 0 & 2.156 \\ -3.037504 & 0 & -12.56 & 1 & 0 & 0 \\ 0 & 0 & -77.6 & 0 & 1 & 0 \\ 19.84 & 0 & -198.4 & 0 & 0 & 0 \\ 0 & 0 & 0 & 0 & 0 & 1 \end{bmatrix}$$

$$G = \begin{bmatrix} 0 \\ 2.156 \\ 0 \\ 0 \\ 0 \\ 0 \end{bmatrix} \qquad L = \begin{bmatrix} 0 & 0 \\ 0 & 2.156 \\ 0 & 0 \\ 0 & 0 \\ 0 & 0 \\ 1 & 0 \end{bmatrix}$$

$$H = \begin{bmatrix} 0 & 0 & 1 & 0 & 0 & 0 \\ 1 & 0 & 0 & 0 & 0 & 0 \end{bmatrix}$$

Five-State Model

$$F = \begin{bmatrix} 0 & 1 & 0 & 0 & 0 \\ -49 & -0.7 & 0 & 0 & 2.156 \\ -2.695 & 0 & -8 & 0 & 0 \\ 4.9 & 0 & -49 & 1 & 0 \\ 0 & 0 & 0 & 0 & 1 \end{bmatrix}$$

$$G = \begin{bmatrix} 0 \\ 2.156 \\ 0 \\ 0 \\ 0 \end{bmatrix} \qquad L = \begin{bmatrix} 0 & 0 \\ 0 & 2.156 \\ 0 & 0 \\ 0 & 0 \\ 1 & 0 \end{bmatrix}$$

$$H = \begin{bmatrix} 0 & 0 & 1 & 0 & 0 \\ 1 & 0 & 0 & 0 & 0 \end{bmatrix}$$

Vita

Phillip L. Toler was born on 29 February 1948 in Madisonville, Kentucky. He graduated from Sylmar High School, Sylmar, California in 1966. He enlisted in the United States Air Force in November 1967 and, while on active duty, continued his education, culminating in the award of a Bachelor of Science Degree in Electrical Engineering from Oklahoma State University in July 1973. In November 1973, upon completion of Officer's Training School, he was commissioned as a Second Lieutenant. During his Air Force career, Captain Toler has attended the Communications - Electronics Officer Course at Keesler Air Force Base and was assigned to Headquarters Air Force Communications Service detached to the Space and Missile Systems Organization at Los Angeles Air Force Station. His current assignment at the Air Force Institute of Technology to pursue a Master of Science Degree in Electrical Engineering began in June 1977. Captain Toler is a member of IEEE.

UNCLASSIFIED

SECURITY CLASSIFICATION OF THIS PAGE (When Data Entered)

REPORT DOCUMENTATION PAGE		READ INSTRUCTIONS BEFORE COMPLETING FORM
1. REPORT NUMBER AFIT/GE/EE/78D-45	2. GOVT ACCESSION NO.	3. RECIPIENT'S CATALOG NUMBER
4. TITLE (and Subtitle) ANALYSIS AND IMPLEMENTATION OF OPTIMAL ESTIMATION AND CONTROL FOR THE FJSRL SEISMIC ISOLATION PLATFORM		5. TYPE OF REPORT & PERIOD COVERED MS Thesis 6. PERFORMING ORG. REPORT NUMBER
7. AUTHOR(s) Phillip L. Toler Captain USAF		8. CONTRACT OR GRANT NUMBER(s)
9. PERFORMING ORGANIZATION NAME AND ADDRESS Air Force Institute of Technology Wright-Patterson AFB, Ohio 45433		10. PROGRAM ELEMENT, PROJECT, TASK AREA & WORK UNIT NUMBERS
11. CONTROLLING OFFICE NAME AND ADDRESS Frank J. Seiler Research Laboratory United States Air Force Academy, Colorado		12. REPORT DATE December 1978 13. NUMBER OF PAGES 146
14. MONITORING AGENCY NAME & ADDRESS(if different from Controlling Office)		15. SECURITY CLASS. (of this report) UNCLASSIFIED 15a. DECLASSIFICATION/DOWNGRADING SCHEDULE

16. DISTRIBUTION STATEMENT (of this Report)
Approved for public release; distribution unlimited

17. DISTRIBUTION STATEMENT (of the abstract entered in Block 20, if different from Report)

18. SUPPLEMENTARY NOTES Approved for public release; IAW AFR 190-17

Joseph P. Hipps, Major, USAF
Director of Information 1-23-79

19. KEY WORDS (Continue on reverse side if necessary and identify by block number)
seismic isolation platform
inertial instrument test methods
digital control of an isolation platform
stochastic estimation and control

20. ABSTRACT (Continue on reverse side if necessary and identify by block number)
The study is directed toward the analysis and implementation of an optimal estimator (Kalman filter) and an optimal regulator to provide active control of the inertial instrument test platform at the Frank J. Seiler Research Laboratory. The design specifications are to maintain angular position within $\pm 1.0 \times 10^{-3}$ arcseconds and angular rate with $\pm 1.667 \times 10^{-5}$ arcseconds/second. + or - .001

A forced separation concept is utilized to allow the independent evaluation of the Kalman filter and the optimal regulator.

DD FORM 1 JAN 73 1473 EDITION OF 1 NOV 65 IS OBSOLETE

+ or - .00001667

UNCLASSIFIED

SECURITY CLASSIFICATION OF THIS PAGE (When Data Entered)

Smgt Page

20. Optimal and suboptimal Kalman filter models are developed and evaluated at physically relizable sampling rates. A general optimal estimation and control algorithm is developed and a proposed sequence of algorithm computations is presented.